Non-fused BODIPY-based acceptor molecules for organic photovoltaics

Fabien Ceugniet,*[a] Amina Labiod,[b] Denis Jacquemin,[c] Benoît Heinrich,[d] Fanny Richard,[e] Patrick Lévêque,*[b] Gilles Ulrich,[a] and Nicolas Leclerc*[a]

[a] Institut de Chimie et Procédés pour l'Énergie, l'Environnement et la Santé (ICPEES), UMR CNRS 7515, École Européenne de Chimie, Polymères et Matériaux (ECPM), 25 Rue Becquerel, 67087 Strasbourg Cedex 02, France. E-mail: fabien.ceugniet@chem.ox.ac.uk and leclercn@unistra.fr

[b] Laboratoire ICube, UMR 7357-CNRS, Université de Strasbourg, 23 rue du Loess, 67037 Strasbourg, France. *E-mail: patrick.leveque@unistra.fr

[c] Nantes Université, CNRS, CEISAM UMR 6230, F-44000, Nantes, France & Institut Universitaire de France, 75005, Paris Cedex 5, France.

[d] Université de Strasbourg, CNRS, IPCMS UMR 7504, F-67034 Strasbourg, France.

[e] Université de Strasbourg, CNRS, Institut de Science et d'Ingénierie Supramoléculaires, 8 allée Gaspard Monge, Strasbourg, 67000, France.

Instrumentation

NMR spectroscopies

^{1}H, ^{11}B, ^{13}C and ^{19}F NMR spectra were recorded on Bucker Advance spectrometer 400 MHz and 500 MHz at 298K (unless specified otherwise). Chemicals shifts are reported to the delta scale in ppm using the predeuderated residual solvent peak as reference for ^{1}H and ^{13}C analysis. The list of solvents used is as follows: $CDCl_3$ (^{1}H : δ = 7.26 ppm, ^{13}C : δ = 77.16 ppm), CD_2Cl_2 (^{1}H : δ = 5.32 ppm, ^{13}C : δ = 54.00 ppm), $C_2D_2Cl_4$ (^{1}H : δ = 6.00 ppm, ^{13}C : δ = 73.78 ppm)

Thermal properties

Thermogravimetric analysis (TGA) measurements were performed with TA Instruments Q50 from instrument.

Differential scanning calorimetry (DSC) measurements were performed with TA Instruments Q1000 instrument, operated at scan rate of 5oC/min on heating and on cooling.

DFT and TD-DFT calculations

All our DFT and TD-DFT calculations have been performed with the Gaussian 16.A.03 code[1] using default threshold and algorithms except for what is noted below. We performed the calculations considering solvent effects ($CHCl_3$) to be consistent with the UV/Vis measurements, using the PCM[2]

model to capture the environmental effects. The structures used in the calculations have the long experimental alkyl chains substituted by methyl groups for obvious computational reasons.

The geometry optimizations were performed with the MN15 hybrid functional[3] combined with the 6-31G(d) atomic basis set. A *tight* convergence criterion was applied and many starting conformers were considered and no symmetry constrains were used. We next performed analytical frequency calculations at the same level of theory to obtain ZPVE energies and to confirm that all structures are true minima of the potential energy surface. Eventually, the vertical transition energies were determined with TD-DFT, using the PCM-MN15/6-31+G(d,p) approach. During these calculations, the *non-equilibrium* limit of the PCM model applied in its *linear-response* version (suited for bright excitations as here) was used. We are well-aware of the limits of TD-DFT for BODIPY derivatives,[4] but we are interested in trends here, and electron-correlared wavefunction calculations are beyond reach for very large compounds.

Absorption and emission spectroscopies

UV-visible spectra in solution were recorded using a Schimadzu UV-3600 dual beam grating spectrophotometer with 1 cm² quartz cells. Steady-state emission and excitation spectra in solution were recorded at 25°C on a HORIBA JobinYvon FluorMax 4P spectrofluorimeter. All fluorescence spectra were corrected. The following equation was used to determine the fluorescence quantum yield (ϕ_F):

$$\phi_F = \phi_{ref} \frac{I \ OD_{ref} \ \eta^2}{I_{ref} \ OD \ \eta_{ref}^{\ 2}}$$

Where ϕ_F stands for fluorescence quantum yield of the analyzed compound, I the integral of the corrected fluorescence spectra, OD the optical density at the excitation wavelength and η the refractive if the measurement solvent. ϕ_{ref}, $I_{ref,}$ $OD_{ref,}$ η_{ref} denote for the reference parameters. Depending on the emission maxima of the analyzed compound, cresyl violet (ϕ_{ref} = 0.50 in EtOH, λ_{ex} = 546 nm) or a reported BODIPY dye (ϕ_{ref} = 0.49 in DCM, λ_{ex} = 650 nm)[197] were used as reference. Fluorescence lifetimes were measured on a HORIBA JobinYvon FluorMax 4P spectrofluorimeter equipped with a HORIBA pulsed diode source NanoLED connected to a HORIBA Single Photon Counting Controller Fluorohub. FS-900 software was used to deconvoluate lifetime using a light-scattering solution (colloidal silica suspension in H_2O) for instrument response.

Cyclic voltammetry

Oxidation and reduction potentials were determined by cyclic voltammetry with a conventional 3-electrode system using a BioLogic potentiostat equipped with a platinum micro disk (2 mm^2) working

electrode and a platinum wire counter electrode. Potentials were calibrated versus the saturated calomel electrode (SCE) at a conventional scan rate of 100 mV/s. Recrystallized tetrabutylammonium hexafluorophosphate (Bu_4NPF_6) was used as the supporting electrolyte (0.1 M) in distilled and anhydrous acetonitrile. Acetonitrile was distilled from CaH_2 under a nitrogen atmosphere. The ferrocene/ferrocenium couple was used as an internal reference.

Photo-Electron Spectroscopy in Air (PESA)

PESA has been performed on an AC-2 Model from Riken Instruments. UV photons are emitted from a deuterium lamp, then monochromated by a grating spectrometer and finally focused on the sample film. The photoelectrons emitted by the sample are detected by an open counter. When the sample's surface is bombarded with a slowly increasing amount of UV energy, photoelectrons start to emit at a certain energy level which corresponds to the photoelectron work function.

Structural analysis

The **SWAXS** patterns were obtained with a transmission Guinier-like geometry. A linear focalized monochromatic Cu Kα1 beam (λ = 1.54056 Å) was obtained using a sealed-tube generator (600 W) equipped with a bent quartz monochromator. The samples were filled in home-made sealed cells of adjustable path. The sample temperature was controlled within ±0.1 °C, and exposure times were of 24 h. The patterns were recorded on image plates and scanned by using Amersham Typhoon IP with 25 µm resolution (periodicities up to 100 Å).

GIWAXS measurements were conducted at PLS-II 9A U-SAXS beamline of Pohang Accelerator Laboratory (PAL) in Korea. The X-rays coming from the vacuum undulator (IVU) were monochromated using Si(111) double crystals and focused on the detector using K-B type mirrors. Patterns were recorded with a 2D CCD detector (Rayonix SX165). The sample-to-detector distance was about 225 mm for energy of 11.09 keV (1.118 Å).

Organic field-effect transistors (OFETs) elaboration and charge-mobility measurements

(Bottom contact/bottom gate) organic field-effect transistors (OFETs) were elaborated on commercially available pre-patterned test structures whose source and drain contacts were composed of a 30 nm thick gold layer on top of a 10 nm thick Indium Tin Oxide (ITO) layer. A 230 nm thick silicon oxide was used as gate dielectric and n-doped ($3x10^{17}/cm^3$) silicon crystal as gate electrode. The channel length and channel width were 20 µm and 10 mm, respectively. The test structures were cleaned in acetone and isopropyl alcohol and subsequently for 30 minutes in an ultra-violet ozone system. Then,

hexamethyldisilazane (HMDS) was spin-coated (500 rpm for 5 s and then 4000 rpm for 50 s) under nitrogen ambient followed by an annealing step at 130°C for 10 minutes. Finally, anhydrous chloroform of NFA solutions (concentration ranging from 5 to 10 mg/mL and stirred 24 hours at room-temperature) were spin coated to complete the FET devices. The samples were then left overnight under vacuum (<10^{-6} mbar) to remove residual solvent traces. Both, the FET elaboration and characterizations were performed in nitrogen ambient. The transistor output and transfer characteristics were recorded using a Keithley 4200 semiconductor characterization system. The charge carrier mobility was extracted in the saturation regime using the usual formalism on as-cast FET devices as well as on isochronally (10 minutes) annealed devices for different temperatures. In this formalism, the source-drain current (I_{DS}) is related to the charge-carrier mobility (μ_{sat}) according to equation (1)

$$I_{DS} = \frac{WC_i\mu_{sat}}{L}(V_{GS} - V_{Th})^2 \qquad (1)$$

where C_i is the capacitance per area of the insulator, W and L are respectively the channel width and length and V_{GS} and V_{Th} are the gate-source and threshold voltages, respectively. The channel width and length were 20 µm and 10 mm, respectively. The charge-carrier mobility in the saturation regime is therefore calculated using equation (2):

$$\mu_{sat} = \frac{2L}{WC_i}\left(\frac{\partial\sqrt{I_{DS}}}{\partial V_{GS}}\right)^2 \qquad (2)$$

Space Charge Limited Current (SCLC) diodes elaboration and charge-mobility measurements

Space charge limited current (SCLC) diodes were elaborated into a glovebox using the structure Glass:ITO/ZnO/**BTT**/Ca (20 nm):Al (120 nm). Glass:ITO substrates from LumTech had a sheet resistance equal to 10 Ω/□. They were cleaned using an ultrasonic bath (45°C, 15 min.) of successively hellmanex™, deionized water, acetone and isopropanol. They were then exposed to UV-O_3 for 30 minutes just before ZnO deposition. The solution of ZnO nanoparticles (2.5 wt% in 2-propanol) from Avantama was filtered (PVDF, 0.45 µm) before spin-coating (5000 rpm, 60 sec.). The ZnO film was then thermally annealed (100°C, 10 min.). The thickness of ZnO, measured by profilometry was around 20 nm. The **BTT** solution was spin-coated, either statically or dynamically, with various conditions to obtain at least two different and homogeneous film thicknesses. The **BTT** thickness was measured by profilometry. No experimental conditions could be found to obtain homogeneous **BTT_{L6}-4F** and **BTT_{L6}-4Cl** films. The electron-only diodes were finally obtained after a thermally evaporated Ca (20 nm):Al (120 nm) bilayer. The charge-carrier mobility (μ_{SCLC}) was extracted using the Mott-Gurney variation of the current-density (J) versus voltage (V) in the space-charge limited regime following equation (3):

$$J = \frac{9}{8}\varepsilon_r\varepsilon_0\mu_{SCLC}\frac{V^2}{d^3} \quad (3)$$

where $\varepsilon_r\varepsilon_0$ is the organic semiconductor dielectric permittivity and d the organic film thickness. The (*J-V*) measurements were performed in the glovebox on non-annealed samples.

Organic solar cells (OSCs) elaboration

OSCs were elaborated using the Glass:ITO/ZnO/AL/MoO_3:Ag structure where AL refers to the active-layer. The elaboration process is the same as for SCLC devices, up to the AL deposition. The AL is a blend of PM6 with the **BTT** molecules ([PM6:**BTT**]) with ratios ranging from [1:1.5] to [1:2] in $CHCl_3$. As an additive, 1-chloronaphthalene (CN) was added in the solution with a ratio 99.5% vol. $CHCl_3$ and 0.5% vol. CN. The solutions were stirred at least 24 hours at room temperature and then at 50°C for one hour before deposition. $\mathbf{BTT_{L6}}$ solutions were spin-coated dynamically at 3000 rpm. $\mathbf{BTT_{R8}}$ solutions were spin-coated statically at 3000 rpm. The device was then thermally annealed for 10 minutes at 110°C (120°C for $\mathbf{BTT_{R8}}$**-4Cl**). The AL thickness has been measured by profilometry and ranged from 80 to 100 nm. The top electrode (7 nm of MoO_3 and 120 nm of Ag) was then thermally evaporated at a pressure lower than $5x10^{-6}$ mbar to complete the device. The (*I-V*) measurements were done in the glovebox using a Keithley 2400 SMU in the dark or under a calibrated (100 mW/cm²) AM1.5G solar spectrum using an ABET TECHNOLOGIES Sun 3000 solar simulator. The diode surface (12 mm²) was defined using a mask. The average results reported below were obtained on at least 10 different devices. Some measurements were performed at lower light-power using neutral filters in order to measure the photovoltaic parameters dependence on the light intensity.

Materials and synthesis

$Pd(PPh_3)_2Cl_2$ was synthetized according to the literature. All other reagents were purchased from commercial suppliers and used without further purifications.

Anhydrous solvents were obtained by distillation over drying agents. DCM was distillated over CaH_2, PhMe over sodium and $MeNO_2$ over KOH.

Compound purifications were performed on standard silica gel (0.063-0.200 mm). Silica plates precoated with fluorescent indicator were used to perform thin layer chromatography.

Synthesis

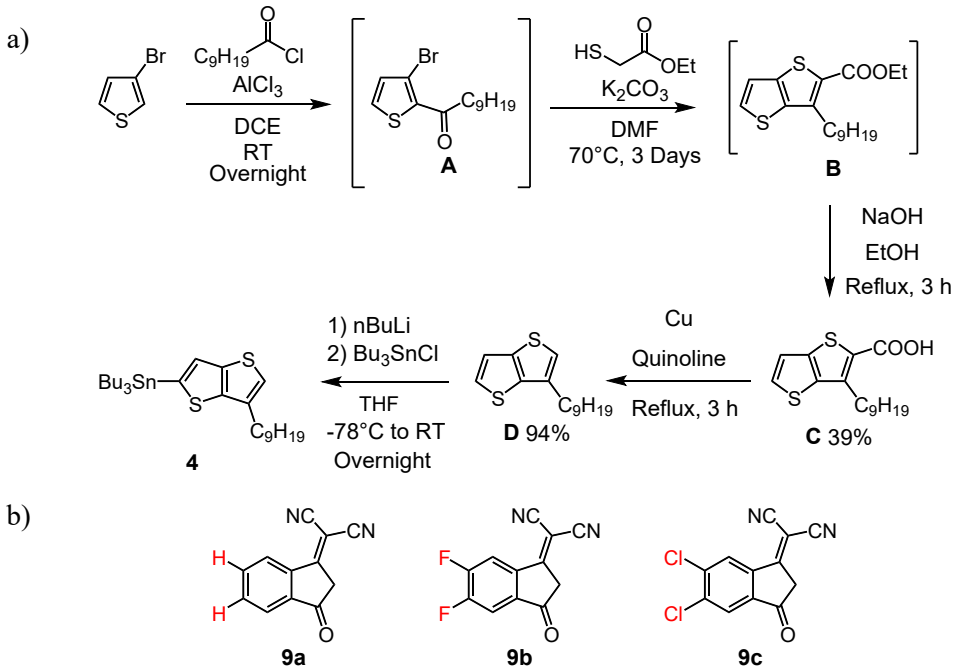

Figure S1. a) Synthesis route toward **4**. b) Terminal acceptors used

General procedure 1: Stille cross-coupling reactions

Dry toluene was added to a dried Schlenk tube loaded with a magnetic stir bar, the halogenated compound (1.0 eq), Compound **4** (3.5 eq) and $Pd(PPh_3)_2Cl_2$ (5%). The reaction was degassed for 30 min with Ar and was heated to 115°C for 24 h. At RT, water was added and the reaction mixture was diluted with DCM. The organic phase was washed several times with water, dried over $MgSO_4$ and the solvent was removed under reduce pressure. Recrystallization from hot ethanol afforded the desired pure compound.

General procedure 2: Vilsmeier-Haack formylation

$POCl_3$ (6.0 eq) was added to a solution of distillated DMF (6.0 eq) in dry DCE at 0°C. The reaction medium was allowed to warm up and stirred for 30 min at RT. The resulting mixture was cannulated into a solution of the appropriate starting material in dry DCE (0.02-0.03M). The reaction was heated to 80°C for 24h. At RT, the reactional mixture was poured to a saturated solution of Na_2CO_3 and stirred for 30 min. The resulting mixture was extracted with DCM, washed with water, dried over $MgSO_4$ and the solvent was removed under reduce pressure. Column chromatography on SiO_2 afforded the desired pure compound.

General procedure 3: Knoevenagel condensation with β-alanine

The formylated BODIPY (1.0 eq), and β-alanine (40 %) were dissolved in a mixture of $CHCl_3$/*i*PrOH (3:1, 6 mM). The appropriate dicyanomethyleneindanone was added and the reaction was heated to reflux for the indicated time. At RT, the reactional mixture was poured in methanol (100 mL) and stirred for 10 min. The precipitate was collected by filtration and purified by several recrystallizations from $CHCl_3$/*i*PrOH to give the desire product.

Compound C[13]

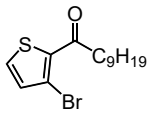

Freshly prepared decanoyl chloride (100 mmol, 1.0 eq) was dissolved in dry DCM (100 mL). 3-bromothiophene (9.11 mL, 100 mmol, 1.0 eq) was added and the mixture was cooldown to 0°C. $AlCl_3$ (13.3 g, 100 mmol, 1.0 eq) was added to the reaction portion-wise at 0°C and the reactional mixture was stirred overnight at RT. Water was slowly added and the solid residue was filtered off. The filtrate was diluted with DCM and washed with an aqueous solution of NaOH 1M. The organic phase was dried over $MgSO_4$ and the solvent was removed under reduce pressure. The crude liquid was dried under vaccum for 3 h and was used without other purification for the next synthetic step (26.4 g).

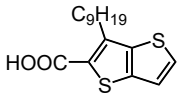

The crude product (26.4 g, 83.2 mmol, 1.0 eq) was dissolved in distillated anhydrous DMF (110 mL). K_2CO_3 (28.7 g, 208 mmol, 2.5 eq) and ethyl 2-mercaptoacetate (9.58 mL, 87.4 mmol, 1.0 eq) were added and the reaction was heated to 60°C for 72 h. At RT, The mixture was diluted with AcOEt and the solid residue was filtered off. The organic phase was washed with an aqueous solution of HCl 1M and brine, dried over $MgSO_4$ and the solvent was removed under reduce pressure. The residue was dissolved in EtOH (250 mL) and NaOH (6.64 g, 166 mmol, 2.0 eq) was added to the reaction. The reactional mixture was heated to reflux for 3h. At RT, the solvent was removed under reduce pressure. Water (100 mL) was added and the pH was acidified to 1 with concentrated HCl. The precipitate was filtrated and purified by trituration in PE. The desire product was obtained as a slightly beige solid (12.2 g, 39.3. 39%). **^{1}H NMR** (400 MHz, $CDCl_3$): δ = 7.61 (d, J = 5.3 Hz, 1H), 7.28 (d, J = 5.3 Hz, 1H), 3.20 (t, J = 7.7 Hz, 2H), 1.76 (m, 2H), 1.46 – 1.20 (m, 17H), 0.87 (t, J = 6.7 Hz, 3H).

Compound D[13]

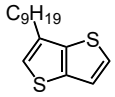

Compound **C** (12.2 g, 39.3 mmol, 1.0 eq) was added to a mixture of copper dust (4.98 g, 78.6 mmol, 2.0 eq) in quinoline (80 mL). The reaction was heated to reflux for 3 h. At RT, The reaction mixture was diluted with AcOEt and the residue of copper was removed by filtration. The organic phase was washed several times with a solution of HCl 1M and water, dried over $MgSO_4$ and the solvent was removed under reduce pressure. The crude product was purified by column chromatography on SiO_2 gel (PE, 100%) to afford the expected product as a colorless oil (9.83g, 36.9 mmol, 94%). **^{1}H NMR** (500 MHz, $CDCl_3$): δ = 7.36 (dd, J = 5.2, 1.5 Hz, 1H), 7.24 (d, J = 5.2 Hz, 1H), 6.99 (d, J = 1.5 Hz, 1H), 2.73 (t, J = 7.8 Hz, 2H), 1.80 – 1.69 (m, 1H), 1.42 – 1.22 (m, 12H) 0.88 (t, J = 6.9 Hz, 3H).

Compound 4

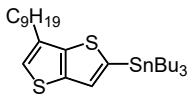

*n*BuLi (2.5M, 1.0 eq) was added dropwise to a solution of compound **D** (9.83g, 36.9 mmol, 1.0 eq) in dry THF (100 mL) at -78°C. The reaction was allowed to warm-up to -30°C and then cooled again to -78°C. Bu_3SnCl (1.05 eq) was slowly added to the reactional mixture at -78°C. The reaction was stirred and allowed to slowly warm-up to RT overnight. Water was added to quench the reaction and the mixture was diluted with AcOEt. The organic phase was washed with water, dried over $MgSO_4$ and the solvent was removed under reduce pressure. The crude was dried under vaccum for 3 h. The crude product was obtained as a yellow oil (20.3 g) and used without other purification for the next synthetic step.

Compound 2

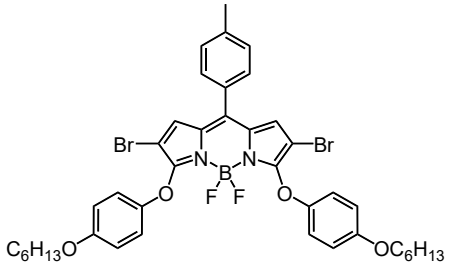

TetrabromoBODIPY **1** (1.00 g, 1.67 mmol, 1.0 eq), 4-(hexyloxy)phenol (1.08 g, 5.52 mmol, 3.3 eq) and Na_2CO_3 (1.07

g, 10.0 mmol, 6.0 eq) were added to 25 mL of dry ACN. The mixture was heated to 100°C for 4h. At RT, the solid residue was filtered off and the solvent was evaporated under reduced pressure. The crude product was purified by flash chromatography on SiO_2 gel (PE/PhMe/DCM, 5:4:1) to give the desire pure product as a golden red solid (1.24 g, 1.50 mmol, 90%). **^{1}H NMR** (400 MHz, $CDCl_3$): δ = 7.41 (d, J = 8.1 Hz, 2H), 7.33 (d, J = 8.1 Hz, 2H), 7.05 (d, J = 9.1 Hz, 4H), 6.89 (s, 2H), 6.83 (d, J = 9.1 Hz, 4H), 3.91 (t, J = 6.6 Hz, 4H), 2.47 (s, 3H), 1.75 (p, J = 6.6 Hz, 4H), 1.51 – 1.39 (m, 4H), 1.38 – 1.25 (m, 8H), 0.90 (t, J = 7.0 Hz, 6H). **^{13}C NMR (**126 MHz, $CDCl_3$): δ = 158.18, 156.21, 149.44, 141.86, 141.37, 132.05, 130.51, 129.60, 129.53, 127.38, 119.21, 115.29, 95.35, 68.60, 31.74, 29.40, 25.86, 22.74, 21.60, 14.18. **^{11}B NMR** (128 MHz, $CDCl_3$): δ = 0.02 (t, J_{B-F} = 26.9 Hz). **^{19}F NMR** (377 MHz, $CDCl_3$): δ = -147.99 (q, J_{F-B} = 26.9 Hz). **HRMS** (ESI-TOF): calcd for $C_{40}H_{43}BBr_2F_2KN_2O_4$ $[M+K]^+$, 863.1272; found 863.1268

Compound 3

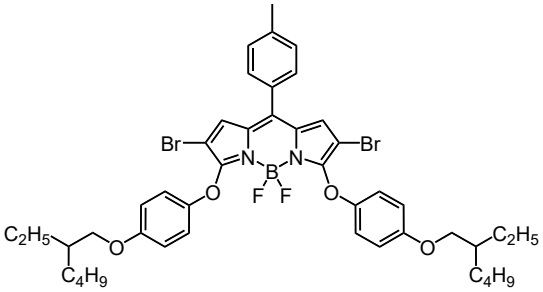

TetrabromoBODIPY **1** (740 mg, 1.24 mmol, 1.0), 4-((2-ethylhexyl)oxy)phenol (908 mg, 4.08 mmol, 3.3 eq) and Na_2CO_3 (787 mg, 7.44 mmol, 6.0 eq) were added to 20 mL of dry ACN. The mixture was heated to 100°C for 4h. At RT, the solid residue was filtered off and the solvent was evaporated under reduced pressure. The crude product was purified by flash chromatography on SiO_2 gel (PE/PhMe/DCM, 5:5:0 to 5:1:4) to give the desire pure product as a golden red sticky solid (931 mg, 1.05 mmol, 85%). **^{1}H NMR** (400 MHz, $CDCl_3$): δ = 7.41 (d, J = 8.1 Hz, 2H), 7.33 (d, J = 8.1 Hz, 2H), 7.11 – 6.98 (m, 4H), 6.89 (s, 2H), 6.86 – 6.75 (m, 4H), 3.79 (d, J = 5.8 Hz, 4H), 2.47 (s, 3H), 1.74 – 1.64 (m, 2H), 1.53 – 1.34 (m, 8H), 1.34 – 1.23 (m, 8H), 0.94 – 0.85 (m, 12H). **^{13}C NMR** (126 MHz, $CDCl_3$): δ = 158.18, 156.46, 149.40, 141.84, 141.36, 132.03, 130.52, 129.61, 129.53, 127.38, 119.15, 115.32, 95.38, 71.14, 39.55, 30.65, 29.24, 23.98, 23.19, 21.60, 14.23, 11.26. **^{11}B NMR** (128 MHz, $CDCl_3$): δ = 0.02 (t, J_{B-F} = 27.1 Hz). **^{19}F NMR** (377 MHz, $CDCl_3$): δ = -147.98 (q, J_{F-B} = 27.1 Hz). **HRMS** (ESI-TOF): calcd for $C_{44}H_{51}BBr_2F_2KN_2O_4$ $[M+K]^+$, 917.1906; found 917.1908.

Compound 5

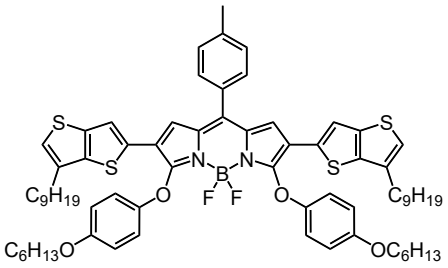

Compound **5** was synthetized according to the **general procedure 1**. Starting from compound **2** (1.24 g, 1.50 mmol, 1.0 eq) and compound **4** (5.26 mmol, 3.5 eq). The desired product was obtained as a blue-violet powder (1.49 g, 1.25 mmol, 83%). **^{1}H NMR** (400 MHz, $CDCl_3$): δ = 7.54 (d, J = 7.9 Hz, 2H), 7.41 (d, J = 7.9 Hz, 2H), 7.03 (s, 2H), 7.00 – 6.92 (m, 6H), 6.87 (s, 2H), 6.73 (d, J = 9.2 Hz, 4H), 3.82 (t, J = 6.6 Hz, 4H), 2.61 (t, J = 7.7 Hz, 4H), 2.53 (s, 3H), 1.74 – 1.62 (m, 8H), 1.44 – 1.36 (m, 4H), 1.35 – 1.16 (m, 32H), 0.92 – 0.85 (m, 12H). **^{13}C NMR** (126 MHz, $CDCl_3$): δ = 158.16, 155.49, 150.73, 142.61, 141.14, 139.21, 138.66, 135.00, 134.45, 130.71, 130.14, 129.57, 128.45, 126.11, 121.80, 118.06, 117.41, 115.42, 68.56, 32.02, 31.73, 30.02, 29.66, 29.53, 29.48, 29.45, 29.39, 28.72, 25.84, 22.82, 22.74, 21.67, 14.26, 14.17. **^{11}B NMR** (128 MHz, $CDCl_3$): δ = 0.23 (t, J = 27.1 Hz). **^{19}F NMR** (377 MHz, $CDCl_3$): δ = -147.33 (q, J = 27.1 Hz). **HRMS** (ESI-TOF): calcd for $C_{70}H_{85}BF_2KN_2O_4S_4$ $[M+K]^+$, 1233.5085; found 1233.5073.

Compound 6

Compound **6** was synthetized according to the **general procedure 1**. Starting from compound **3** (911 mg, 1.03 mmol, 1.0 eq) and compound **4** (3.60 mmol, 3.5 eq). The desired product was obtained as a blue-violet powder (1.01 g, 0.807 mmol, 78%). **^{1}H NMR** (400 MHz, $CDCl_3$): δ = 7.54 (d, J = 8.0 Hz, 2H), 7.41 (d, J = 8.0 Hz, 2H), 7.04 (s, 2H), 7.00 – 6.94 (m, 6H), 6.87 (s, 2H), 6.74 (d, J = 9.1 Hz, 4H), 3.71 (d, J = 5.9 Hz, 4H), 2.62 (t, J = 7.7 Hz, 4H), 2.53 (s, 3H), 1.74 – 1.59 (m, 6H), 1.49 – 1.22 (m, 40H), 0.93 – 0.84 (m, 18H). **^{13}C NMR** (126 MHz, $CDCl_3$): δ = 158.17, 155.74, 150.68, 142.58, 141.13, 139.22, 138.63, 134.99, 134.47, 130.71, 130.14, 129.57, 128.45, 126.09, 121.79, 118.07, 117.36, 115.44, 71.06, 39.52, 32.02, 30.63, 30.02, 29.66, 29.53, 29.48, 29.45, 29.21, 28.72, 23.95, 23.18, 22.82, 21.67, 14.26, 14.22, 11.23. **^{11}B NMR** (128 MHz, $CDCl_3$): δ = 0.24 (t, J_{B-F} = 27.2 Hz). **^{19}F NMR** (377 MHz, $CDCl_3$): δ = -147.31 (q, J_{F-B} = 27.2 Hz). **HRMS** (ESI-TOF): calcd for $C_{74}H_{93}BF_2N_2O_4S_4$ $[M]^+$, 1250.6074; found 1250.6058

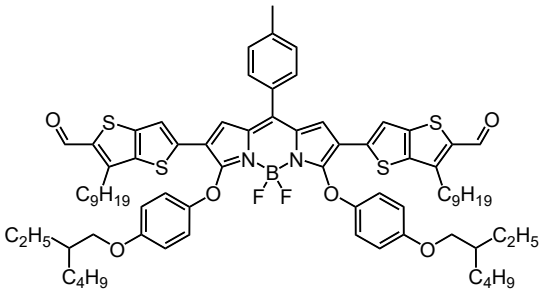

Compound 7

Compound **7** was synthetized according to the **general procedure 2**. Starting from compound **5** (783 mg, 0.655 mmol, 1.0 eq). Column chromatography on silica gel (DCM, 100%) with solid deposit on cellite affords the desired product as a blue-violet powder (655 mg, 0.531 mmol, 81%). **^{1}H NMR** (400 MHz, $CDCl_3$): δ = 10.01 (s, 2H), 7.54 (d, J = 8.0 Hz, 2H), 7.44 (d, J = 8.0 Hz, 2H), 7.09 (s, 2H), 7.04 (s, 2H), 6.96 (d, J = 9.1 Hz, 4H), 6.74 (d, *J* = 9.1 Hz, 4H), 3.83 (t, J = 6.6 Hz, 4H), 2.99 (t, J = 7.6 Hz, 4H), 2.54 (s, 3H), 1.78 – 1.63 (m, 8H), 1.50 – 1.16 (m, 36H), 0.94 – 0.82 (m, 12H). **^{13}C NMR** (126 MHz, $CDCl_3$): δ = 182.23, 158.51, 155.76, 150.46, 145.09, 144.94, 143.61, 141.64, 140.73, 139.75, 138.74, 130.68, 129.75, 129.73, 128.74, 127.10, 118.14, 117.47, 117.31, 115.44, 68.58, 31.96, 31.70, 29.98, 29.55, 29.43, 29.39, 29.35, 28.39, 25.82, 22.78, 22.71, 21.70, 14.23, 14.15. **^{11}B NMR** (128 MHz, $CDCl_3$): δ = 0.22 (t, J_{B-F} = 26.9 Hz). **^{19}F NMR** (377 MHz, $CDCl_3$): δ = -146.99 (q, J_{F-Bz} = 26.9 Hz). **HRMS** (ESI-TOF): calcd for $C_{72}H_{85}BF_2N_2NaO_6S_4$ $[M+Na]^+$, 1273.5244; found 1273.5234.

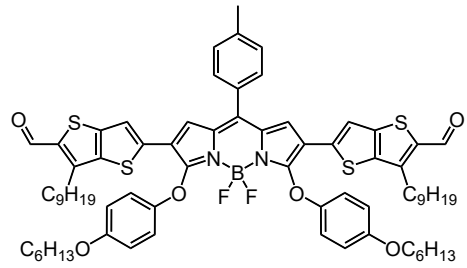

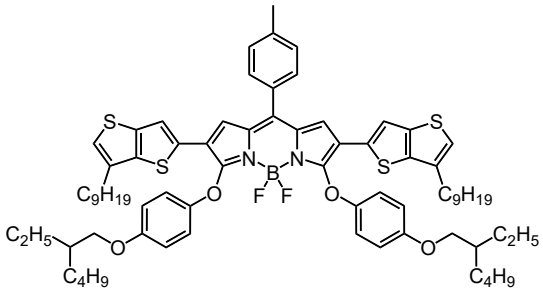

Compound 8

Compound **8** was synthetized according to the **general procedure 2**. Starting from compound **6** (919 mg, 0.734 mmol, 1.0 eq). Column chromatography on silica gel (DCM/AcOEt, 100:0 to 100:1) with solid deposit on celite affords the desired product as a blue-violet powder (656 mg, 0.502 mmol, 68%). **^{1}H NMR** (400 MHz, $CDCl_3$): δ = 10.01 (s, 2H), 7.55 (d, J = 8.0 Hz, 2H), 7.44 (d, J = 8.0 Hz, 2H), 7.09 (s, 2H), 7.05 (s, 2H), 6.96 (d, J = 9.1 Hz, 4H), 6.75 (d, J = 9.1 Hz, 4H), 3.71 (d, J = 6.4 Hz, 4H), 2.99 (t, J = 7.6 Hz, 4H), 2.54 (s, 3H), 1.76 – 1.60 (m, 6H), 1.49 – 1.21 (m, 40H), 0.94 – 0.83 (m, 18H). **^{13}C NMR** (126 MHz, $CDCl_3$): δ = 182.22, 158.53, 156.02, 150.42, 145.11, 144.93, 143.59, 141.63, 140.74, 139.74, 138.74, 130.69, 129.77, 129.73, 128.75, 127.09, 118.15,

117.43, 117.33, 115.48, 71.11, 39.49, 31.96, 30.60, 29.99, 29.55, 29.43, 29.39, 29.19, 28.39, 23.92, 23.16, 22.79, 21.70, 14.24, 14.20, 11.21. **^{11}B NMR** (128 MHz, $CDCl_3$): δ = 0.22 (t, J_{B-F} = 26.3 Hz). **^{19}F NMR** (377 MHz, $CDCl_3$): δ = -146.97 (q, J_{F-B} = 26.3 Hz). **HRMS** (ESI-TOF): calcd for $C_{76}H_{94}BF_2N_2O_6S_4$ $[M+H]^+$, 1307.6050; found 1307.6009.

BTT_{L6}

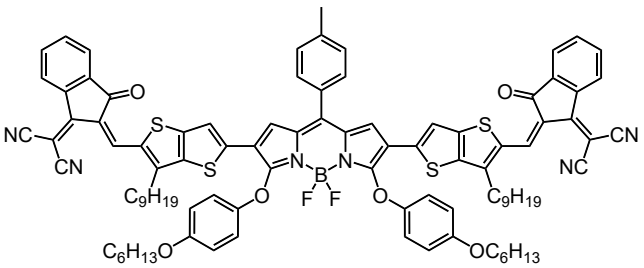

BTT_{L6} was synthetized according to the **general procedure 3**. Starting from compound **7** (120 mg, 0.096 mmol, 1.0 eq) and compound **9a** (74 mg, 0.38 mmol, 4.0 eq). The reaction was heated for 48h. The desired product was obtained as a black powder (139 mg, 0.087 mmol, 90%). **^{1}H NMR** (500 MHz, $CDCl_3$): δ = 8.82 (s, 2H), 8.64 – 8.42 (m, 2H), 7.90 – 7.85 (m, 2H), 7.74 – 7.66 (m, 6H), 7.54 (d, J = 8.0 Hz, 2H), 7.12 (s, 2H), 6.98 (s, 2H), 6.91 (d, J = 9.2 Hz, 4H), 6.75 (d, J = 9.2 Hz, 4H), 3.82 (t, J = 6.6 Hz, 4H), 2.94 (t, J = 7.9 Hz, 4H), 2.62 (s, 3H), 1.72 – 1.61 (m, 8H), 1.43 – 1.33 (m, 8H), 1.33 – 1.20 (m, 28H), 0.92 – 0.80 (m, 12H). **^{13}C NMR** (126 MHz, $CDCl_3$): δ = 188.23, 160.86, 158.34, 155.78, 151.69, 151.29, 150.27, 143.79, 142.12, 140.22, 139.95, 136.99, 135.09, 135.00, 134.61, 134.50, 131.11, 129.95, 129.62, 129.06, 126.87, 125.18, 123.84, 121.28, 117.76, 117.23, 116.97, 115.65, 115.29, 114.95, 68.66, 68.55, 32.00, 31.70, 30.74, 30.10, 29.78, 29.58, 29.57, 29.43, 29.35, 25.81, 22.82, 22.70, 21.83, 14.27, 14.13. **^{11}B NMR** (160 MHz, $CDCl_3$): δ = 0.05 (t, J = 27.3 Hz). **^{19}F NMR** (471 MHz, $CDCl_3$): δ = -146.12 (s, broad). **HRMS** (ESI-TOF): calcd for $C_{96}H_{93}BF_2KN_6O_6S_4$ $[M+K]^+$, 1641.5732; found 1641.5680.

BTT_{L6}-4F

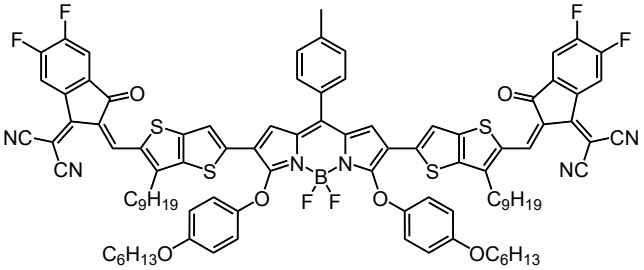

BTT_{L6}-4F was synthetized according to the **general procedure 3**. Starting from compound **7** (150 mg, 0.120 mmol, 1.0 eq) and compound **9b** (110 mg, 0.480 mmol, 4.0 eq). The reaction was heated for 24h. The desired product was obtained as a black powder (177 mg, 0.106 mmol, 88%). **^{1}H NMR** (500 MHz, $CDCl_3$): δ = 8.82 (s, 2H), 8.44 (dd, J = 9.9, 6.4 Hz, 2H), 7.67 (d, J = 7.7 Hz, 2H), 7.63 (t, J = 7.5 Hz, 2H), 7.54 (d, J = 7.7 Hz, 2H), 7.11 (s, 2H), 7.01 (s, 2H), 6.90 (d, J = 9.2 Hz, 4H), 6.75 (d, J = 9.2 Hz, 4H), 3.83 (t, J = 6.6 Hz, 4H), 2.95 (t, J = 8.0 Hz, 4H), 2.63 (s, 3H), 1.73 – 1.60 (m, 8H), 1.44 – 1.32 (m, 8H), 1.31 – 1.19 (m, 28H), 0.92 – 0.82 (m, 12H). **^{13}C NMR** (101 MHz, CD_2Cl_4, 80°C, Q-DEPT): δ = 185.29, 158.89, 158.59, 155.85, 155.45, 152.99, 152.85, 151.90, 150.08, 144.43, 143.75, 141.73, 140.57, 136.29, 135.32, 134.45, 134.27, 130.53, 129.55, 129.25, 128.92, 127.14, 120.56, 118.05, 117.24, 116.97, 115.77, 114.55, 114.54 (d, $^3J_{F-C}$ = 21.8 Hz), 114.27, 112.37 (d, $^3J_{F-C}$ = 18.7 Hz), 68.98, 68.76, 31.60, 31.33, 30.36, 29.80, 29.37, 29.15, 29.07, 28.97, 25.44, 22.40, 22.30, 21.38, 13.82, 13.71. **^{11}B NMR** (160 MHz, $CDCl_3$): δ = 0.04 (t, J_{B-F} = 25.3 Hz). **^{19}F NMR** (471 MHz, $CDCl_3$): δ = -122.66 – -122.81 (m), -123.72 – -123.86 (m), -146.06 (s, broad). **HRMS** (ESI-TOF): calcd for $C_{96}H_{89}BF_6KN_6O_6S_4$ $[M+K]^+$, 1713.5355; found 1713.5350.

BTT_{L6}-4Cl

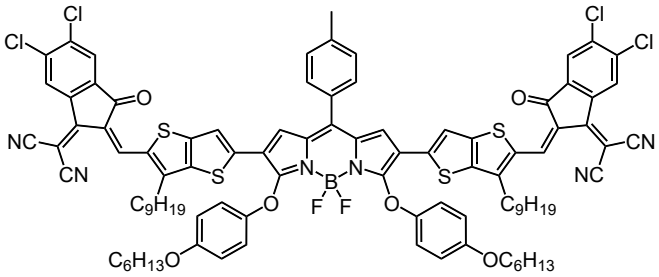

BTT_{L6}-4Cl was synthetized according to the **general procedure 3**. Starting from compound **9c** (170 mg, 0.136 mmol, 1.0 eq) and compound **3.14** (143 mg, 0.544 mmol, 4.0 eq). The reaction was heated for 24h. The desired product was obtained as a black powder (202 mg, 0.116 mmol, 85%). **^{1}H NMR** (400 MHz, $CDCl_3$): δ = 8.87 (s, 2H), 8.68 (s, 2H), 7.89 (s, 2H), 7.66 (d, J = 7.6 Hz, 2H), 7.54 (d, J = 7.8 Hz, 2H), 7.12 (s, 2H), 7.03 (s, 2H), 6.91 (d, J = 9.1 Hz, 4H), 6.76 (d, J = 9.1 Hz, 4H), 3.82 (t, J = 6.5 Hz, 4H), 2.96 (t, J = 8.2 Hz, 4H), 2.62 (s, 3H), 1.73 – 1.60 (m, 8H), 1.44 – 1.32 (m, 8H), 1.33 – 1.19 (m, 28H), 0.90 – 0.81 (m, 12H). **^{13}C NMR** (101 MHz, $C_2D_2Cl_4$, 80°C, Q-DEPT): δ = 185.37, 158.71, 158.57, 155.86, 152.29, 152.13, 150.07, 144.74, 143.77, 141.78, 140.65, 139.35, 139.12, 138.44, 135.99, 135.79, 134.59, 130.57, 129.57, 129.24, 128.96, 127.11, 126.56, 124.97, 120.48, 118.00, 117.23, 116.97, 115.77, 114.63, 114.26, 69.02, 68.76, 31.61, 31.33, 30.35, 29.84, 29.39, 29.16, 29.07 (2C), 28.97, 25.44, 22.40, 22.30, 21.40, 13.83, 13.71. **^{11}B NMR** (128 MHz, $C_2D_2Cl_4$, 80°C): δ = 0.22 (t, J = 26.1 Hz). **HRMS** (ESI-TOF): calcd for $C_{96}H_{89}BCl_4F_2N_6NaO_6S_4$ $[M+Na]^+$, 1761.4443; found 1761.4386.

BTT_{R8}

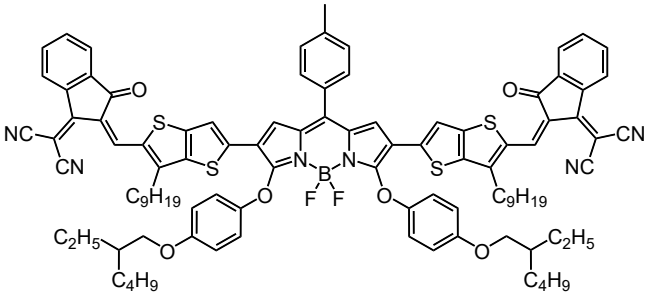

BTT_{R8} was synthetized according to the **general procedure 3**. Starting from compound **8** (160 mg, 0.122 mmol, 1.0 eq) and compound **9a** (95 mg, 0.49 mmol, 4.0 eq). The reaction was heated for 48h. The desired product was obtained as a black powder (153 mg, 0.092 mmol, 75%). **^{1}H NMR** (500 MHz, $CDCl_3$): δ = 8.76 (s, 2H), 8.56 (d, J = 7.0 Hz, 2H), 7.90 – 7.84 (m, 2H), 7.74 – 7.66 (m, 6H), 7.56 (d, J = 7.7 Hz, 2H), 7.12 (s, 2H), 6.94 (s, 2H), 6.89 (d, J = 9.2 Hz, 4H), 6.75 (d, J = 9.2 Hz, 4H), 3.74 – 3.66 (m, 4H), 2.92 (t, J = 8.0 Hz, 4H), 2.64 (s, 3H), 1.70 – 1.59 (m, 6H), 1.46 – 1.33 (m, 10H), 1.32 – 1.21(m, 30H), 0.90 – 0.80 (m, 18H). **^{13}C NMR** (126 MHz, $CDCl_3$, APT): δ = 188.21, 160.81, 158.32, 156.00, 151.72, 151.27, 150.22, 143.82, 143.78, 142.13, 140.18, 139.94, 136.99, 135.08, 134.94, 134.63, 134.50, 131.15, 129.95, 129.63, 129.06, 126.86, 125.16, 123.84, 121.25, 117.74, 117.22, 116.89, 115.69, 115.28, 114.95, 71.06, 68.65, 39.49, 32.00, 30.73, 30.58, 30.10, 29.79, 29.59, 29.57, 29.43, 29.18, 23.90, 23.14, 22.82, 21.84, 14.27, 14.18, 11.21. **^{11}B NMR** (160 MHz, $CDCl_3$): δ = 0.04 (t, J = 27.5 Hz). **^{19}F NMR** (471 MHz, $CDCl_3$): δ = -146.01 (s, broad). **HRMS** (ESI-TOF): calcd for $C_{100}H_{101}BF_2KN_6O_6S_4$ $[M+K]^+$, 1697.6358; found 1697.6389.

BTT_{R8}-4F

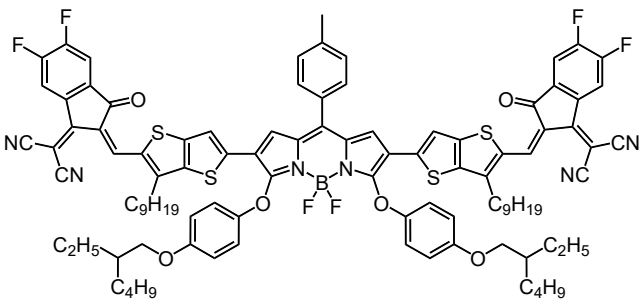

BTT_{R8}-4F was synthetized according to the **general procedure 3.2**. Starting from compound **8** (200 mg, 0.153 mmol, 1.0 eq) and compound **9b** (141 mg, 0.612 mmol, 4.0 eq). The reaction was heated for 24h. The desired product was obtained as a black powder. (221 mg, 0.128 mmol, 83%). **^{1}H NMR** (500 MHz,

$CDCl_3$): δ = 8.83 (s, 2H), 8.44 (dd, J = 9.9, 6.4 Hz, 2H), 7.67 (d, J = 7.6 Hz, 2H), 7.63 (t, J = 7.5 Hz, 2H), 7.54 (d, J = 7.6 Hz, 2H), 7.11 (s, 2H), 7.02 (s, 2H), 6.90 (d, J = 9.2 Hz, 4H), 6.76 (d, J = 9.2 Hz, 4H), 3.75 – 3.65 (m, 4H), 2.95 (t, J = 7.9 Hz, 4H), 1.71 – 1.58 (m, 6H), 1.43 – 1.33 (m, 10H), 1.31 – 1.22 (m, 30H), 0.91 – 0.81 (m, 18H). **^{13}C NMR** (126 MHz, $CDCl_3$, APT): δ =185.88, 158.50, 158.24, 156.01, 155.65, 155.62, 155.54, 155.51, 153.55, 153.44, 152.37, 152.05, 150.15, 144.54, 143.83, 142.37, 140.34, 136.48, 134.77, 134.59, 134.57, 134.54, 134.52, 130.01, 129.48, 129.10, 126.77, 120.19, 117.68, 117.11, 116.79, 115.69, 114.89 (d, $^3J_{F-C}$ = 22.1 Hz), 114.77, 114.71, 114.50, 112.65 (d, $^3J_{F-C}$ = 18.6 Hz), 71.02, 69.13, 39.46, 31.99, 30.76, 30.56, 30.17, 29.79, 29.57, 29.54, 29.42, 29.16, 23.87, 23.13, 22.81, 21.87, 14.27, 14.18, 11.20. **^{11}B NMR** (160 MHz, $CDCl_3$): δ = 0.05 (t, J = 22.5 Hz). **^{19}F NMR** (471 MHz, $CDCl_3$): δ = 122.62 – -122.91 (m), -123.61 – -124.12 (m), -146.10 (s, broad). **HRMS** (ESI-TOF): calcd for $C_{100}H_{97}BF_6N_6O_6S_4$ $[M]^+$, 1730.6344; found 1730.6348.

BTT_{R8}-4Cl

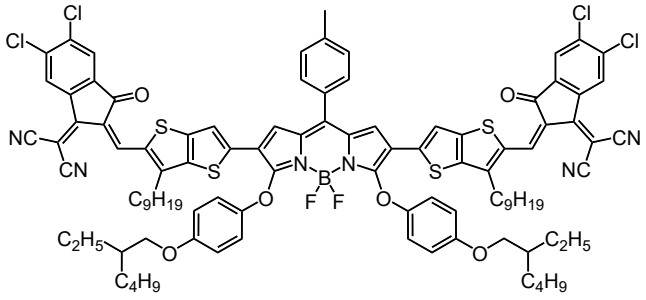

BTT_{R8}-4Cl was synthetized according to the **general procedure 3**. Starting from compound **8** (200 mg, 0.153 mmol, 1.0 eq) and compound **9c** (161 mg, 0.612 mmol, 4.0 eq). The reaction was heated for 24h. The desired product was obtained as a black powder (230 mg, 0.128 mmol, 84%). **^{1}H NMR** (400 MHz, $CDCl_3$): δ = 8.75 (s, 2H), 8.62 (s, 2H), 7.86 (s, 2H), 7.74 (d, J = 7.7 Hz, 2H), 7.58 (d, J = 7.7 Hz, 2H), 7.13 (s, 2H), 6.94 (s, 2H), 6.86 (d, J = 9.2 Hz, 4H), 6.75 (d, J = 9.2 Hz, 4H), 3.70 (d, J = 5.9 Hz, 4H), 2.92 (t, J = 8.0 Hz, 4H), 2.66 (s, 3H), 1.68 – 1.58 (m, 6H), 1.44 – 1.31 (m, 10H), 1.30 – 1.21 (m, 30H), 0.91 – 0.80 (m, 18H). **^{13}C NMR** (126 MHz, $CDCl_3$): δ = 185.95, 158.44, 158.33, 156.06, 152.73, 152.30, 150.18, 144.83, 143.92, 142.38, 140.49, 139.72, 139.52, 138.61, 136.12, 135.36, 134.80, 131.27, 130.02, 129.51, 129.14, 126.92, 126.81, 125.23, 120.20, 117.70, 117.16, 116.86, 115.72, 114.90, 114.56, 71.08, 69.31, 39.49, 32.00, 30.77, 30.58, 30.24, 29.82, 29.59, 29.55, 29.43, 29.18, 23.90, 23.14, 22.82, 21.87, 14.27, 14.18, 11.21. **^{11}B NMR** (160 MHz, $C_2D_2Cl_4$) δ = 0.02 (t, J_{B-F} = 27.4 Hz).**^{19}F NMR** (471 MHz, $CDCl_3$): δ = -145.85 (s, broad). **HRMS** (ESI-TOF): calcd for $C_{100}H_{97}BCl_4F_2N_6NaO_6S_4$ $[M+Na]^+$, 1817.5060; found 1817.5021.

NMR and mass spectra of synthesized compounds

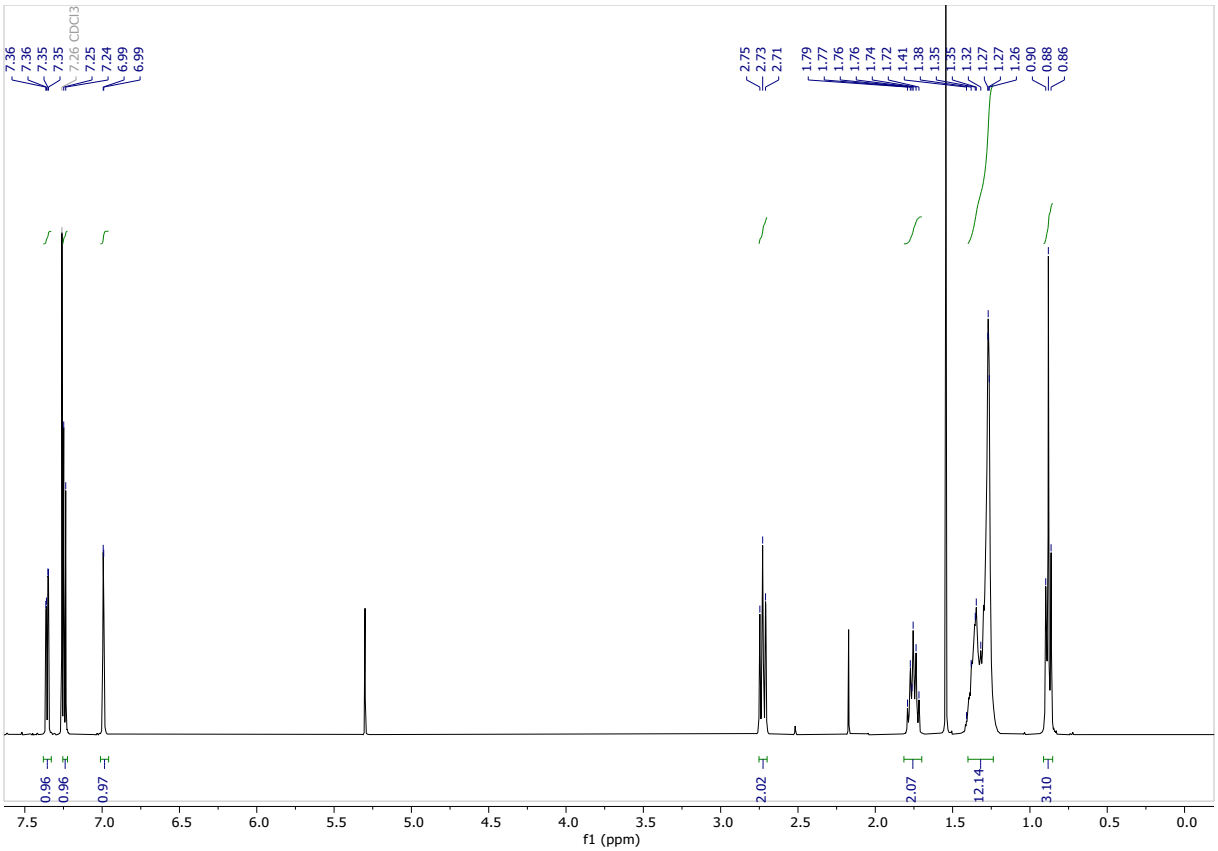

Figure S2. [1]H NMR of compound **D**

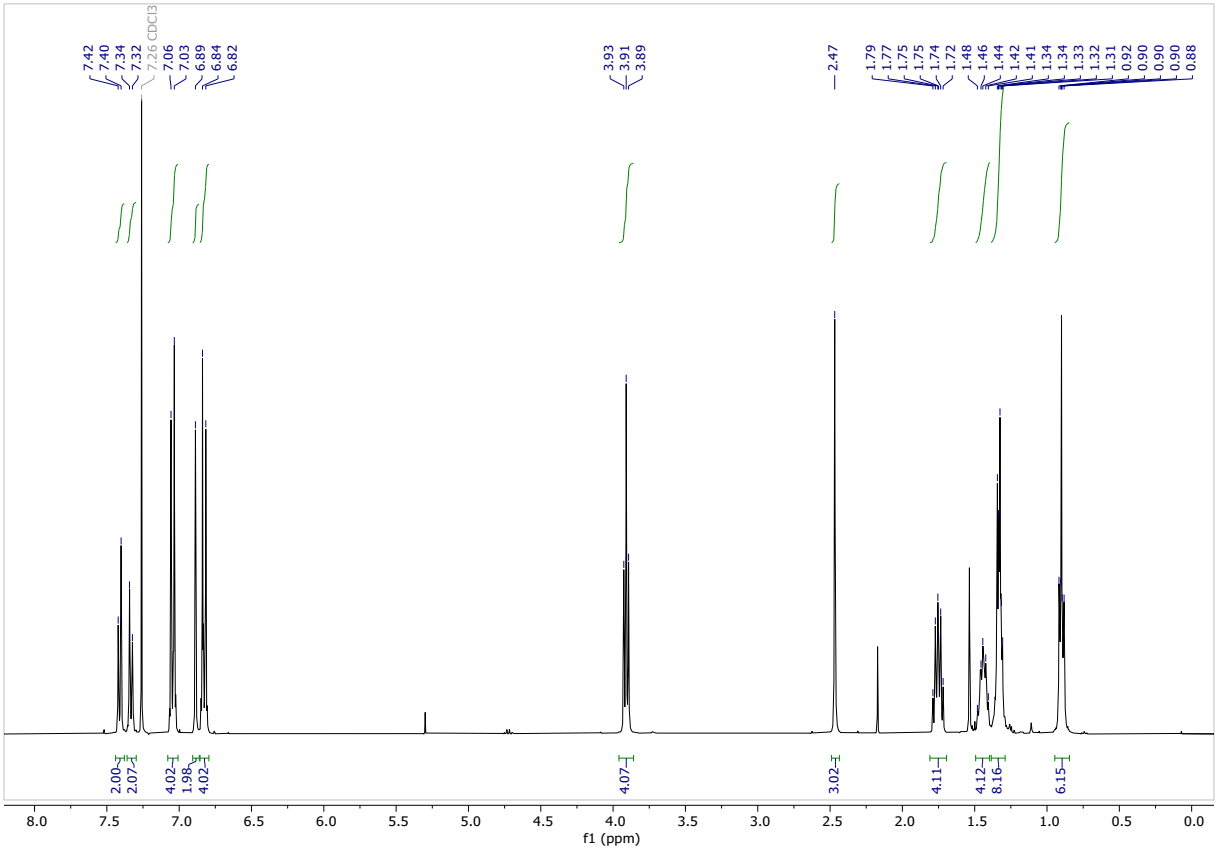

Figure S3. [1]H NMR of compound **2**

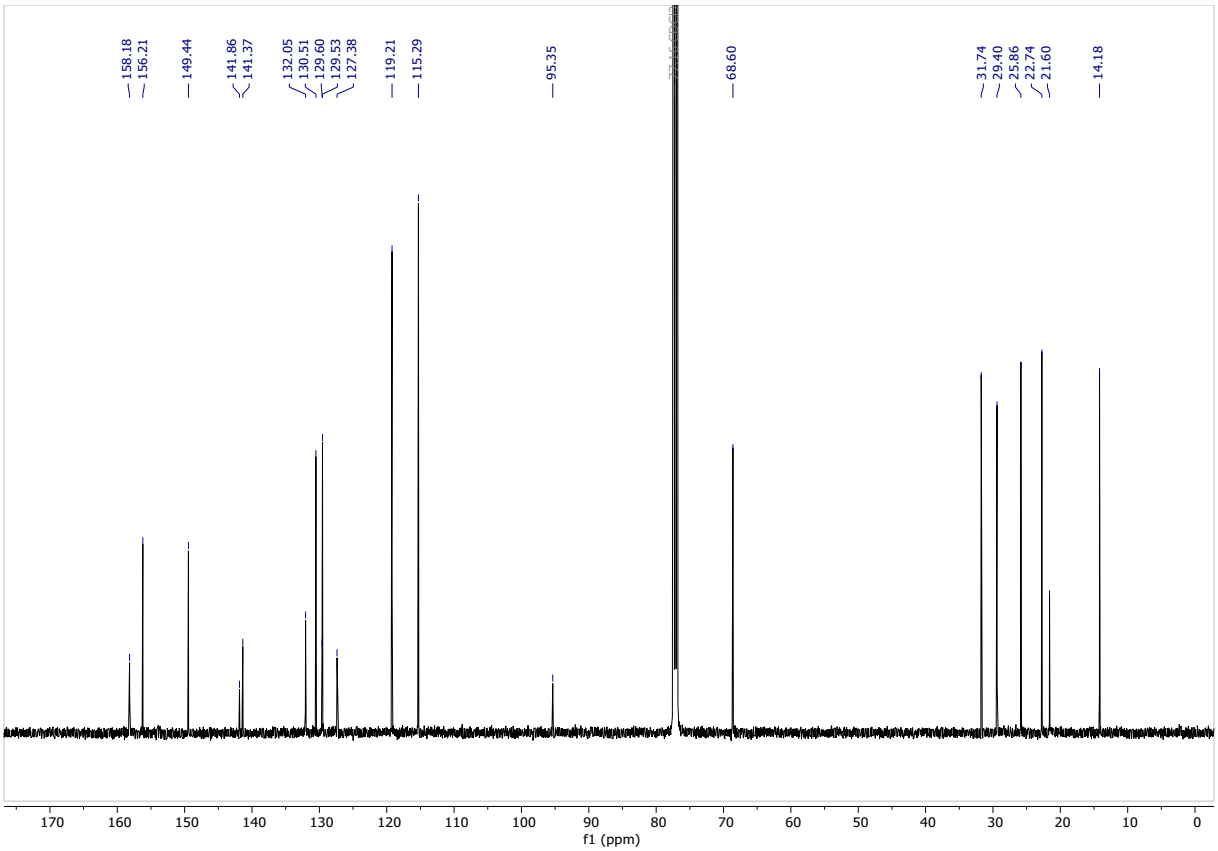

Figure S4. ^{13}C NMR of compound **2**

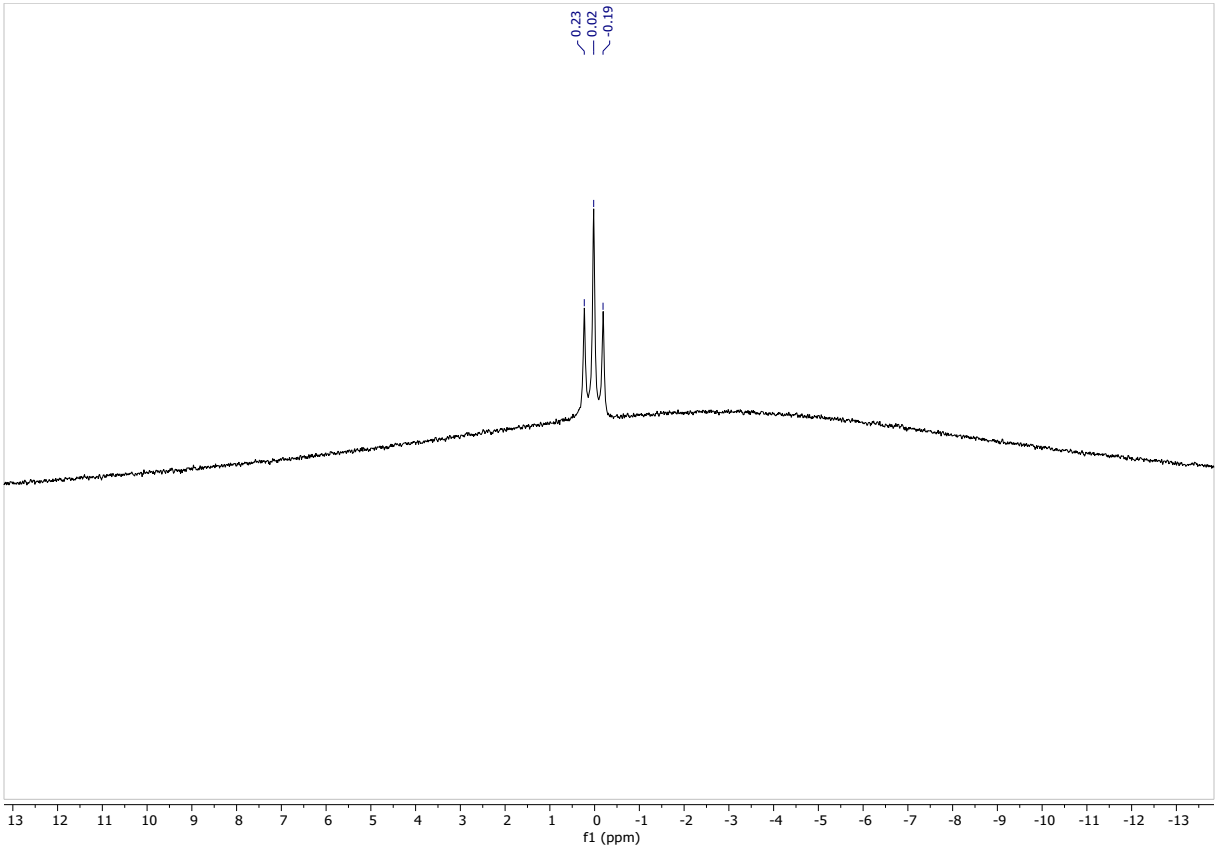

Figure S5. ^{11}B NMR of compound **2**

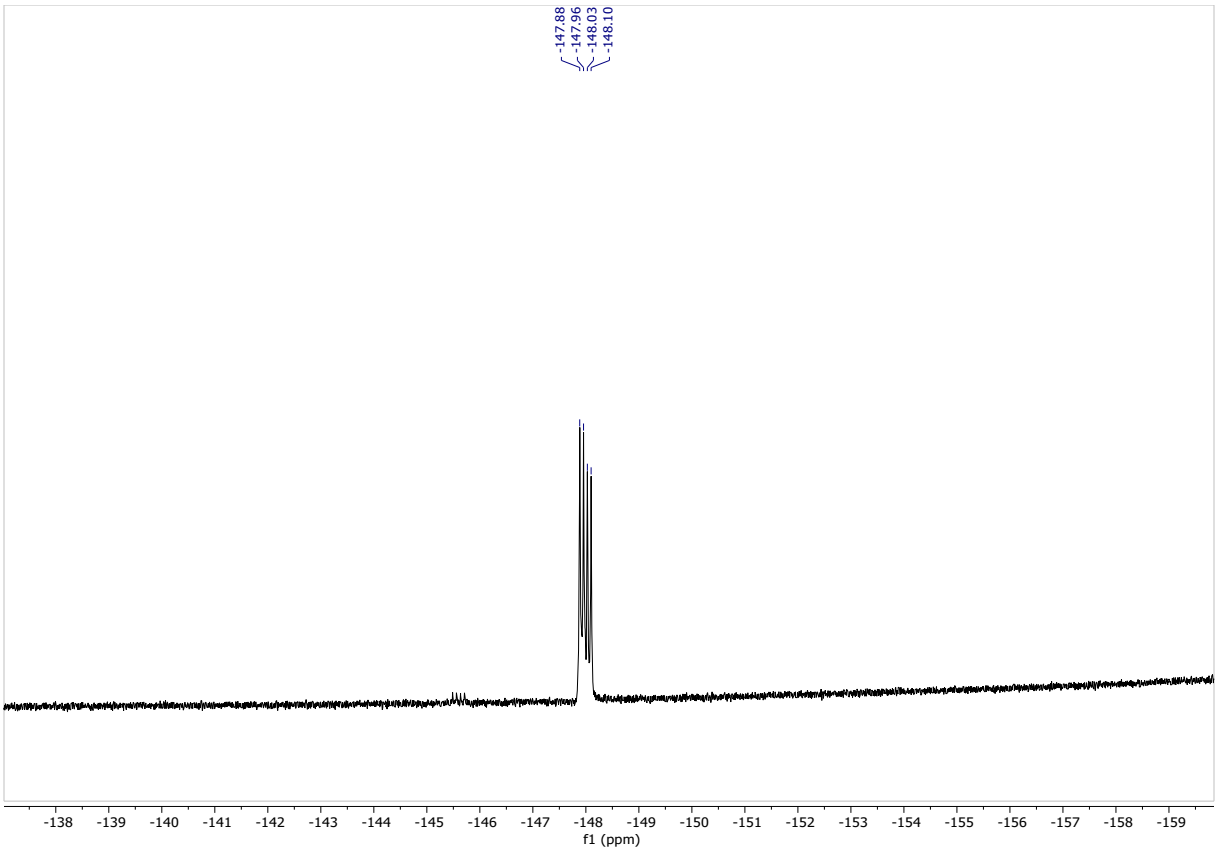

Figure S6. ^{19}F NMR of compound **2**

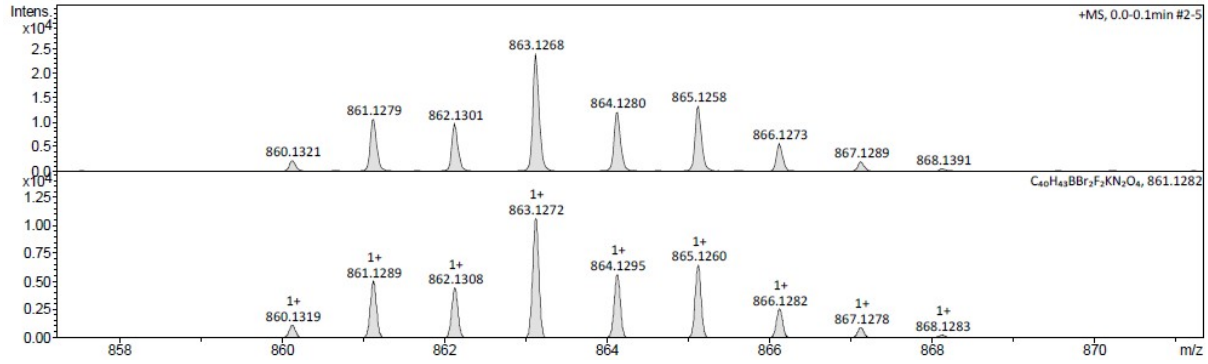

Figure S7. HRMS of compound **2**

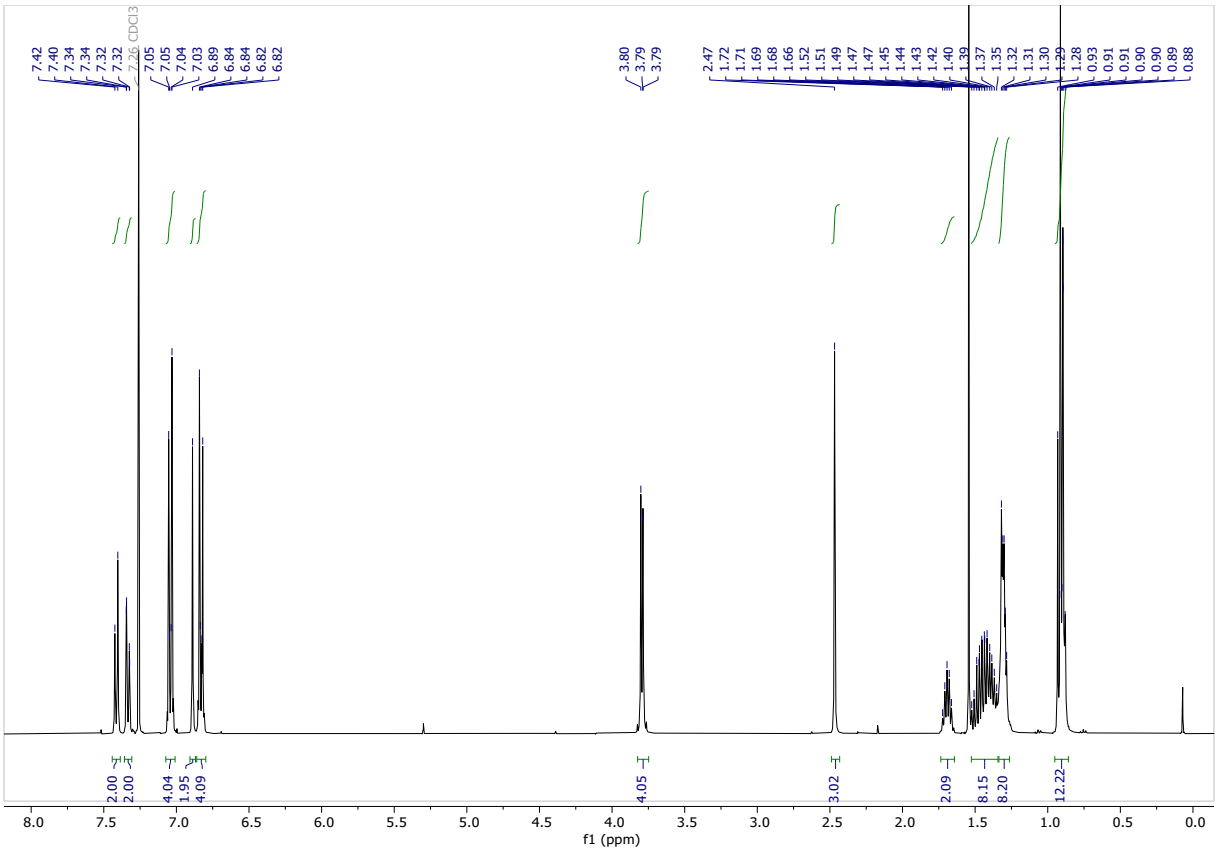

Figure S8. ^{1}H NMR of compound **3**

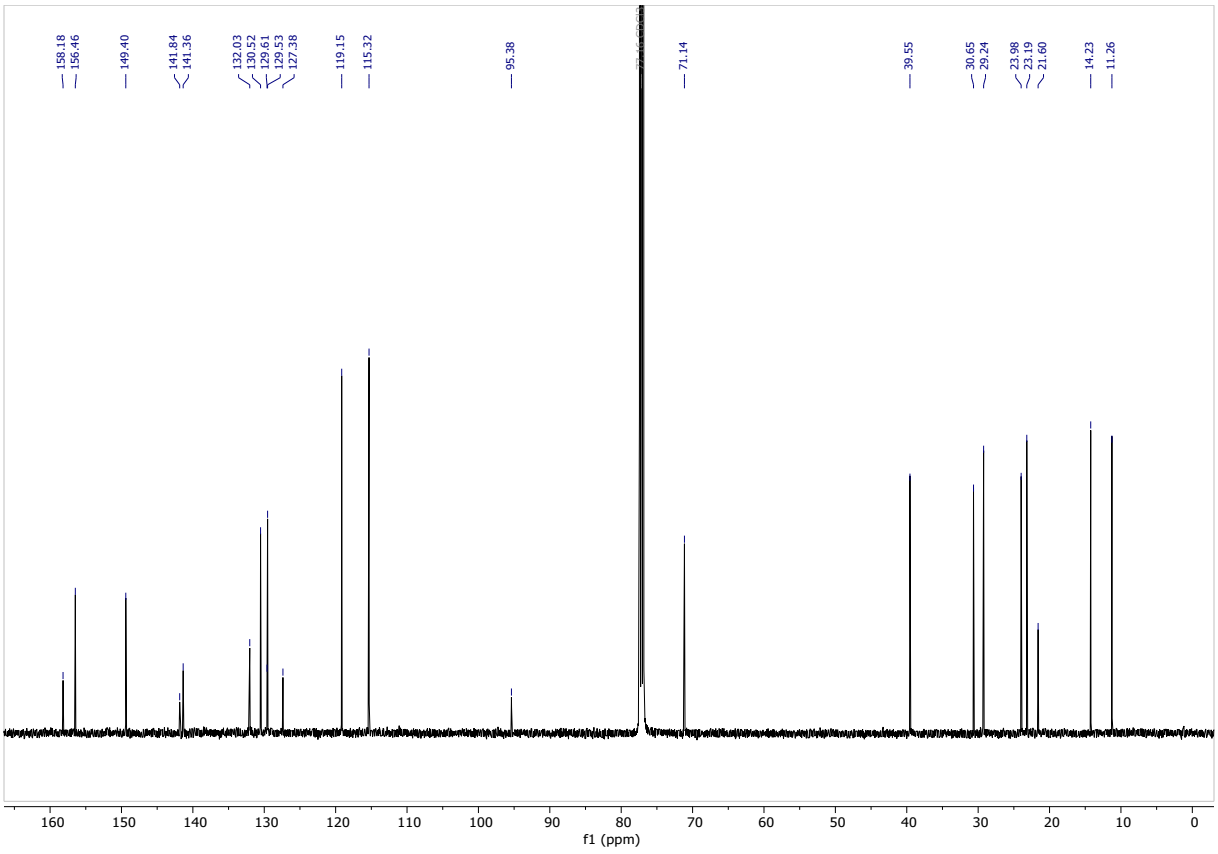

Figure S9. ^{13}C NMR of compound **3**

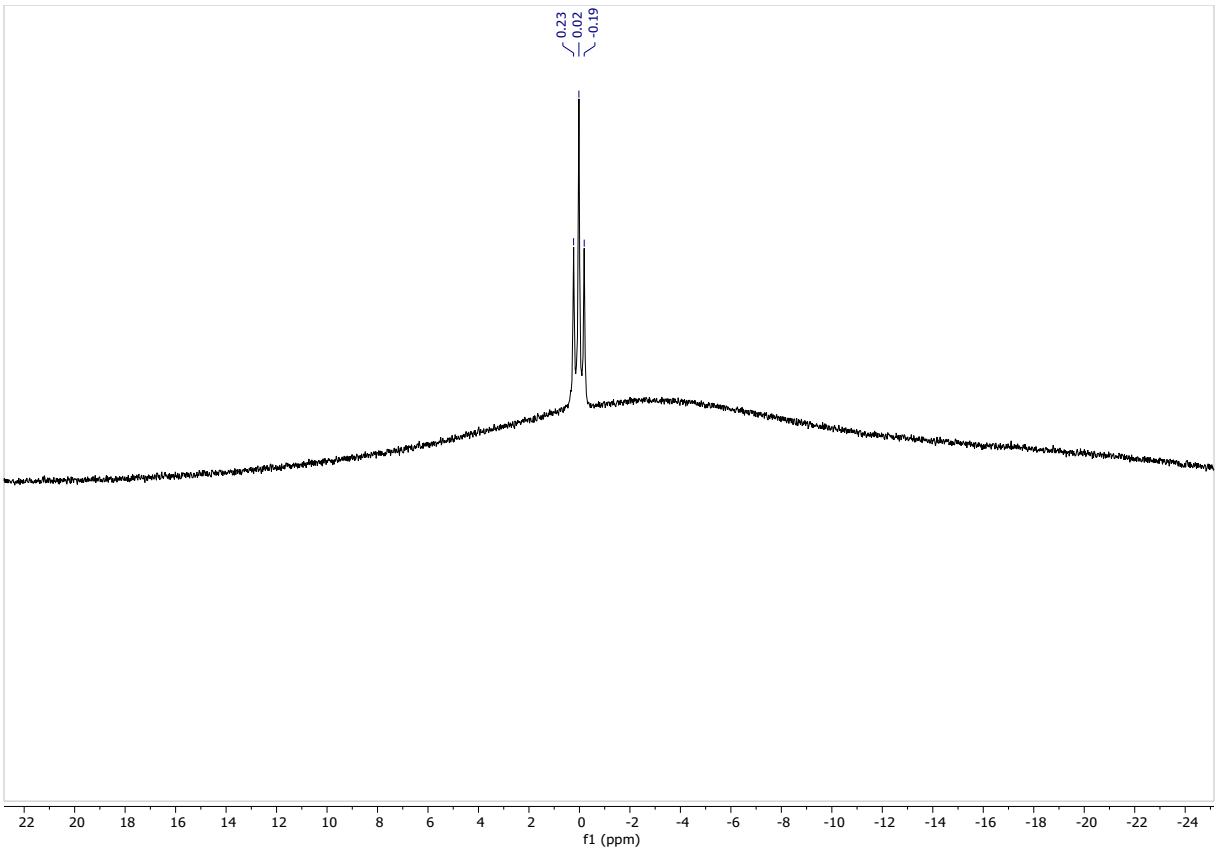

Figure S10. ^{11}B NMR of compound **3**

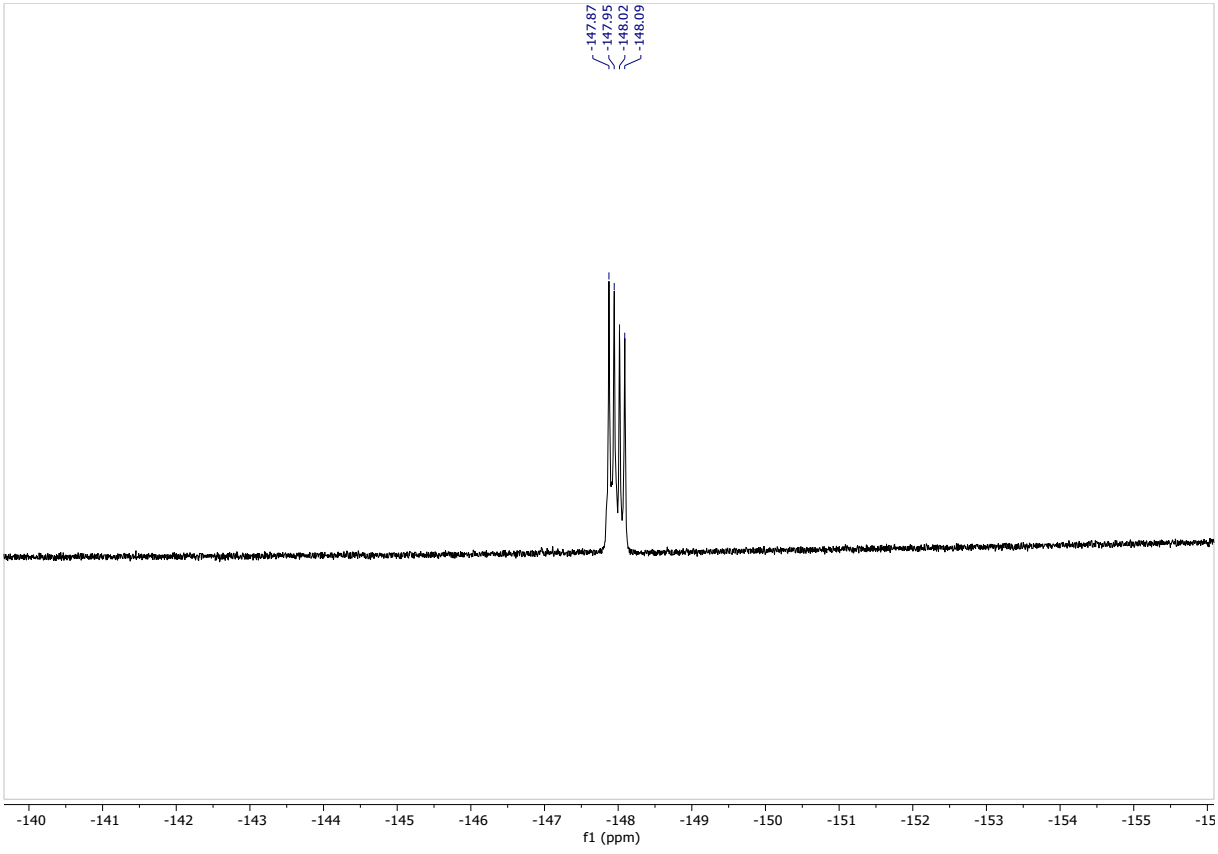

Figure S11. ^{19}F NMR of compound **3**

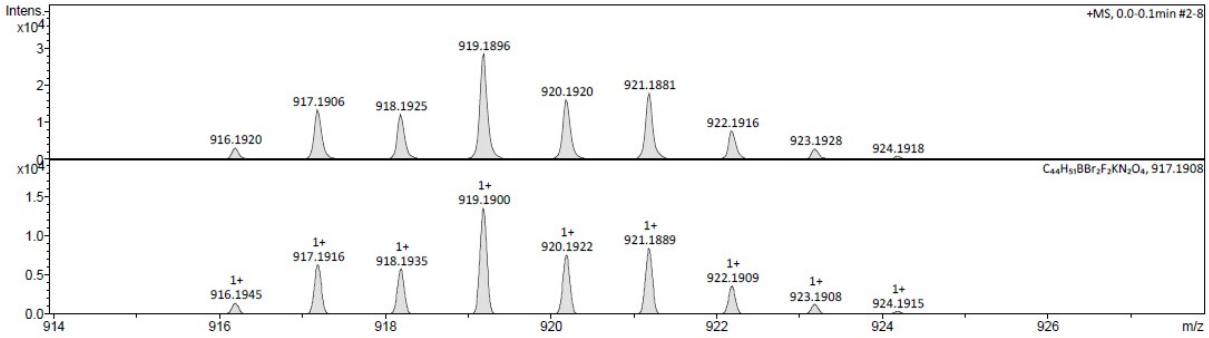

Figure S12. HRMS of compound **3**

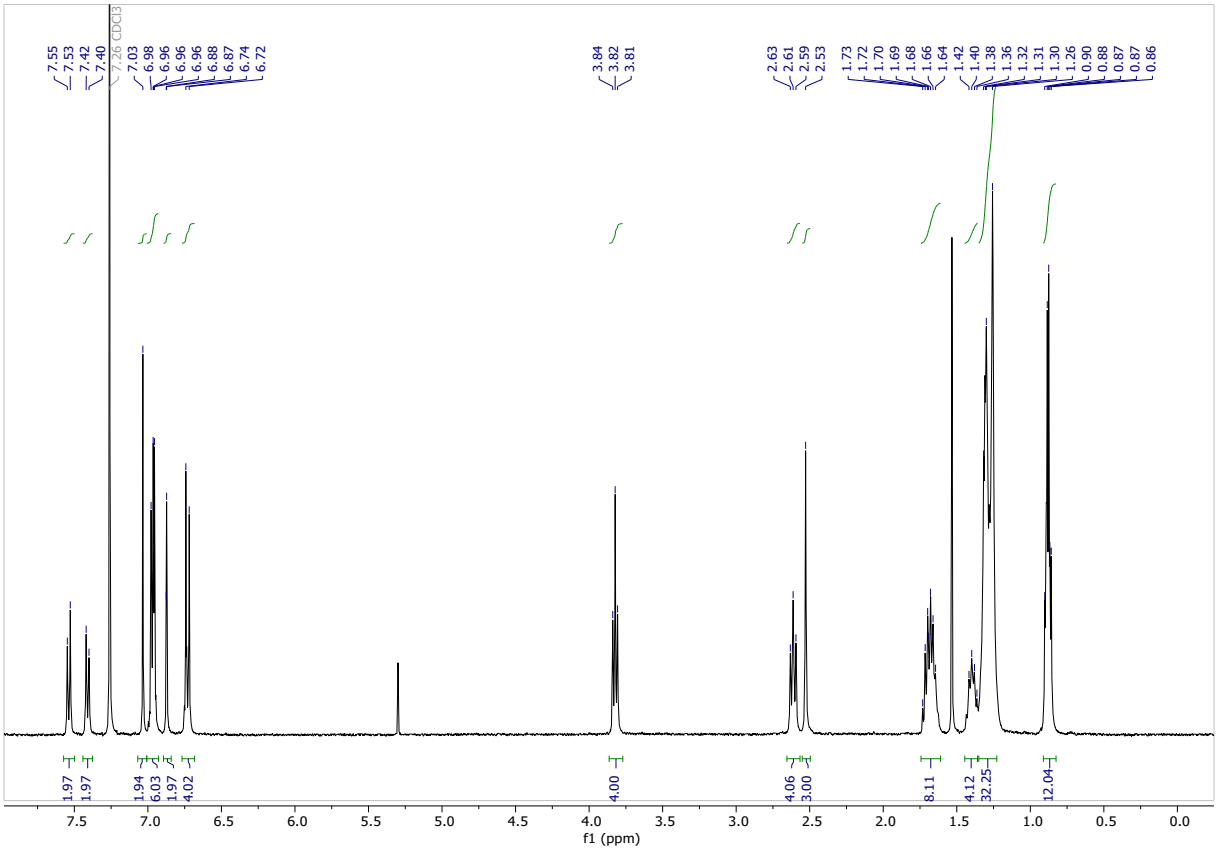

Figure S13. ^{1}H NMR of compound **5**

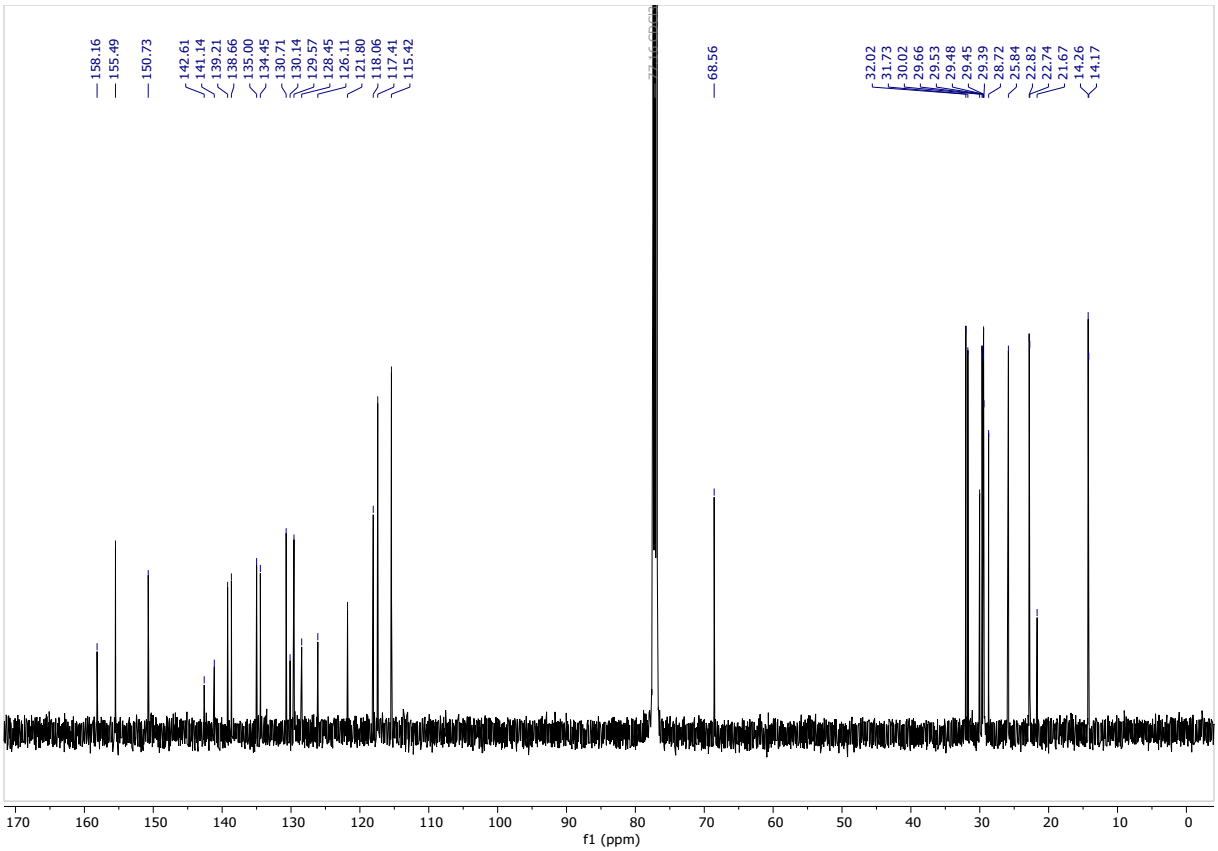

Figure S14. ^{13}C NMR of compound **5**

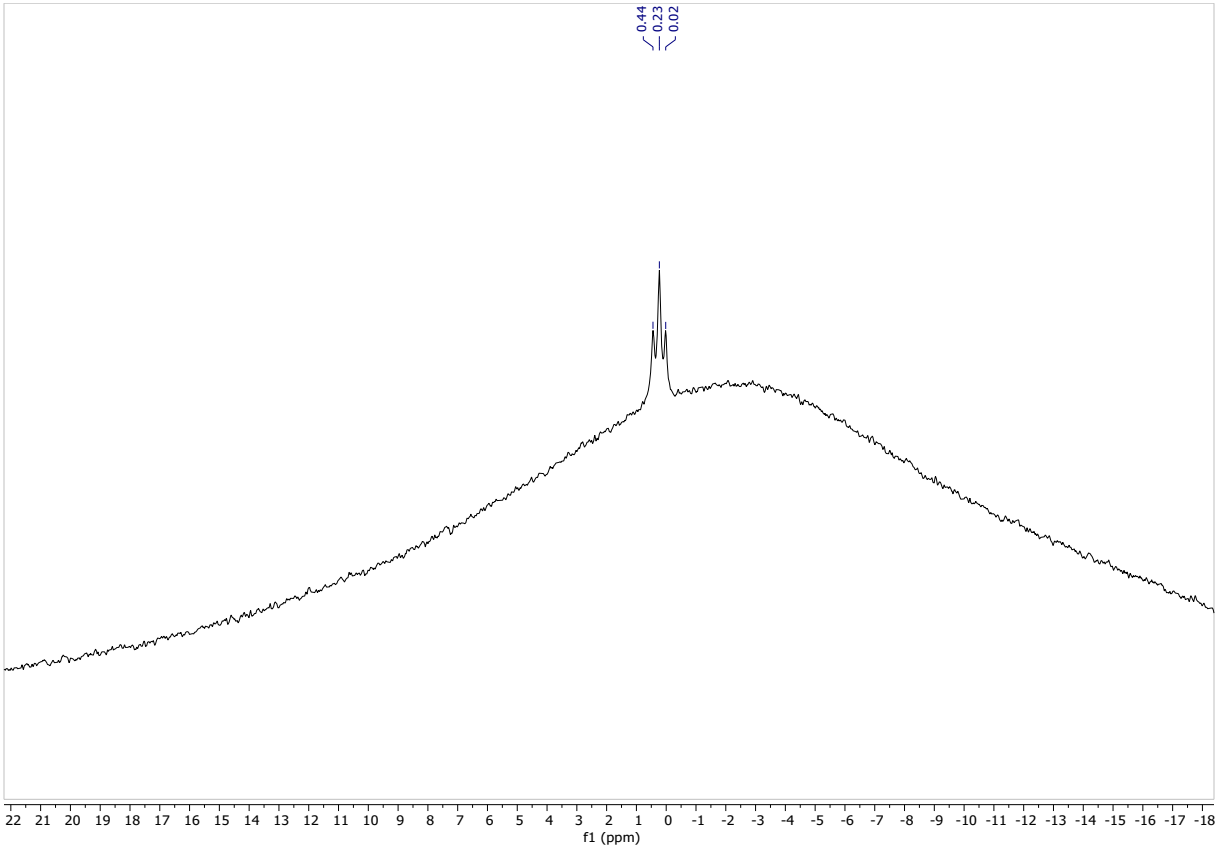

Figure S15. ^{11}B NMR of compound **5**

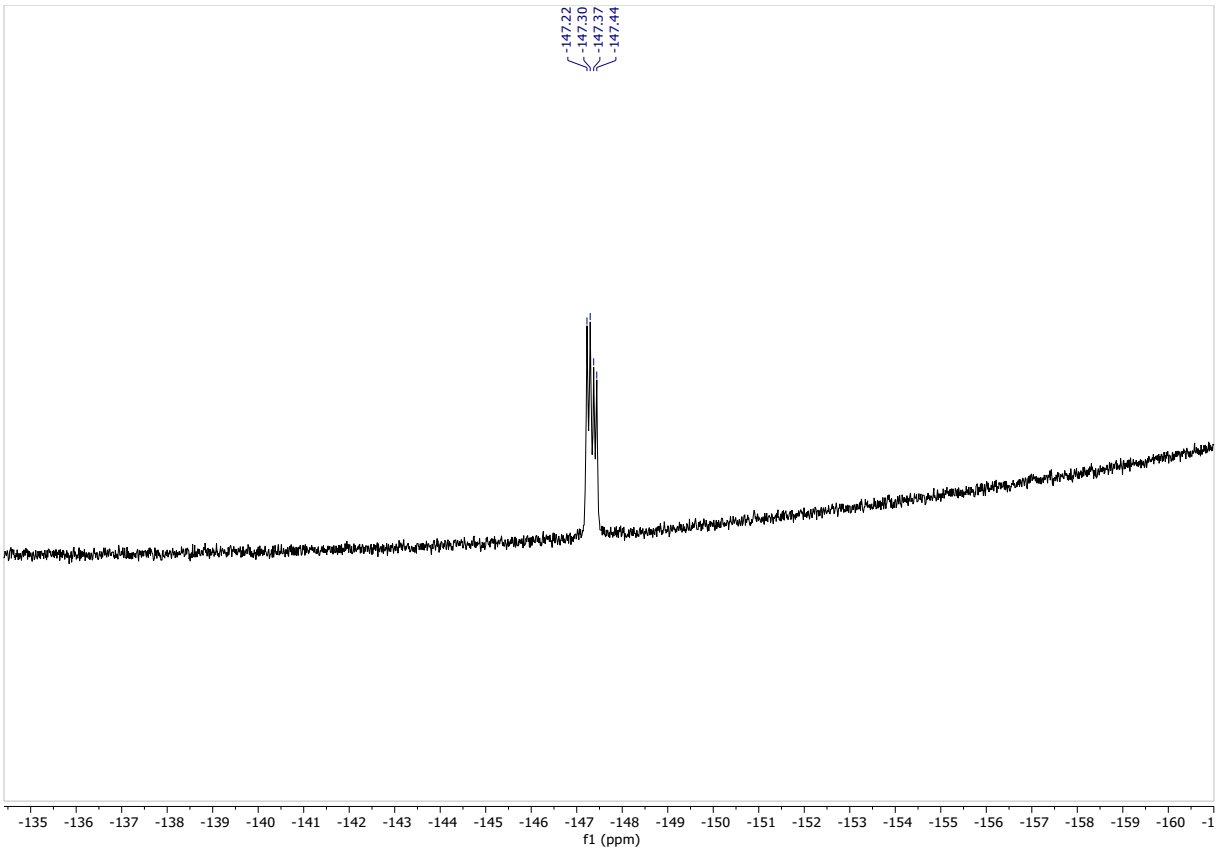

Figure S16. ^{19}F NMR of compound **5**

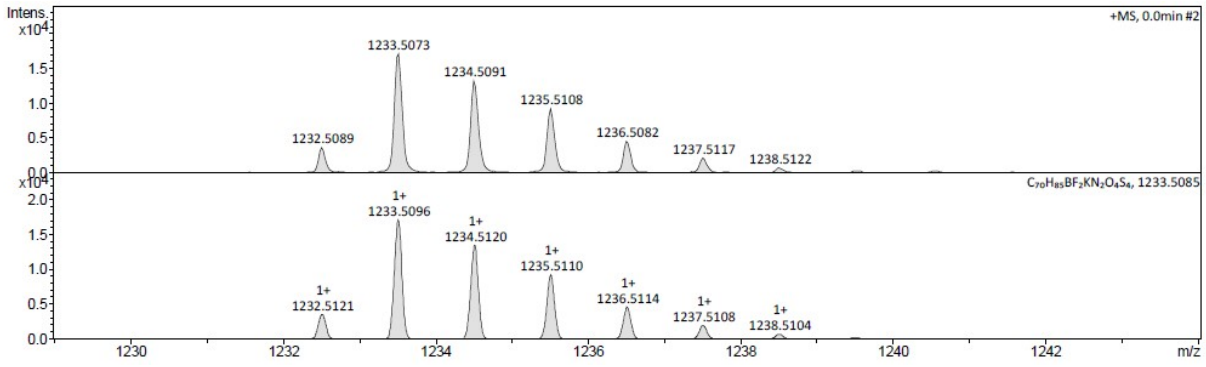

Figure S17. HRMS of compound **5**

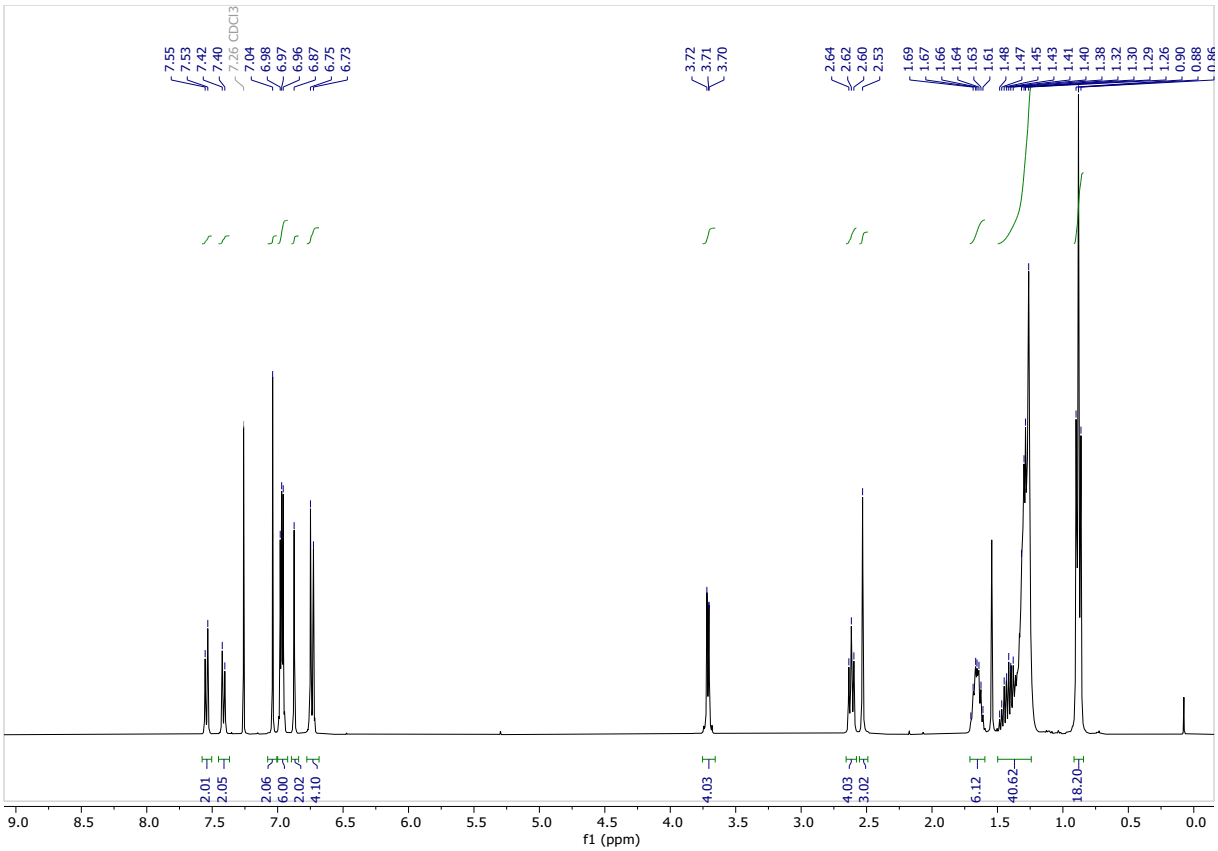

Figure S18. ^{1}H NMR of compound **6**

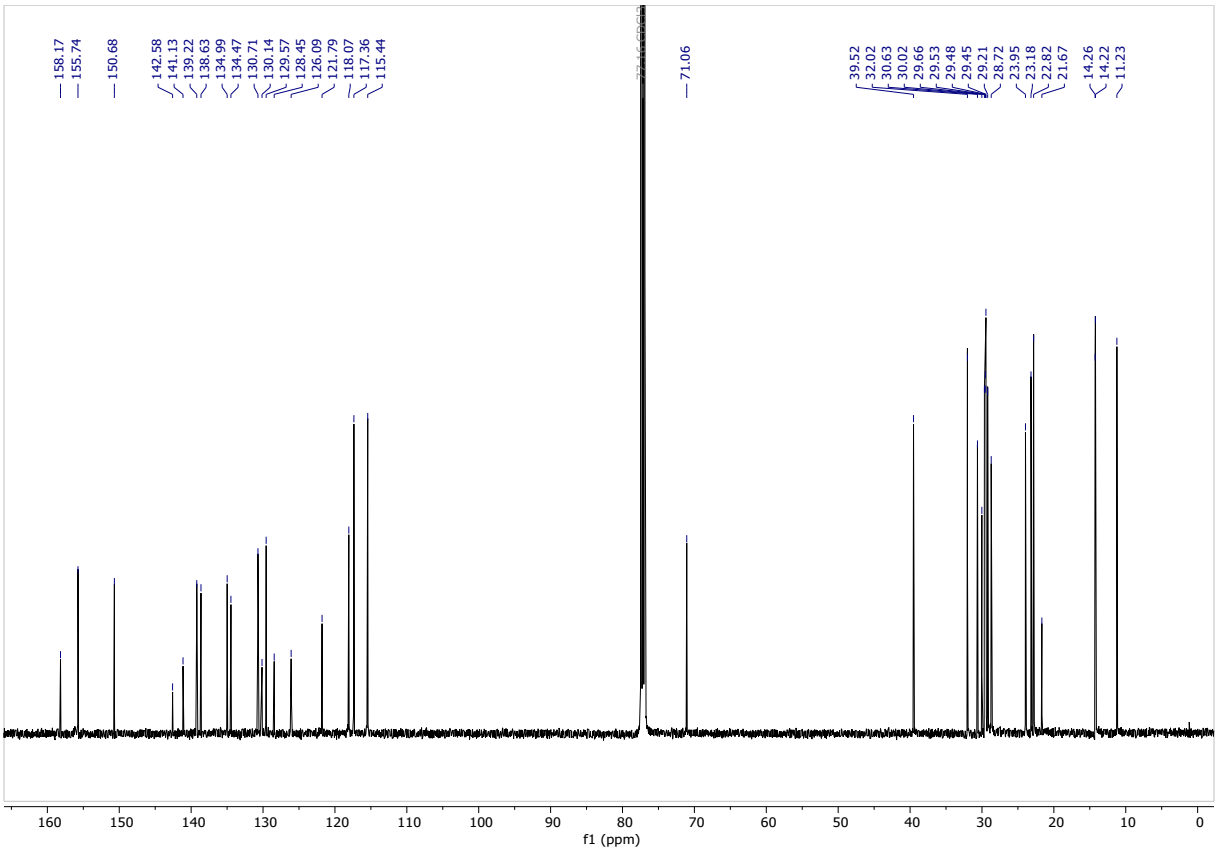

Figure S19. ^{13}C NMR of compound **6**

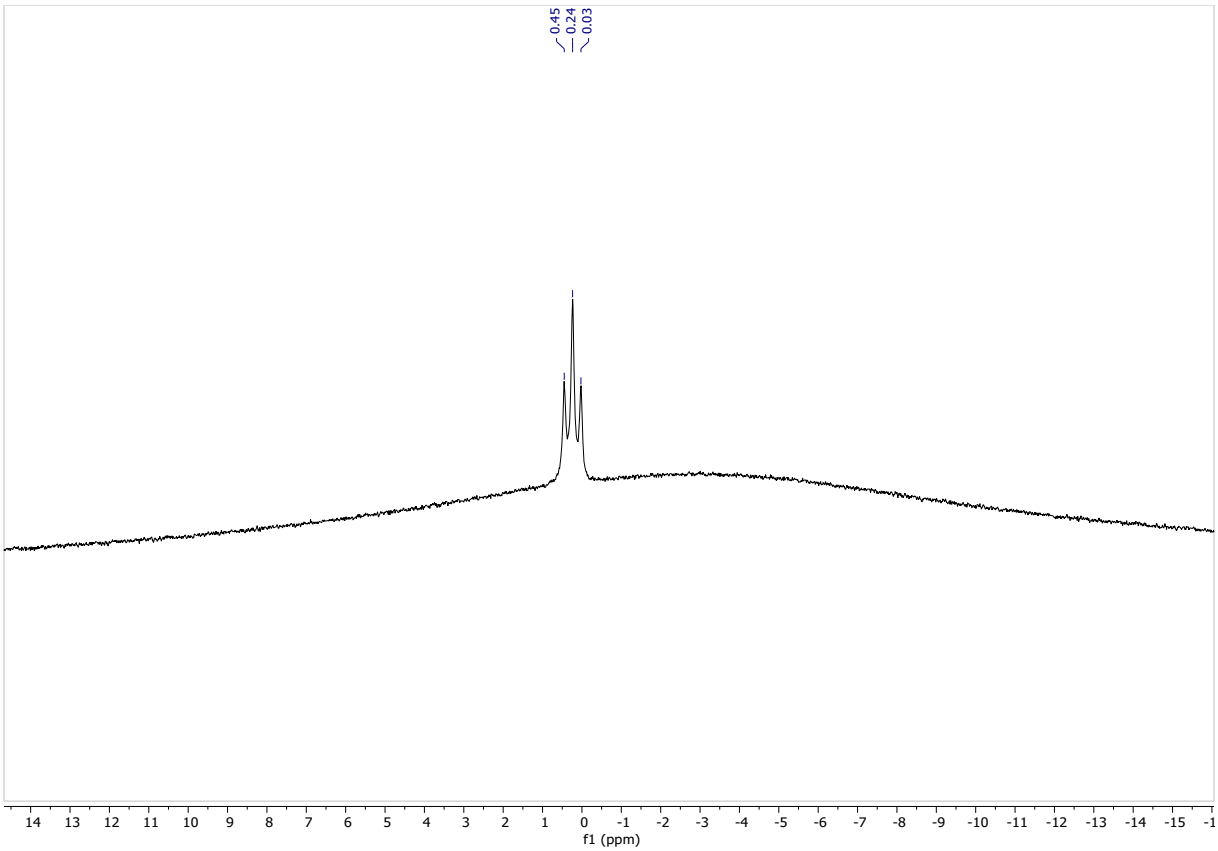

Figure S20. ^{11}B NMR of compound **6**

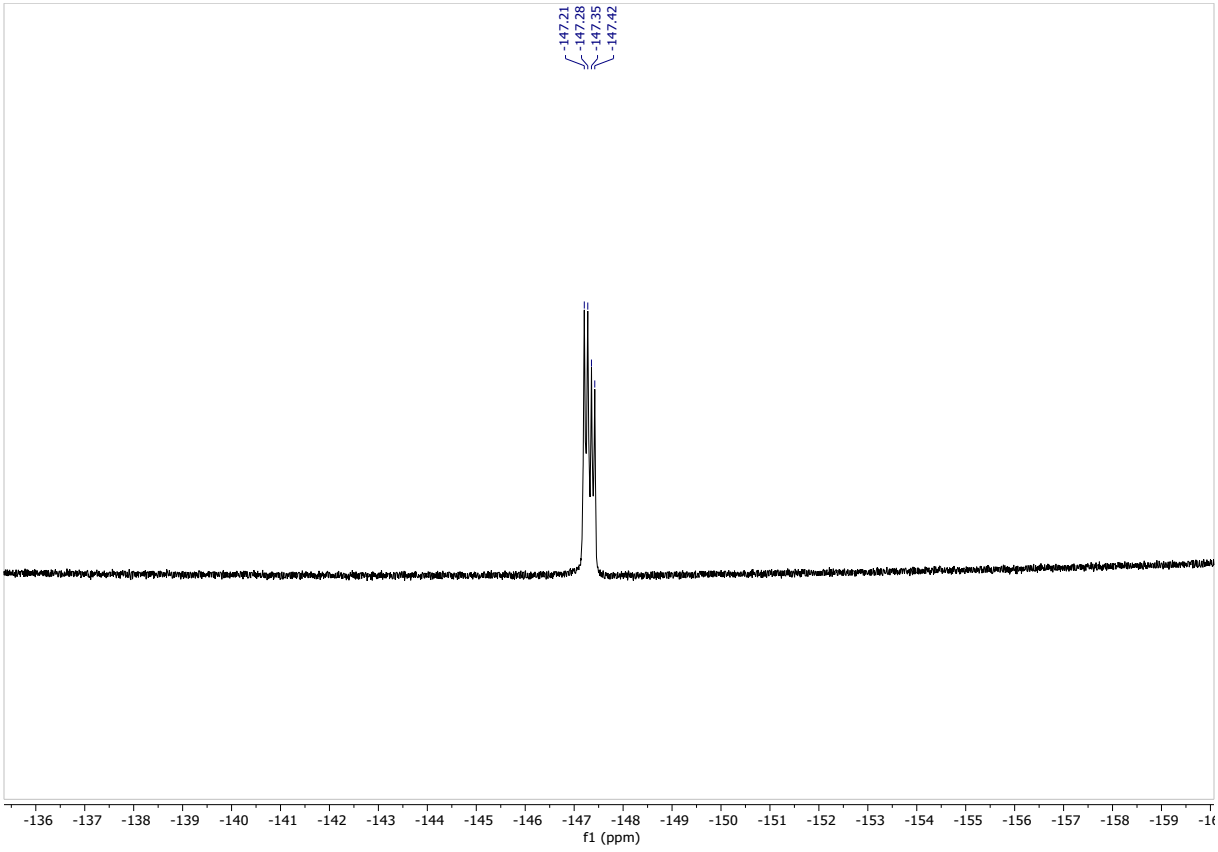

Figure S21. ^{19}F NMR of compound **6**

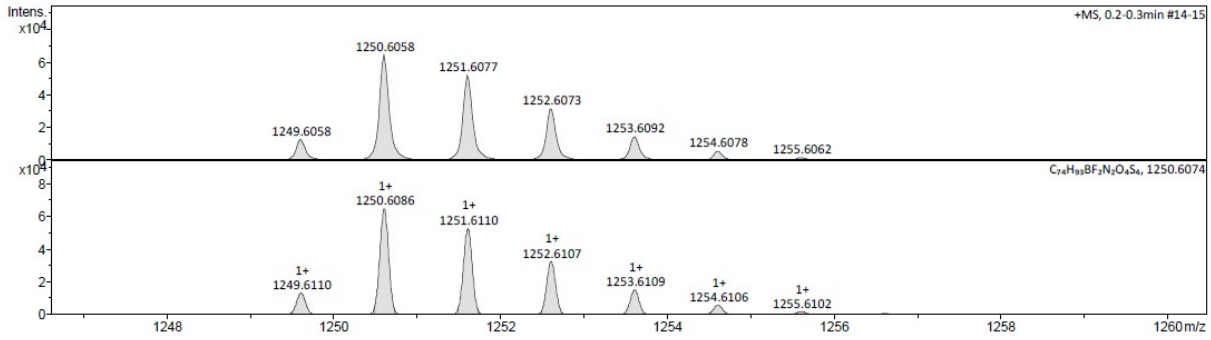

Figure S22. HRMS of compound **6**

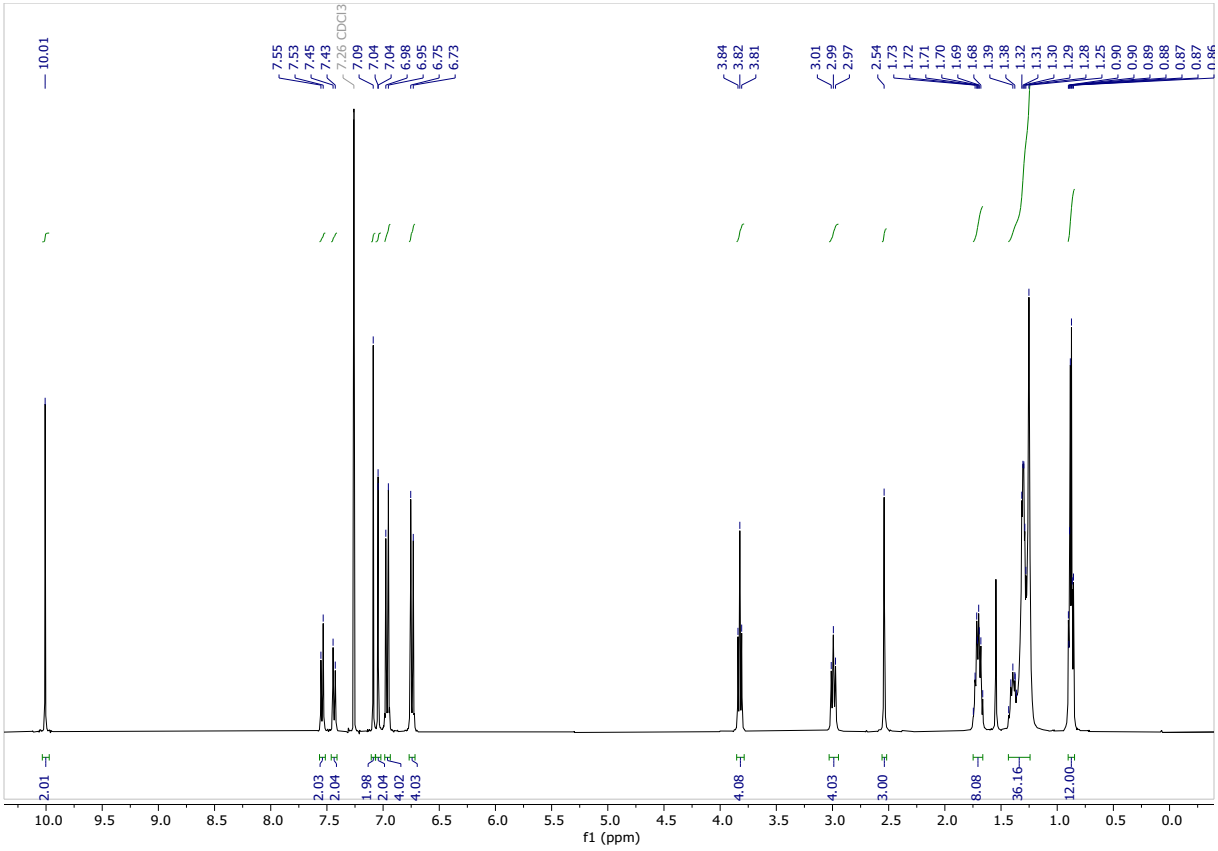

Figure S23. ^{1}H NMR of compound **7**

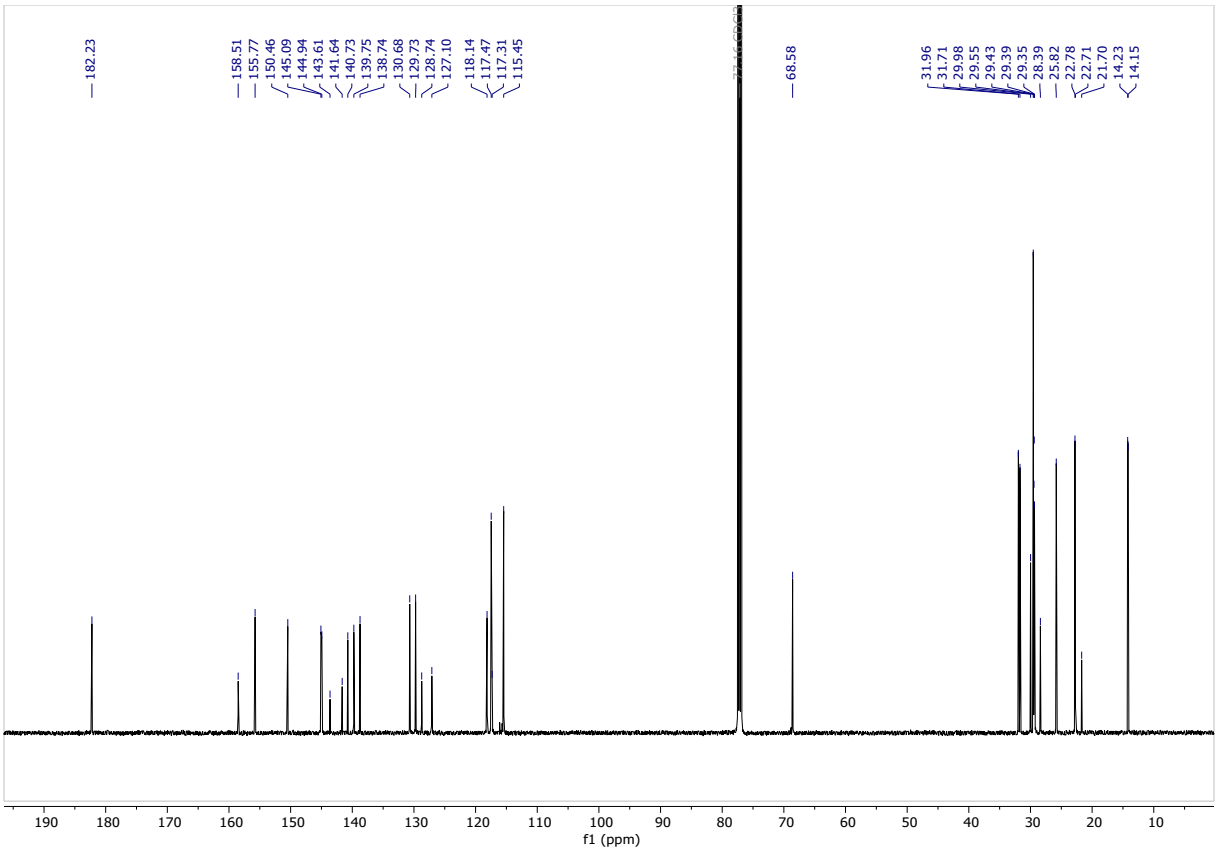

Figure S24. ^{13}C NMR of compound **7**

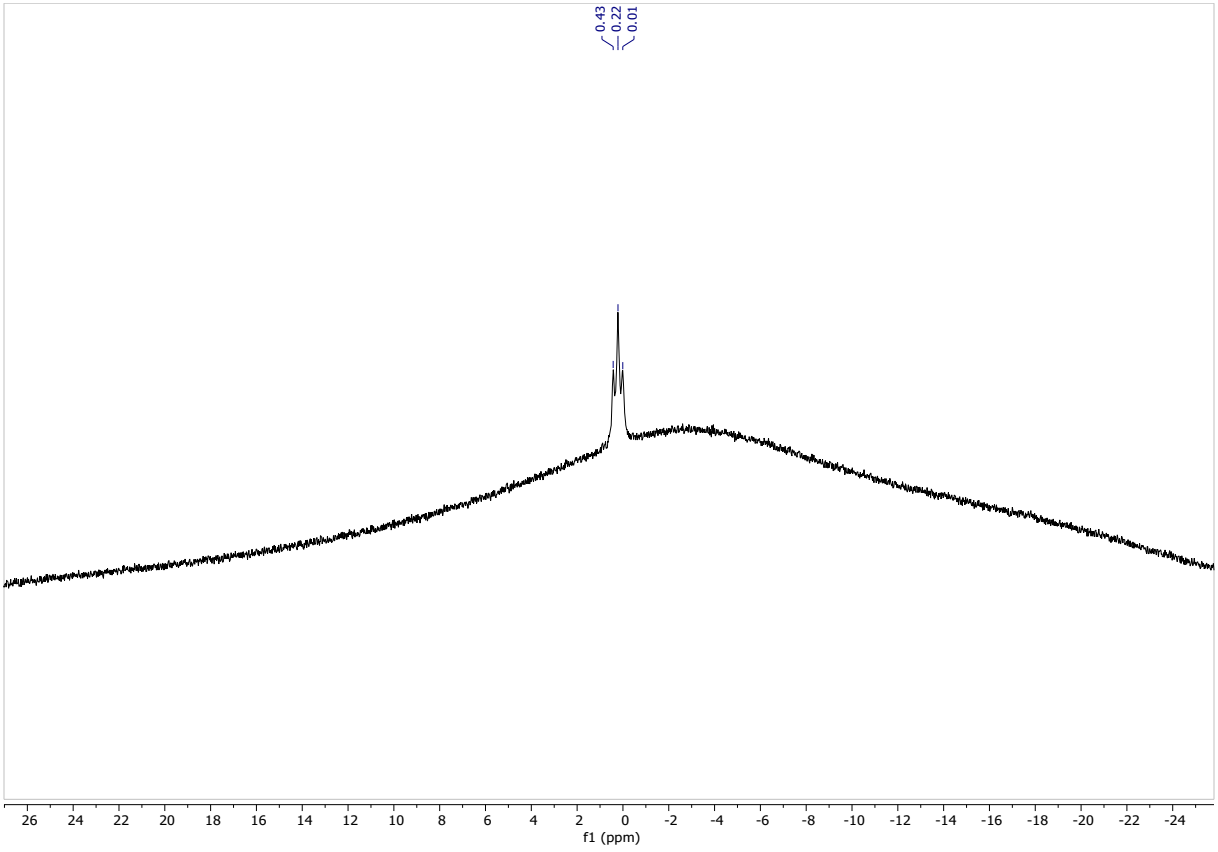

Figure S25. ^{11}B NMR of compound **7**

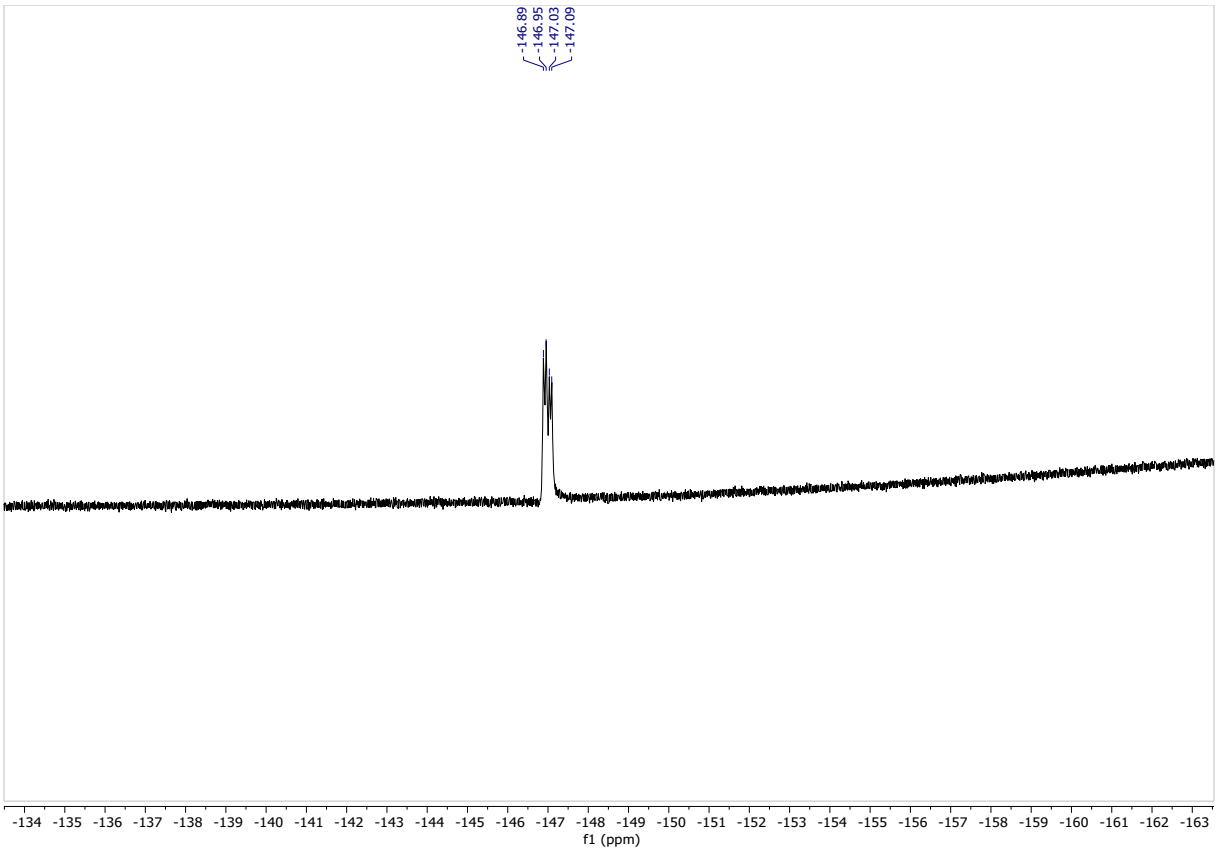

Figure S26. ^{19}F NMR of compound **7**

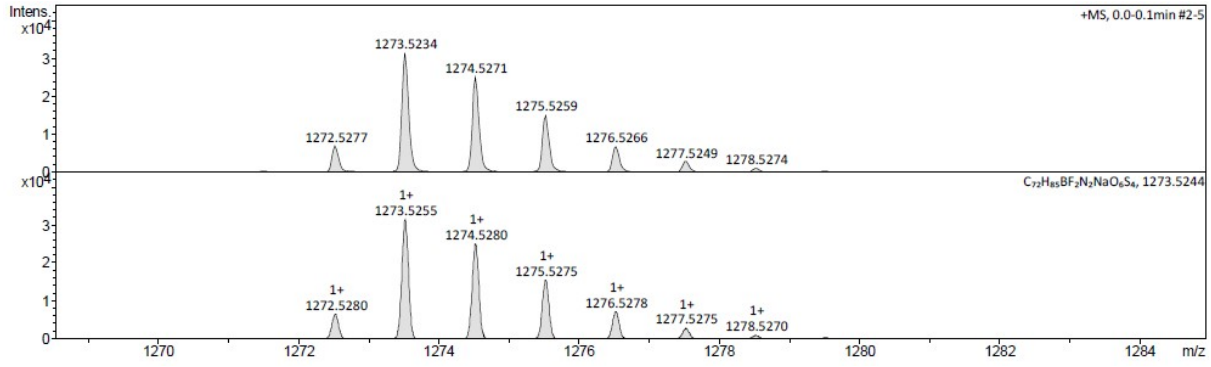

Figure S27. HRMS of compound **7**

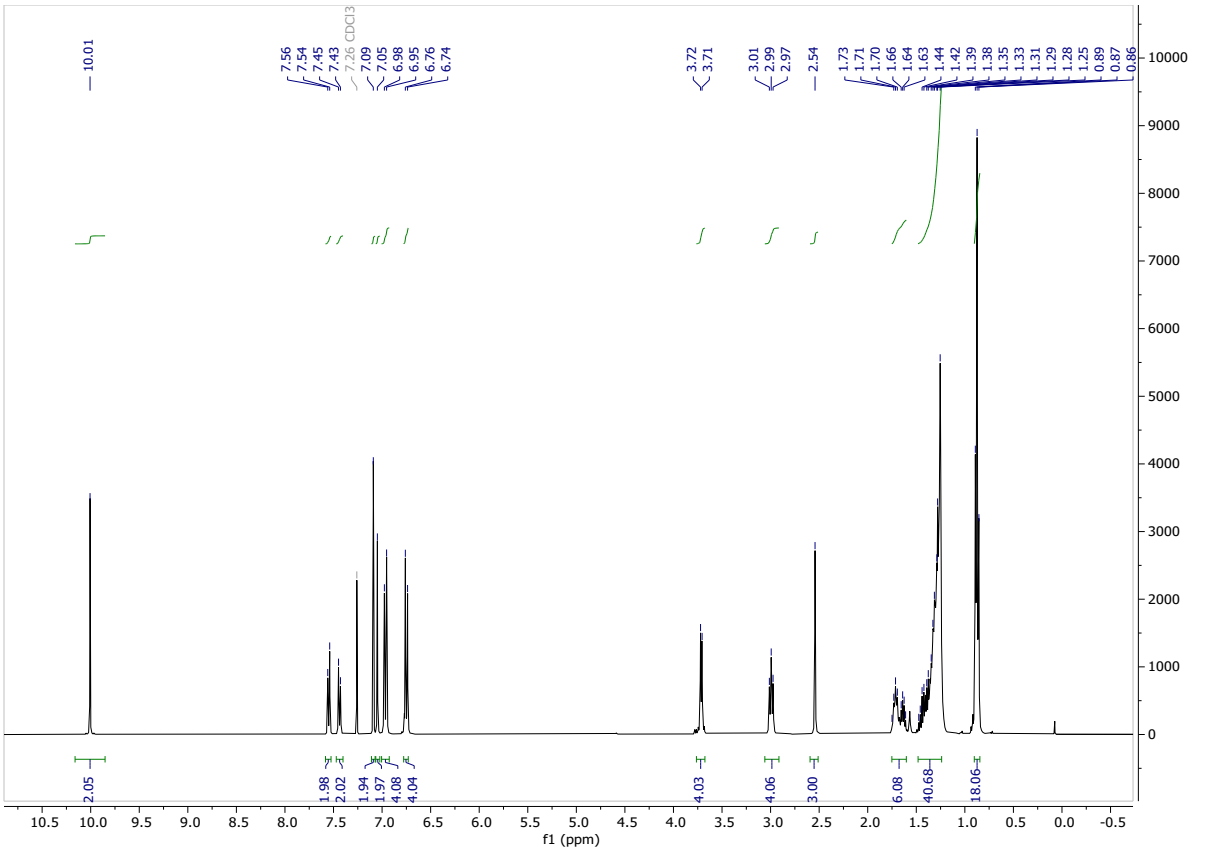

Figure S28. ^{1}H NMR of compound **8**

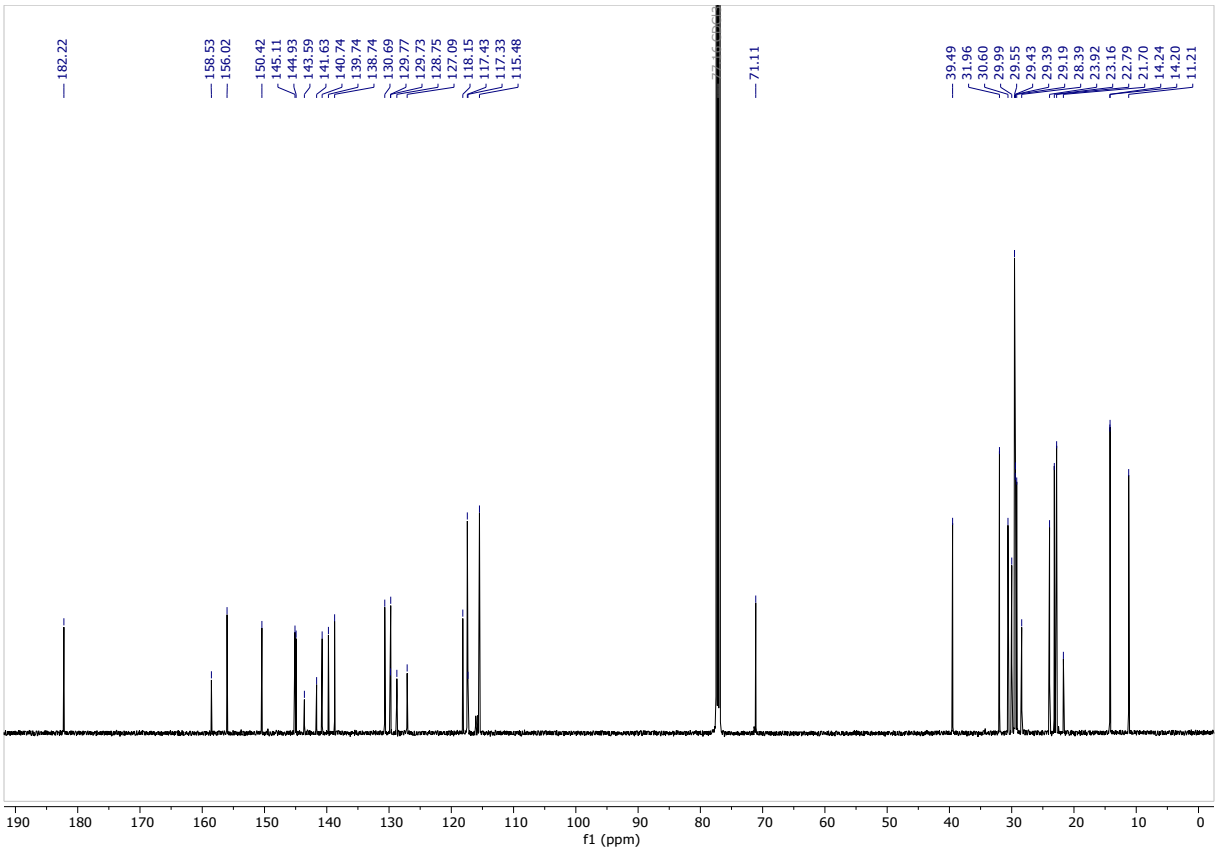

Figure S29. ^{13}C NMR of compound **8**

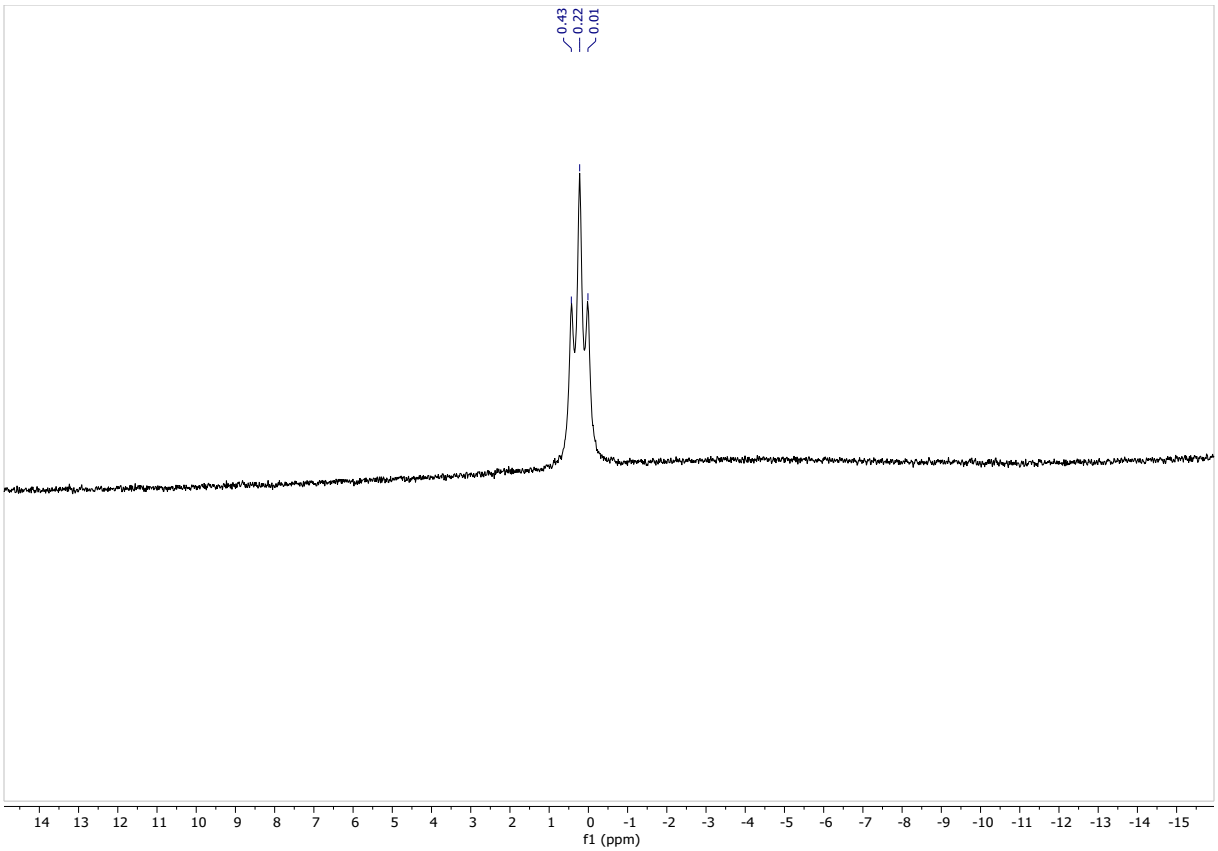

Figure S30. ^{11}B NMR of compound **8**

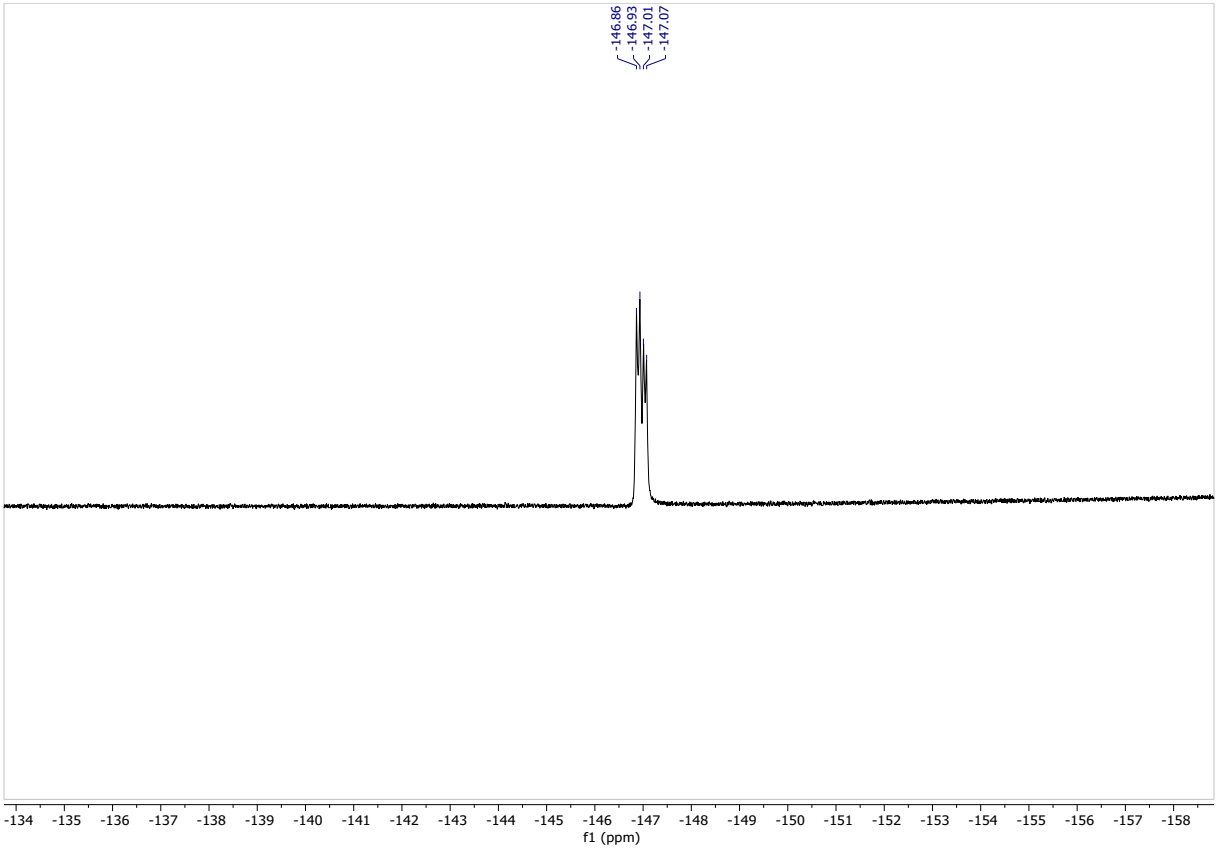

Figure S31. ^{19}F NMR of compound **8**

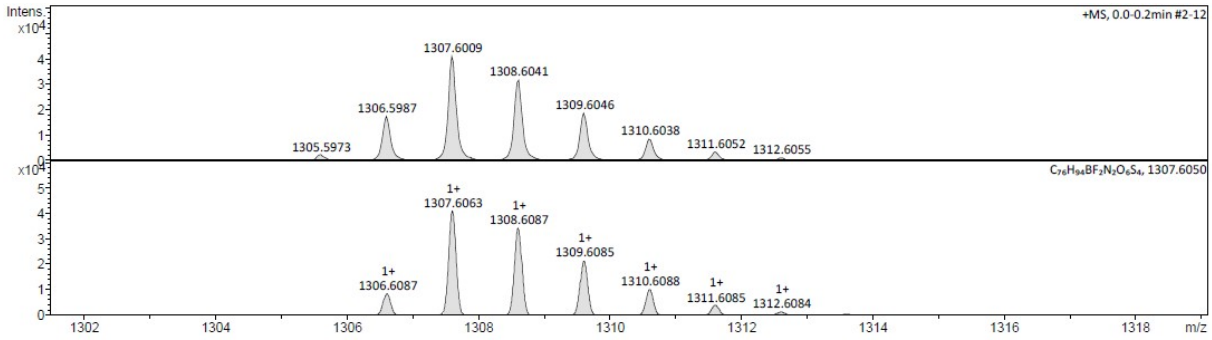

Figure S32. HRMS of compound **8**

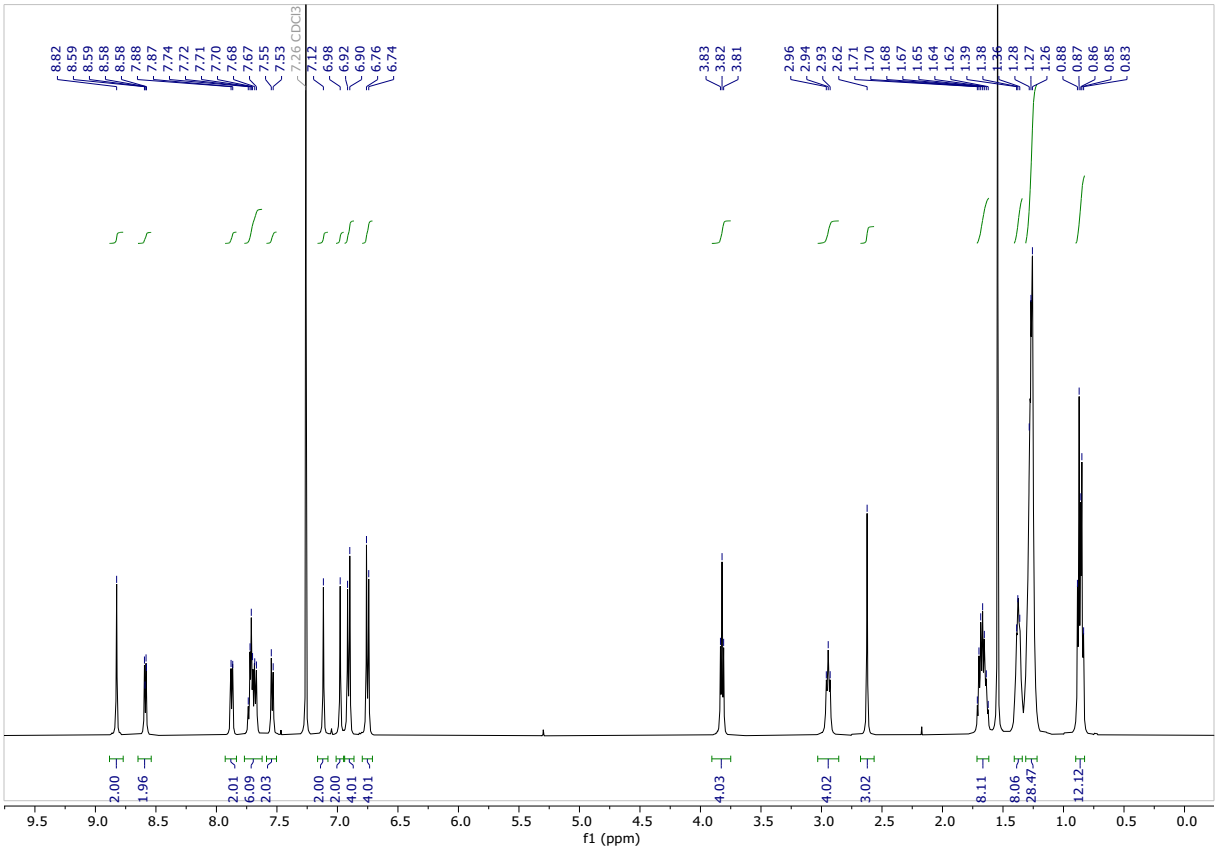

Figure S33. ^{1}H NMR of compound $\mathbf{BTT_{L6}}$

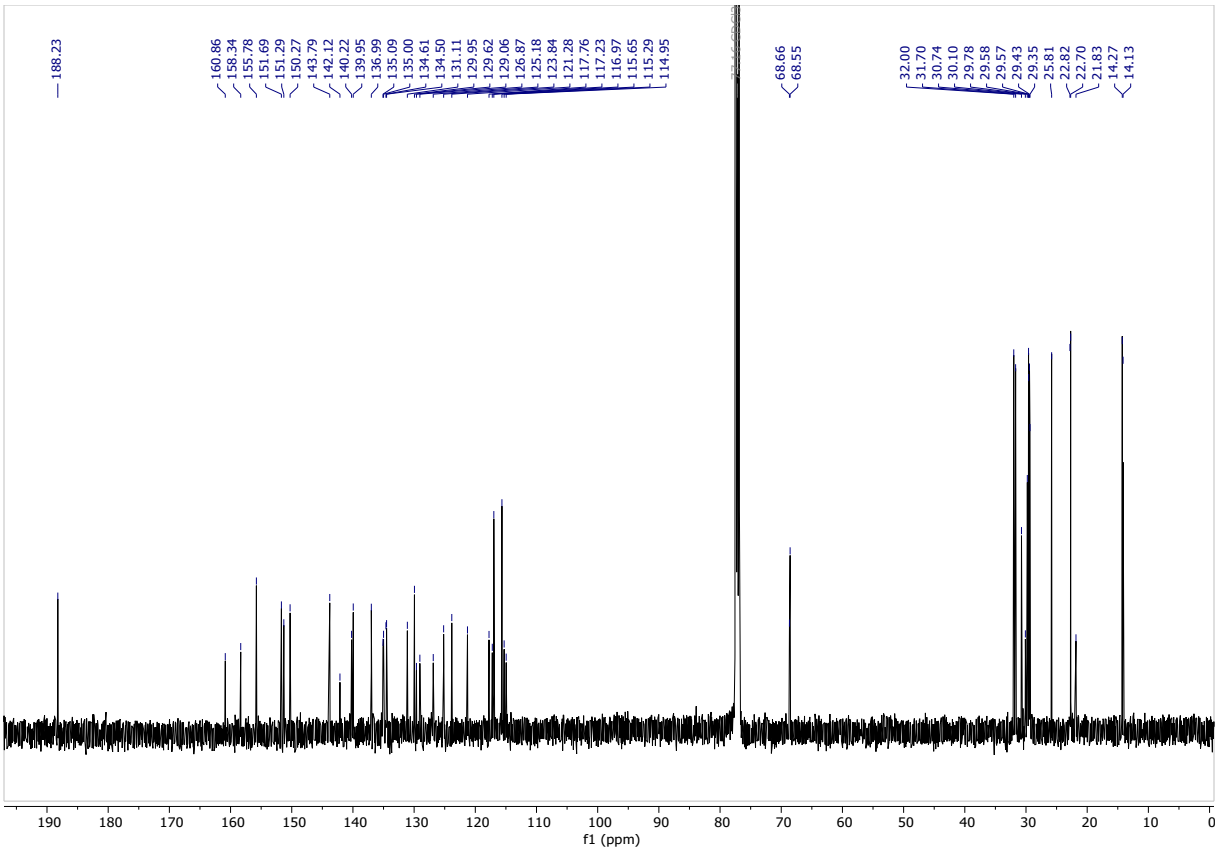

Figure S34. ^{13}C NMR of compound $\mathbf{BTT_{L6}}$

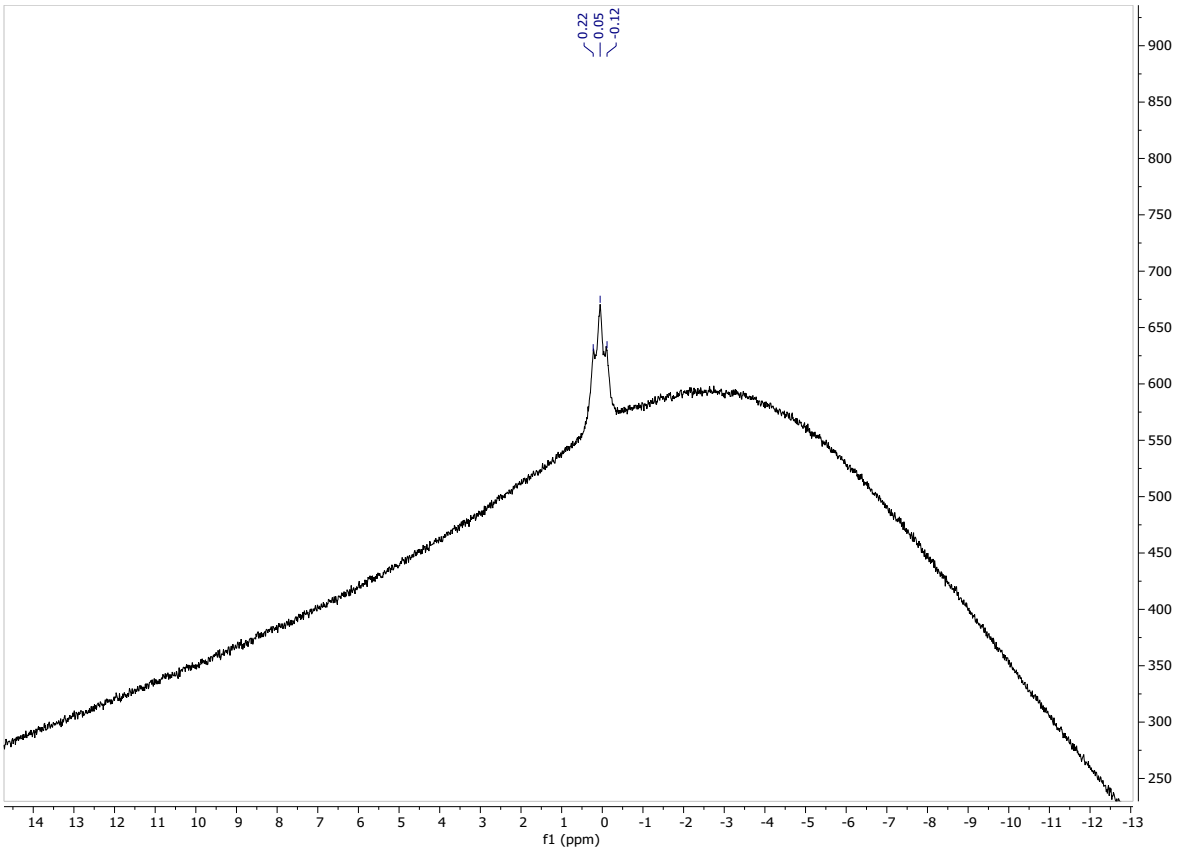

Figure S35. ^{11}B NMR of compound $\mathbf{BTT_{L6}}$

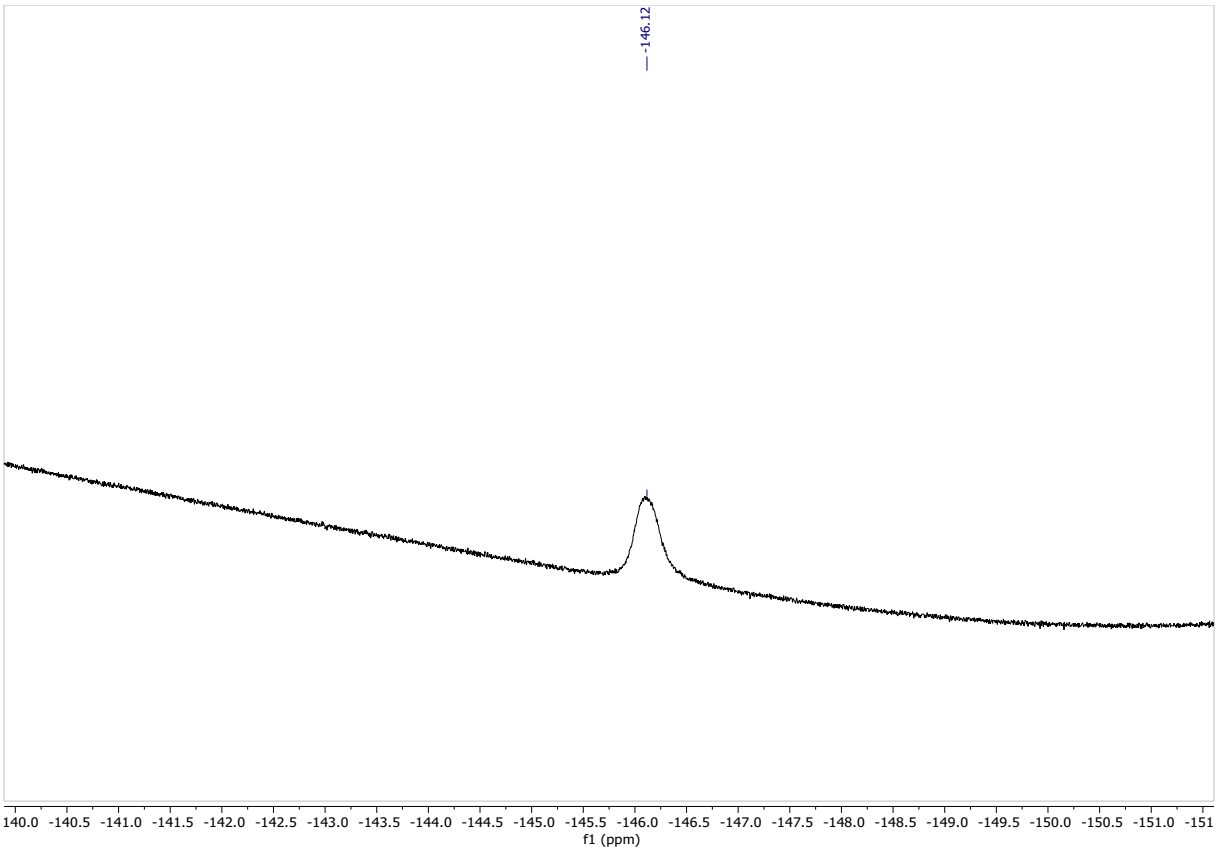

Figure S36. ^{19}F NMR of compound $\mathbf{BTT_{L6}}$

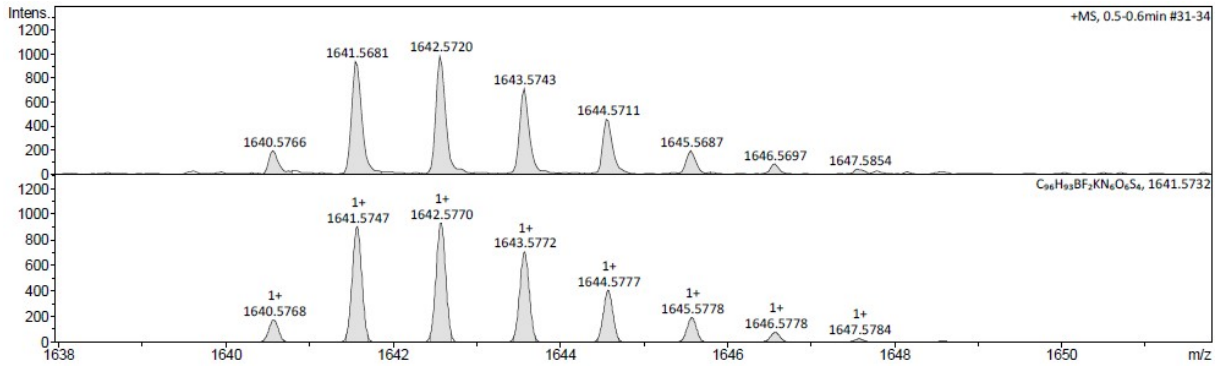

Figure S37. HRMS of compound $\mathbf{BTT_{L6}}$

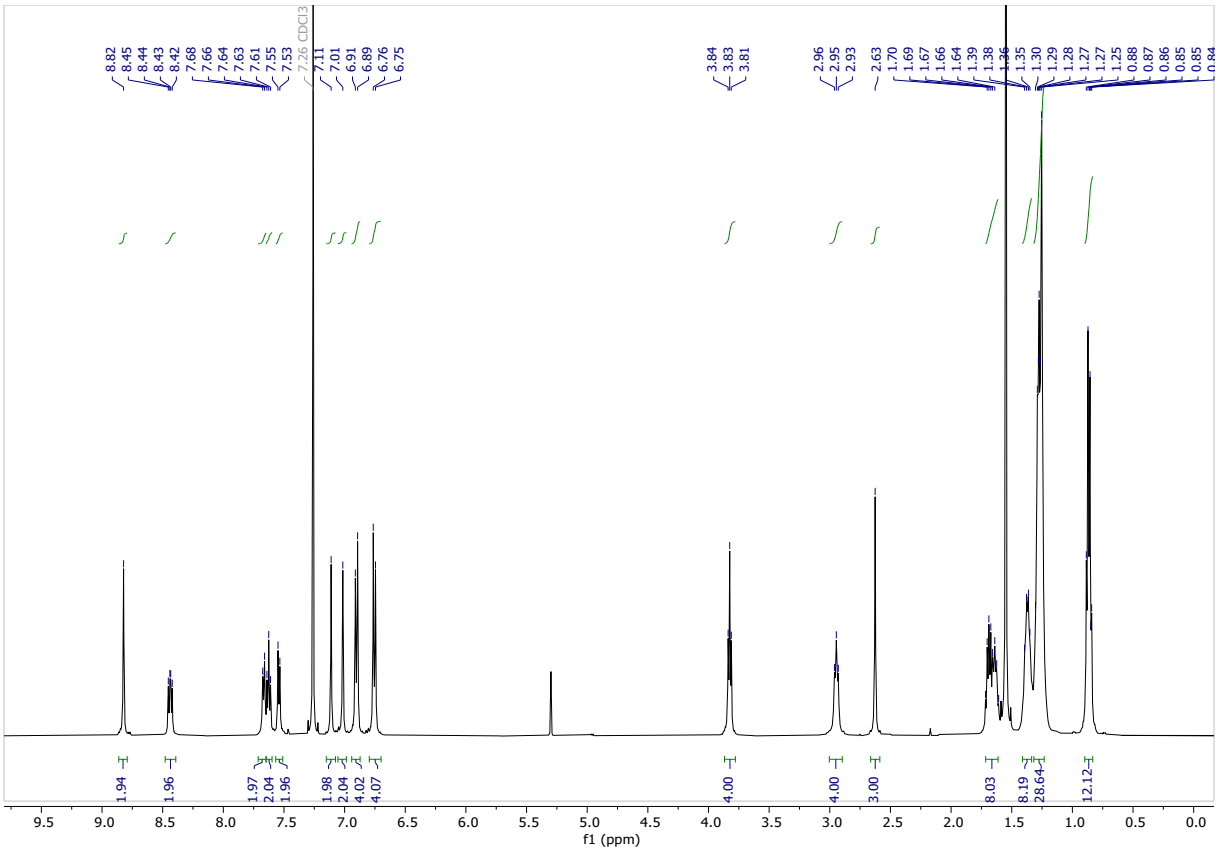

Figure S38. ^{1}H NMR of compound **BTT$_{L6}$-4F**

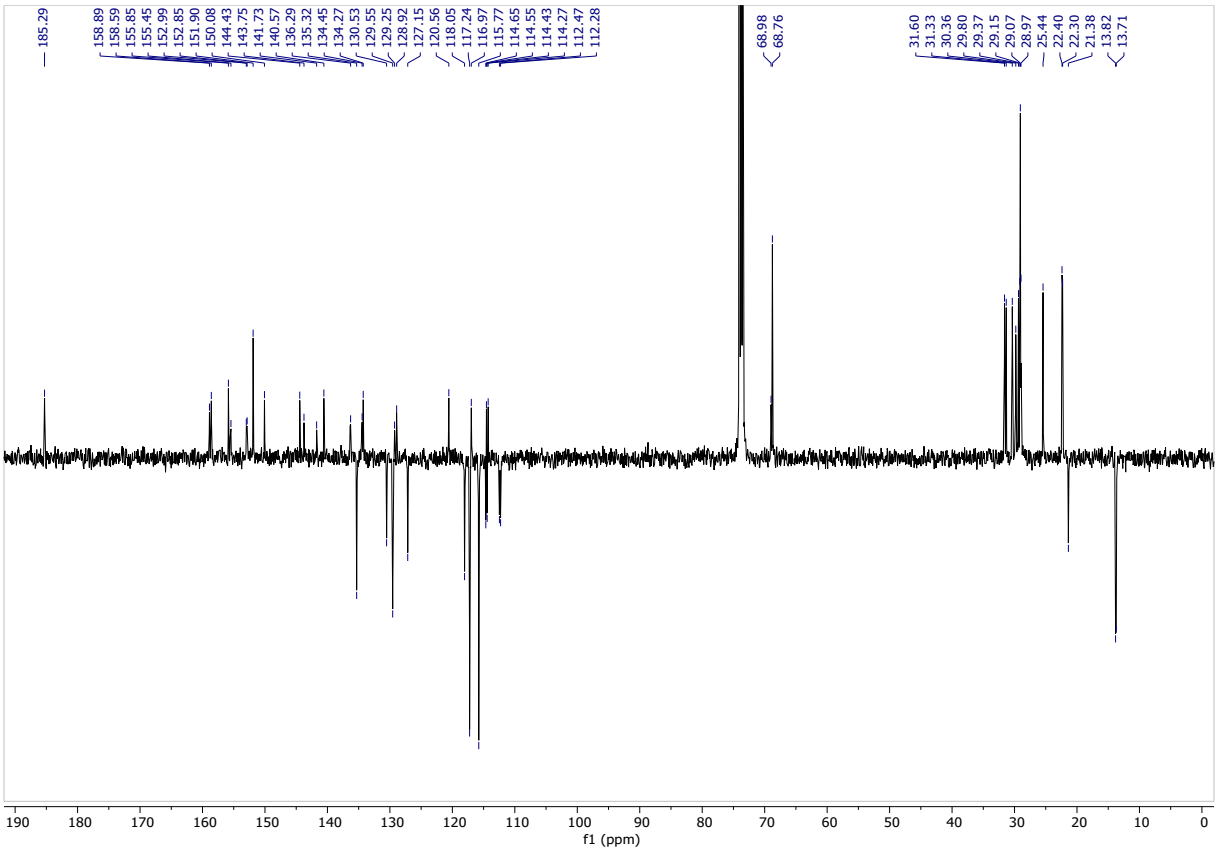

Figure S39. ^{13}C NMR of compound **BTT$_{L6}$-4F**

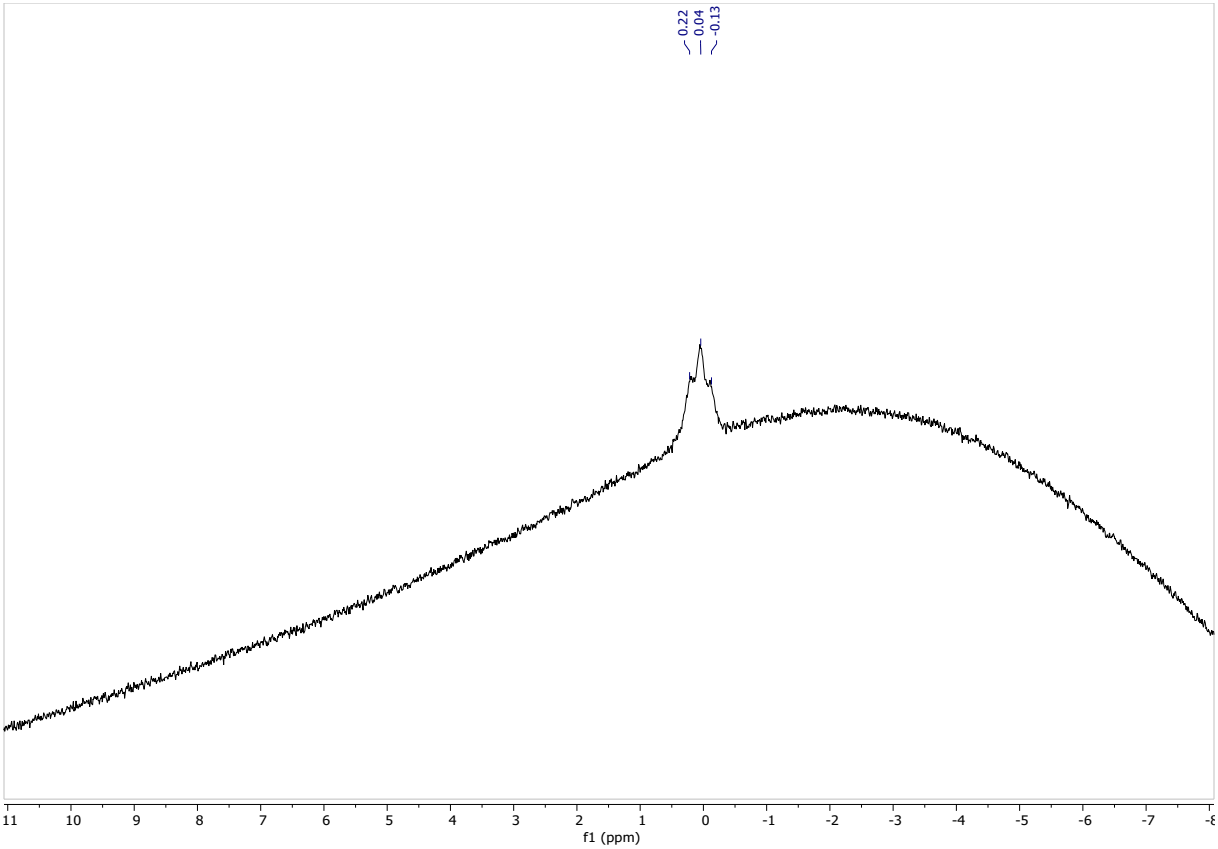

Figure S40. ^{11}B NMR of compound **BTT$_{L6}$-4F**

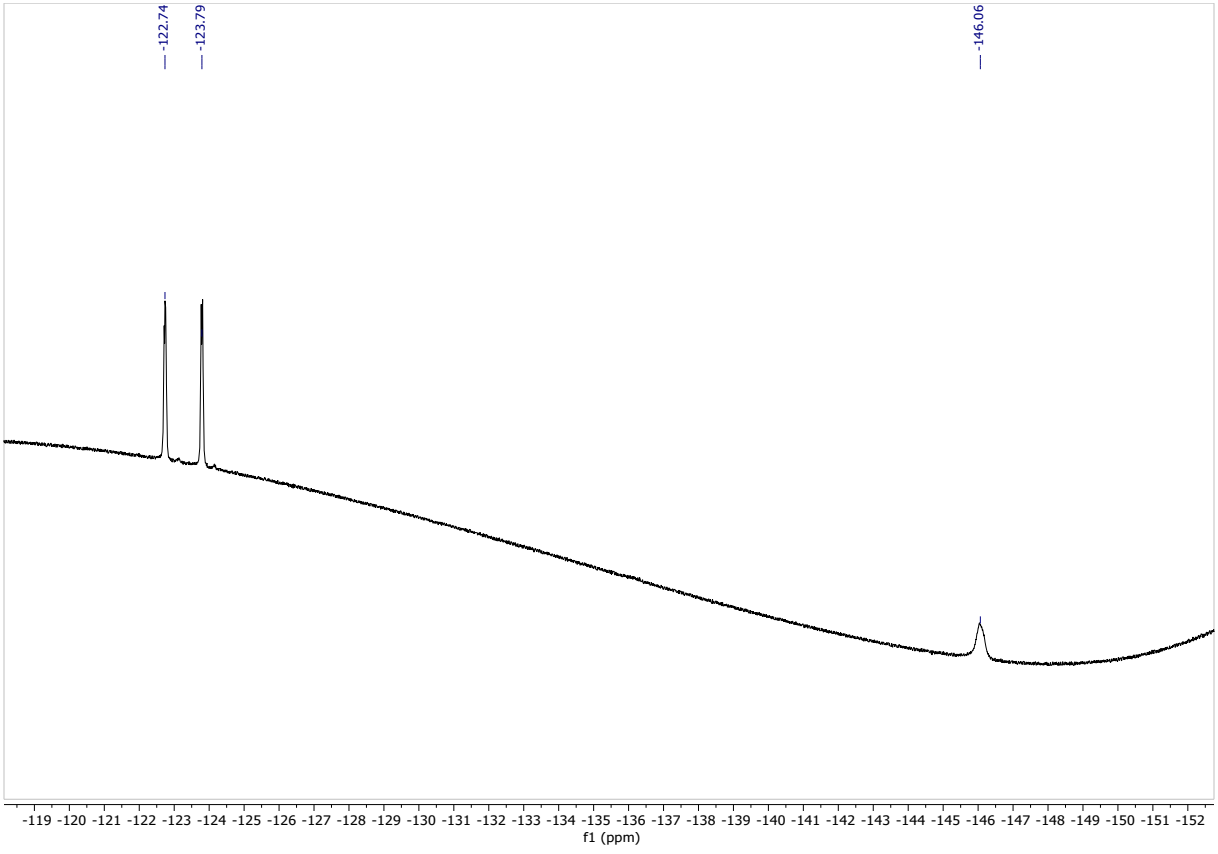

Figure S41. ^{19}F NMR of compound **BTT$_{L6}$-4F**

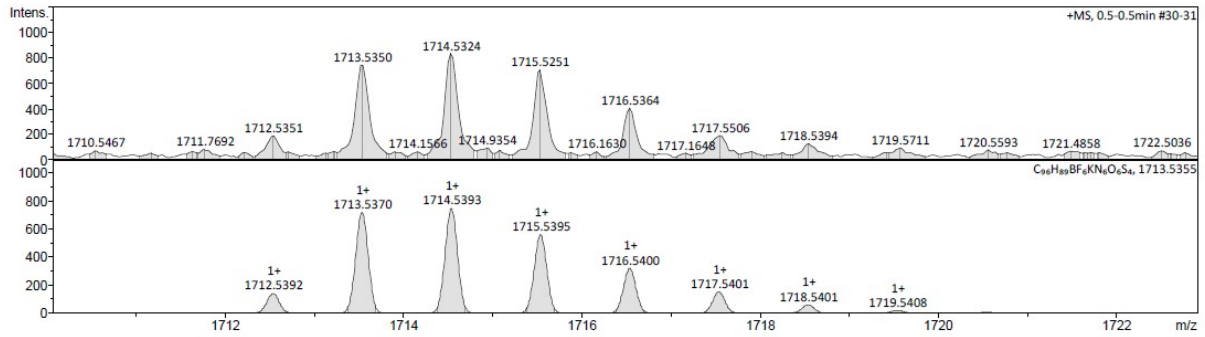

Figure S42. HRMS of compound **BTT_{L6}-4F**

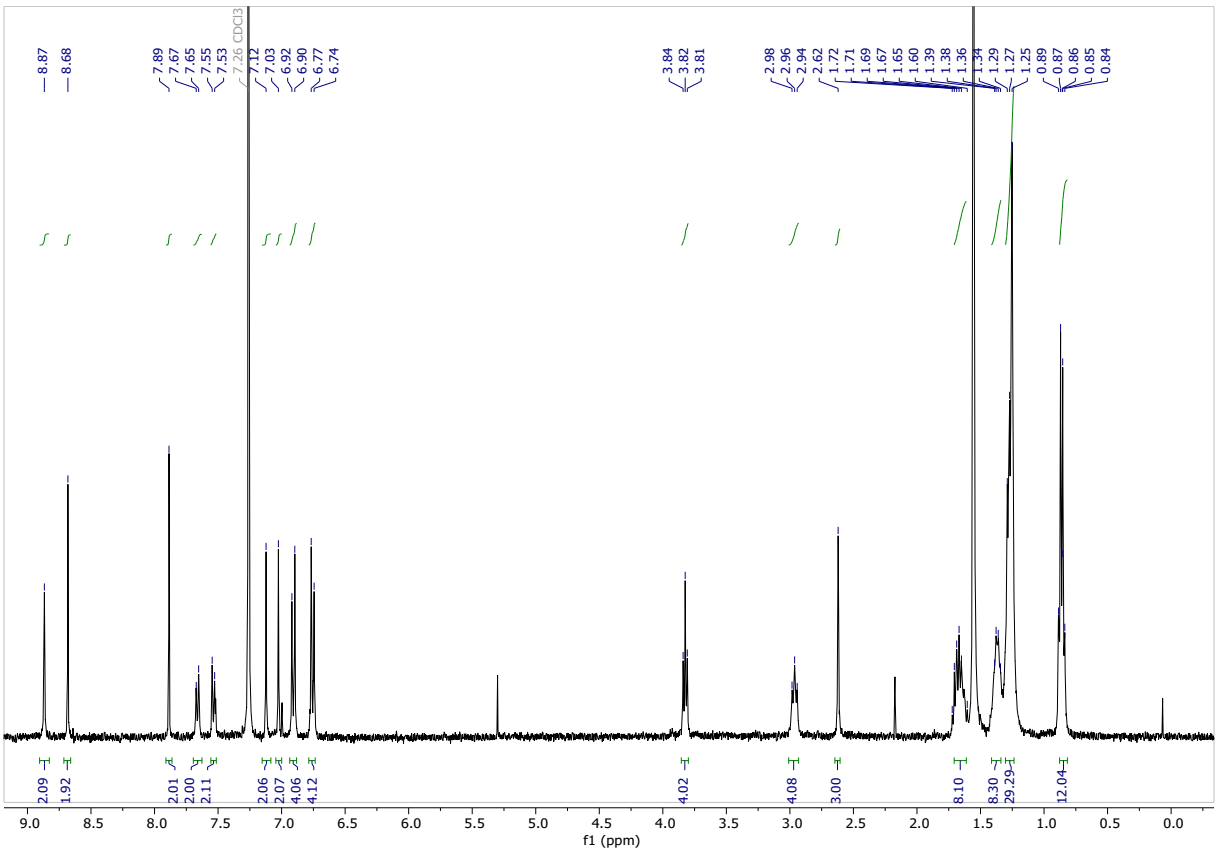

Figure S43. ^{1}H NMR of compound **BTT_{L6}-4Cl**

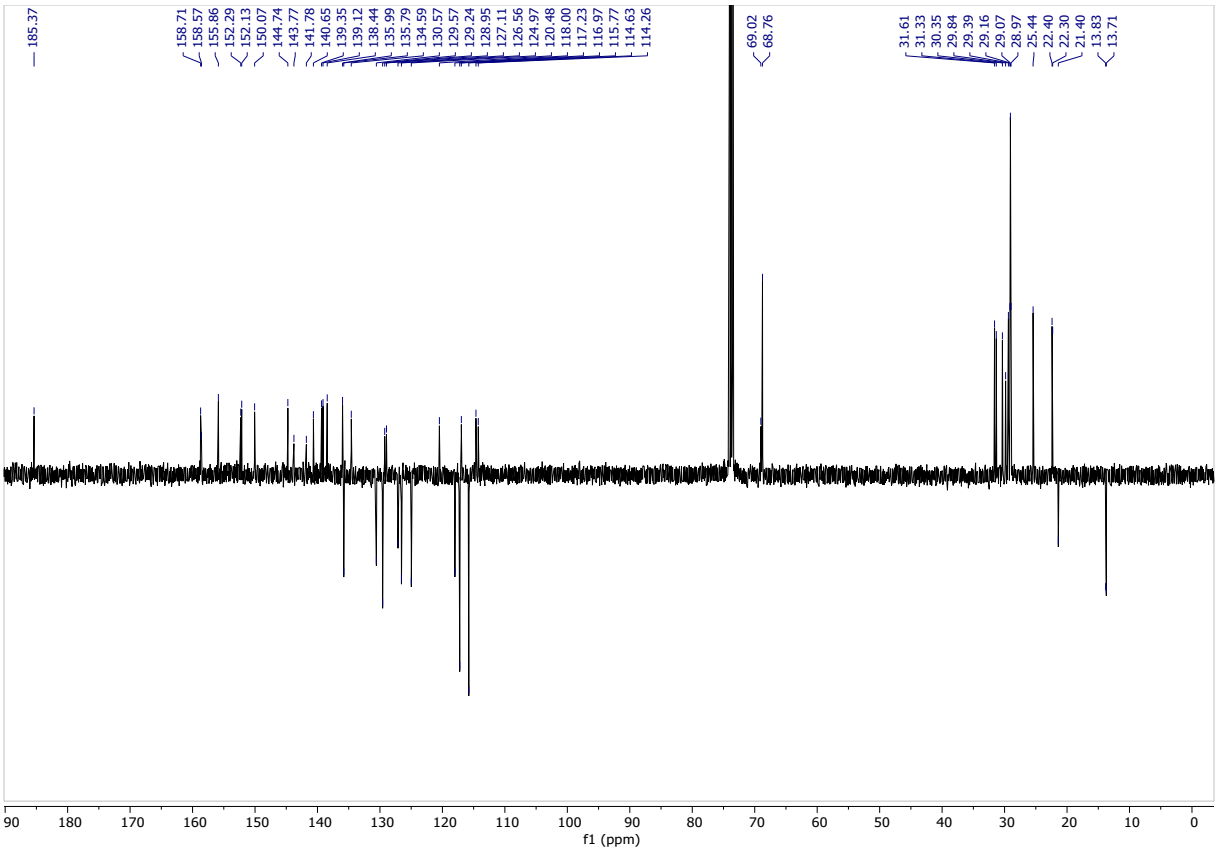

Figure S44. ^{13}C NMR of compound **BTTL6-4Cl**

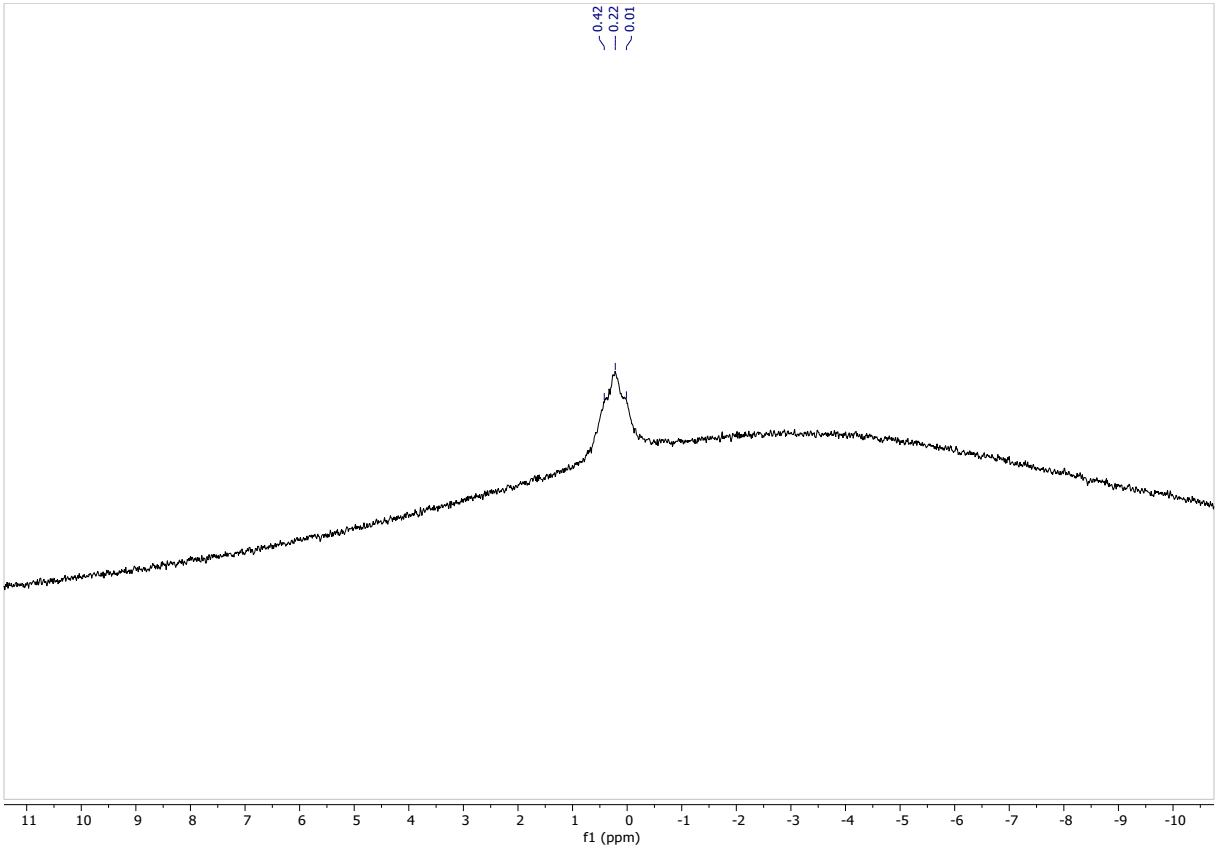

Figure S45. ^{11}B NMR of compound **BTT$_{L6}$-4Cl**

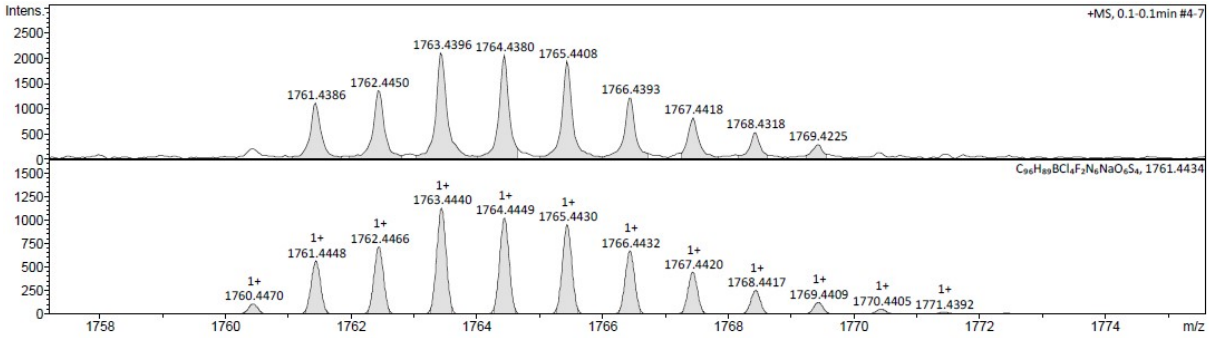

Figure S46. HRMS of compound **BTT$_{L6}$-4Cl**

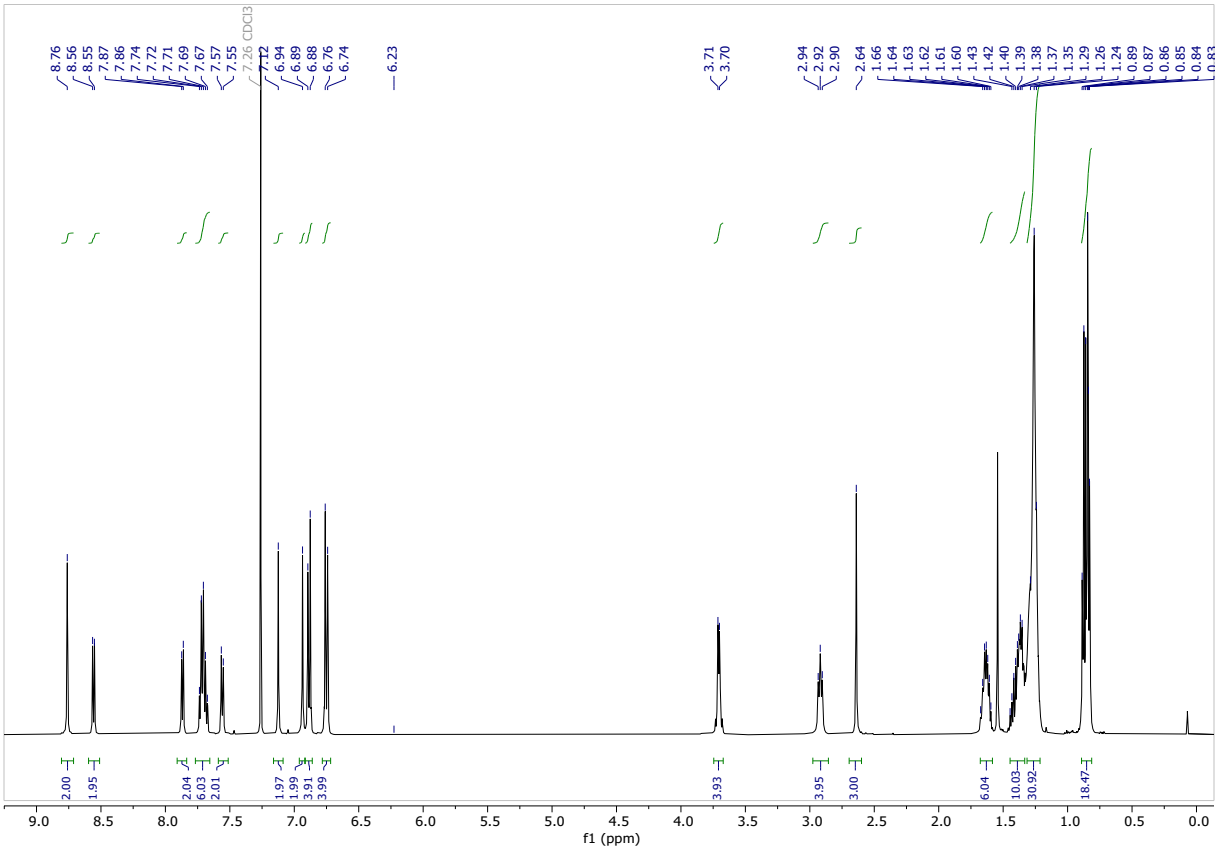

Figure S47. ^{1}H NMR of compound **BTT$_{R8}$**

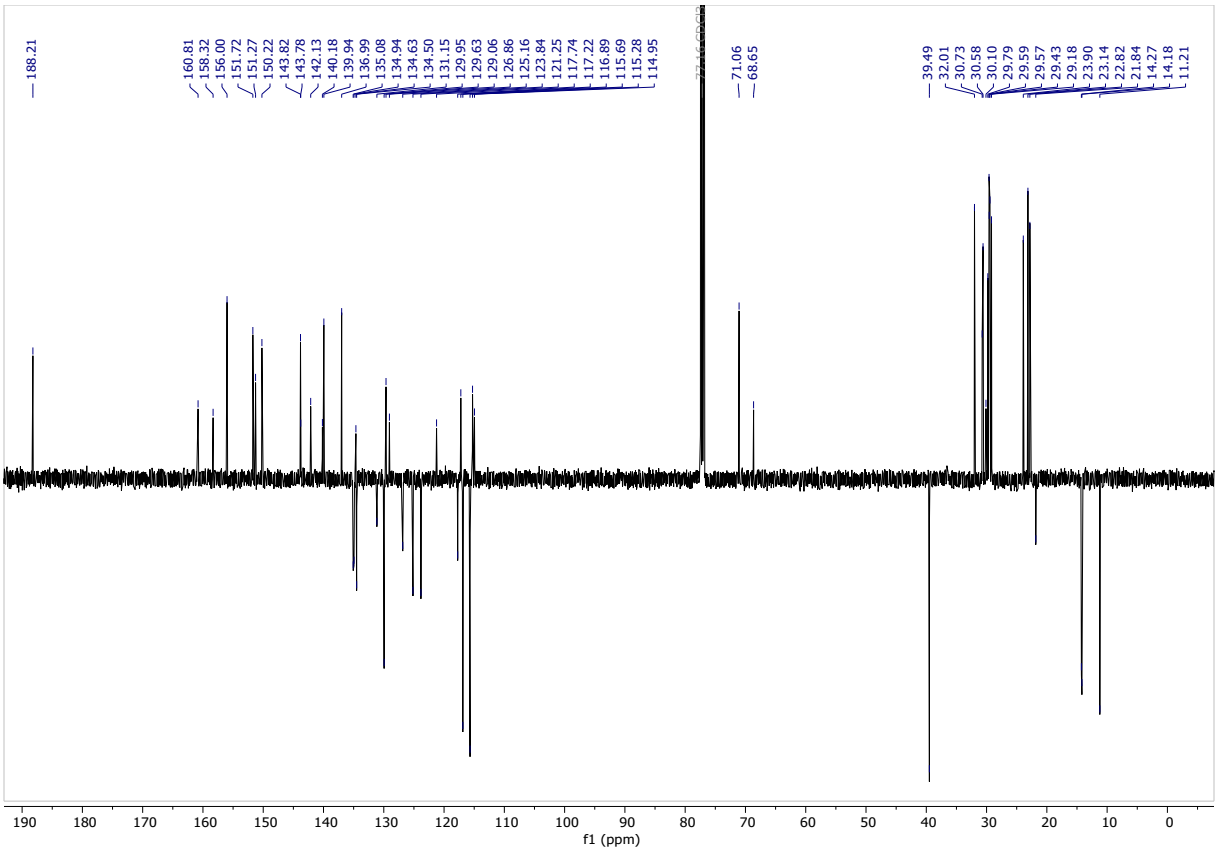

Figure S48. ^{13}C NMR of compound $\mathbf{BTT_{R8}}$

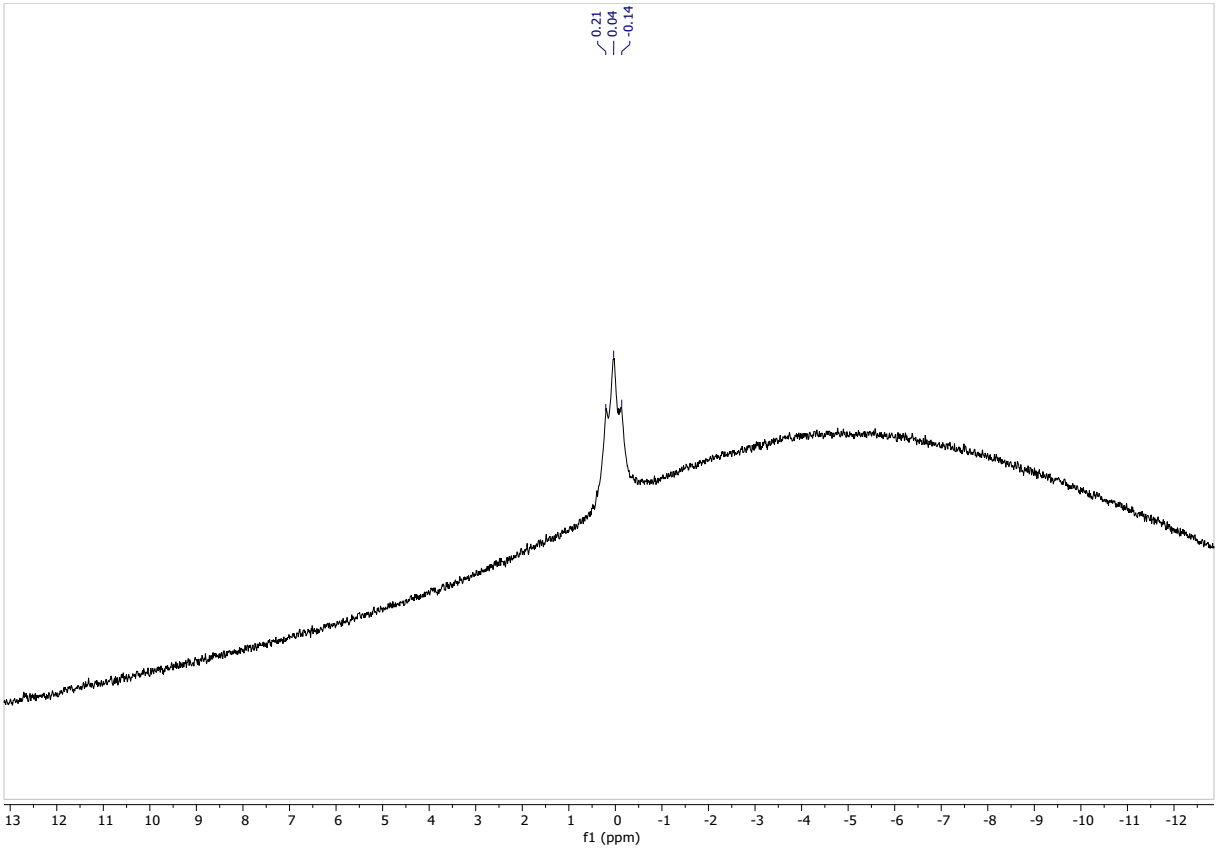

Figure S49. ^{11}B NMR of compound $\mathbf{BTT_{R8}}$

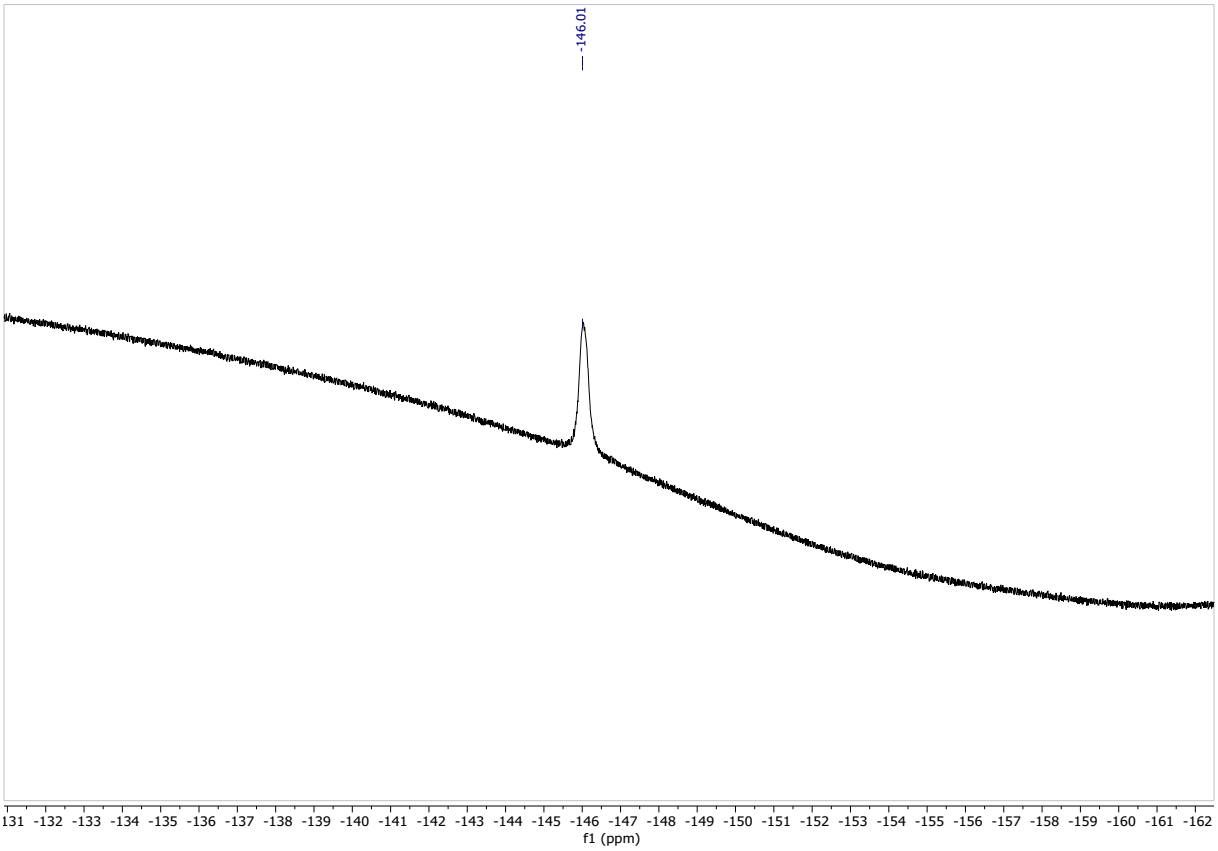

Figure S50. ^{19}F NMR of compound $\mathbf{BTT_{R8}}$

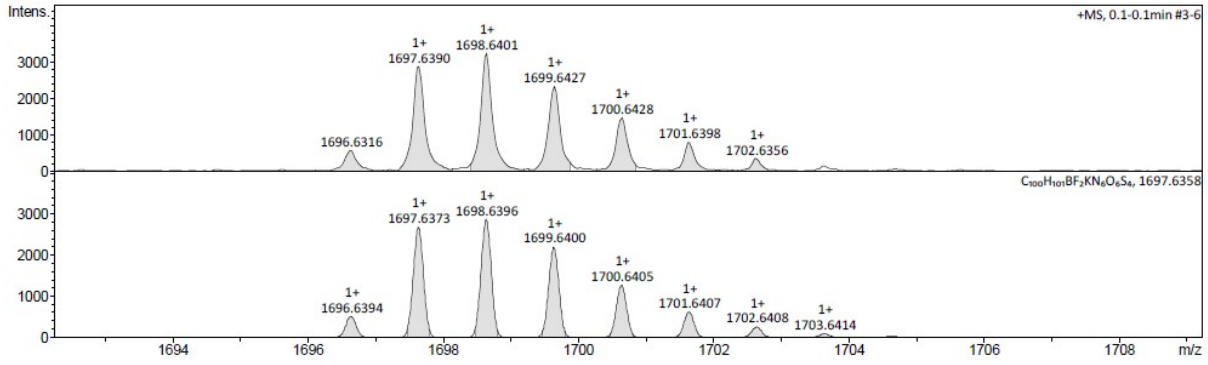

Figure S51. HRMS of compound $\mathbf{BTT_{R8}}$

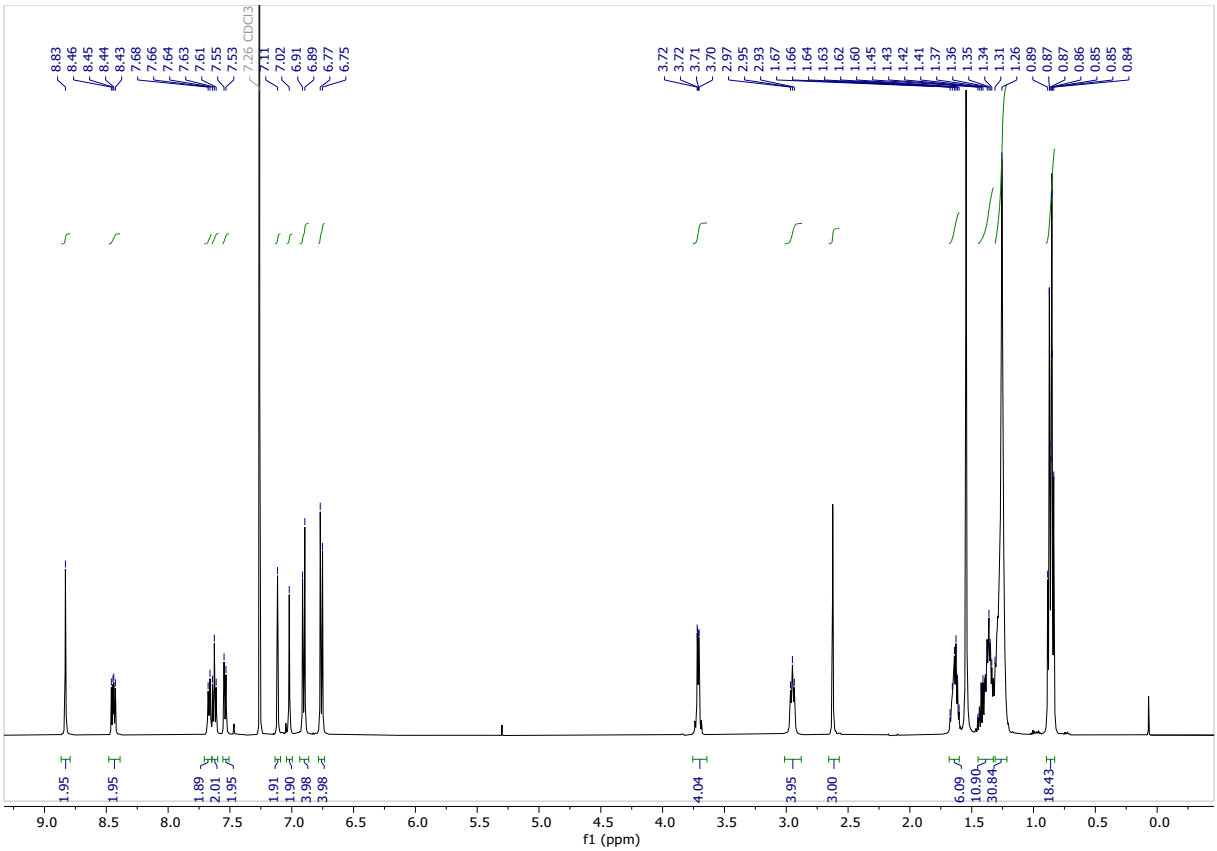

Figure S52. ^{1}H NMR of compound **BTT_{R8}-4F**

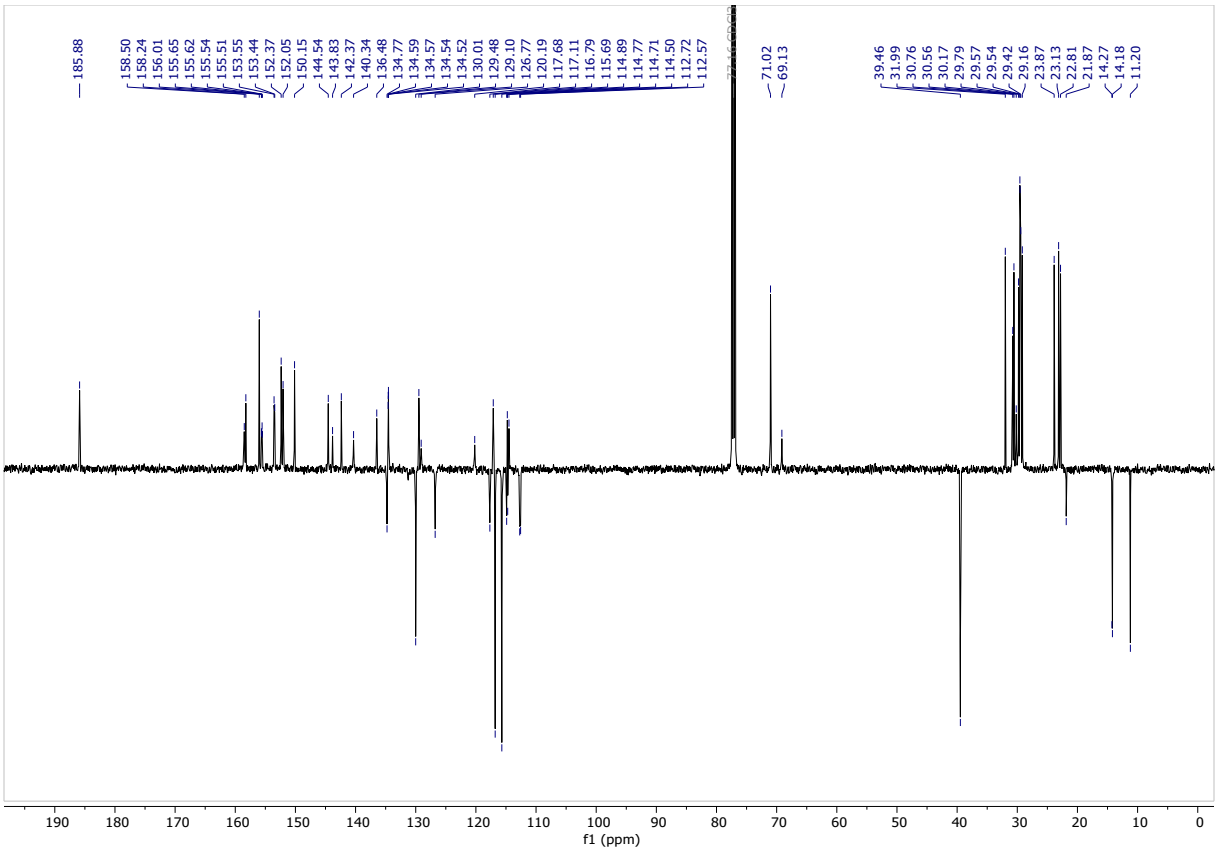

Figure S53. ^{13}C NMR of compound **BTT_{R8}-4F**

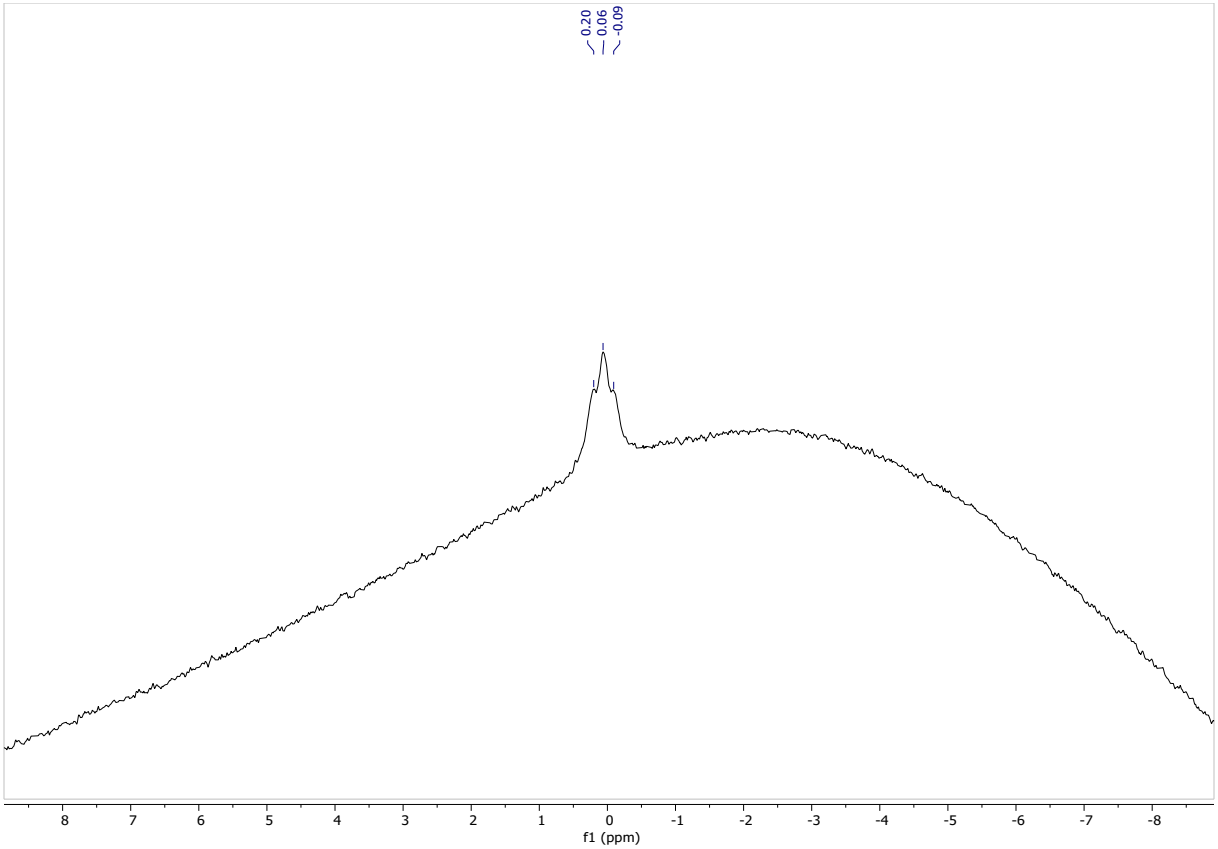

Figure S54. ^{11}B NMR of compound **BTT_{R8}-4F**

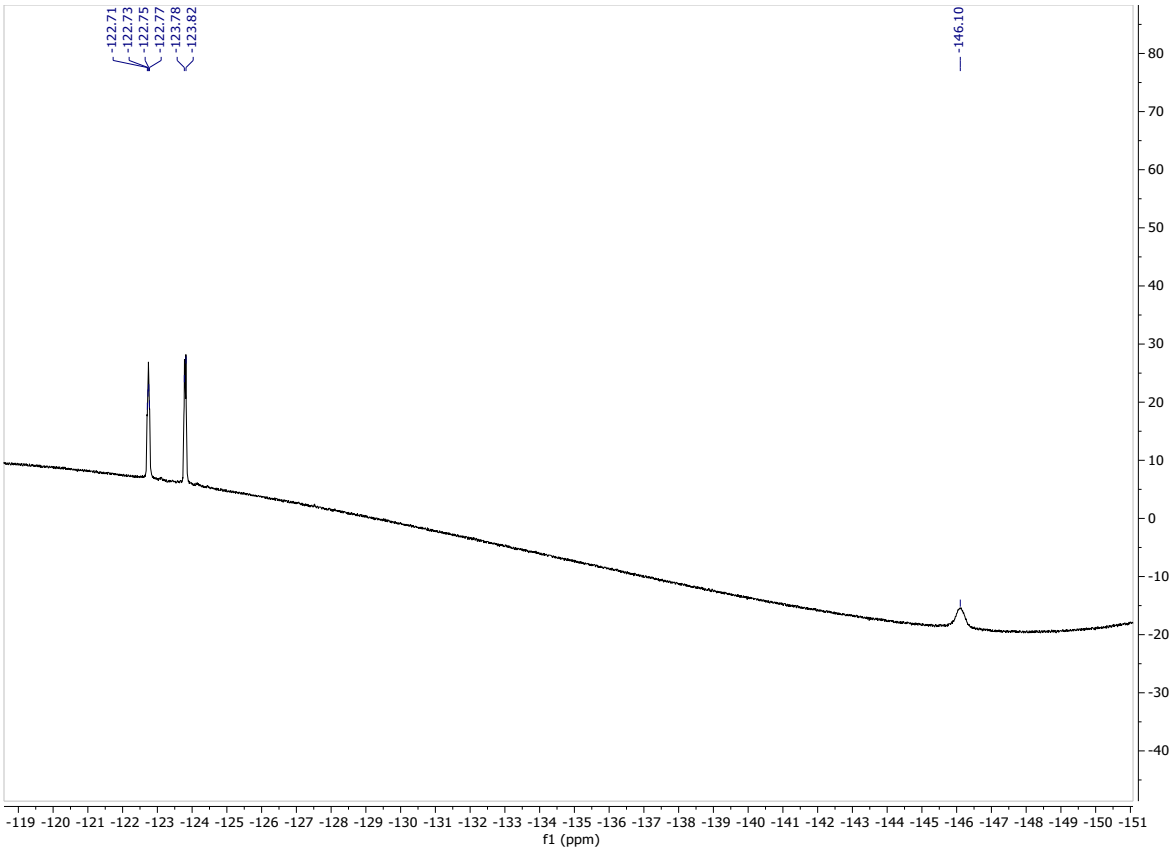

Figure S55. ^{19}F NMR of compound **BTT$_{R8}$-4F**

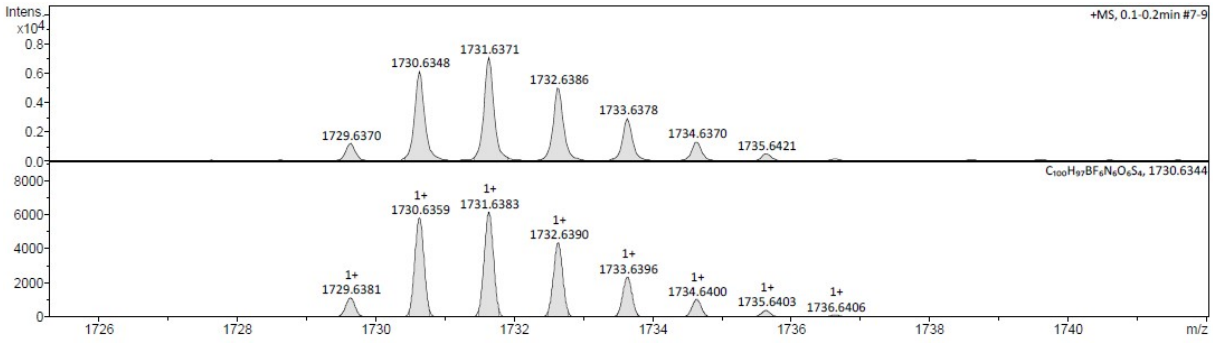

Figure S56. HRMS of compound **BTT$_{R8}$-4F**

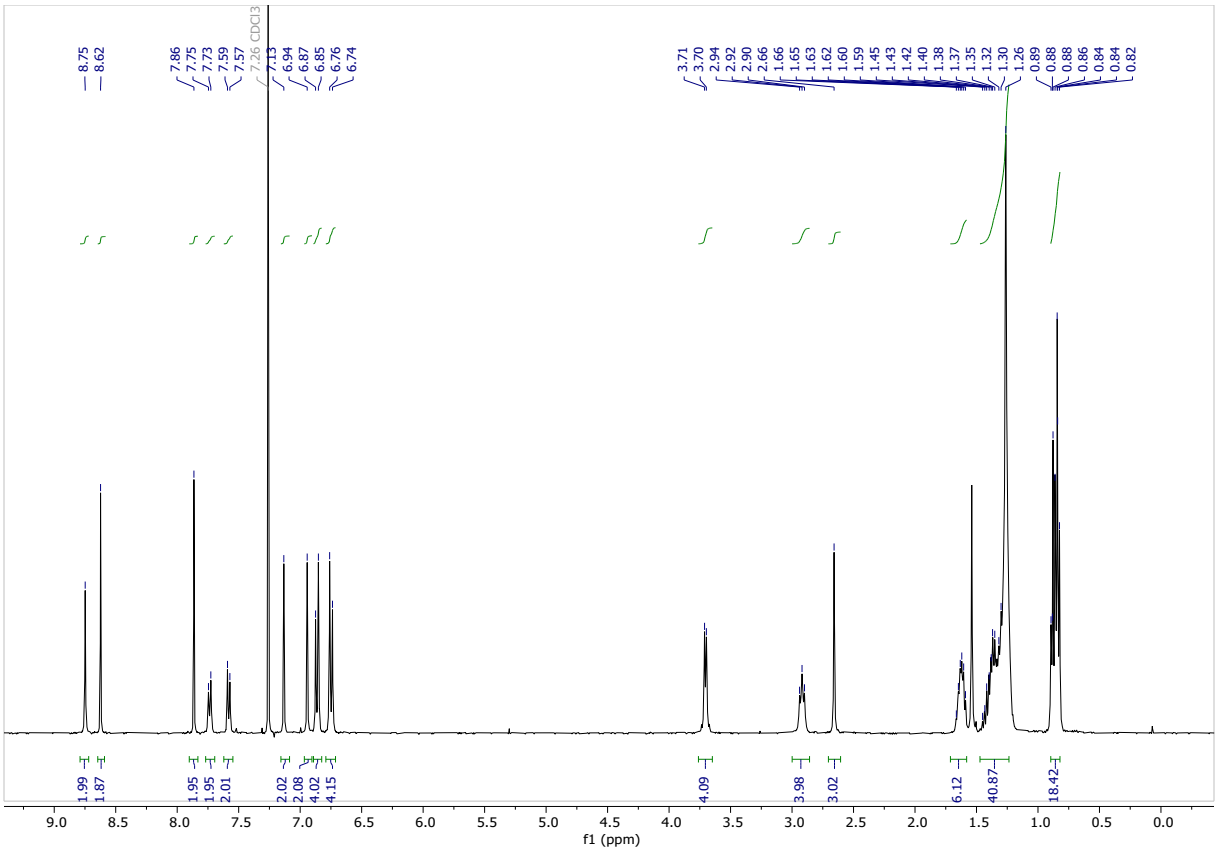

Figure S57. ^{1}H NMR of compound **BTT_{R8}-4Cl**

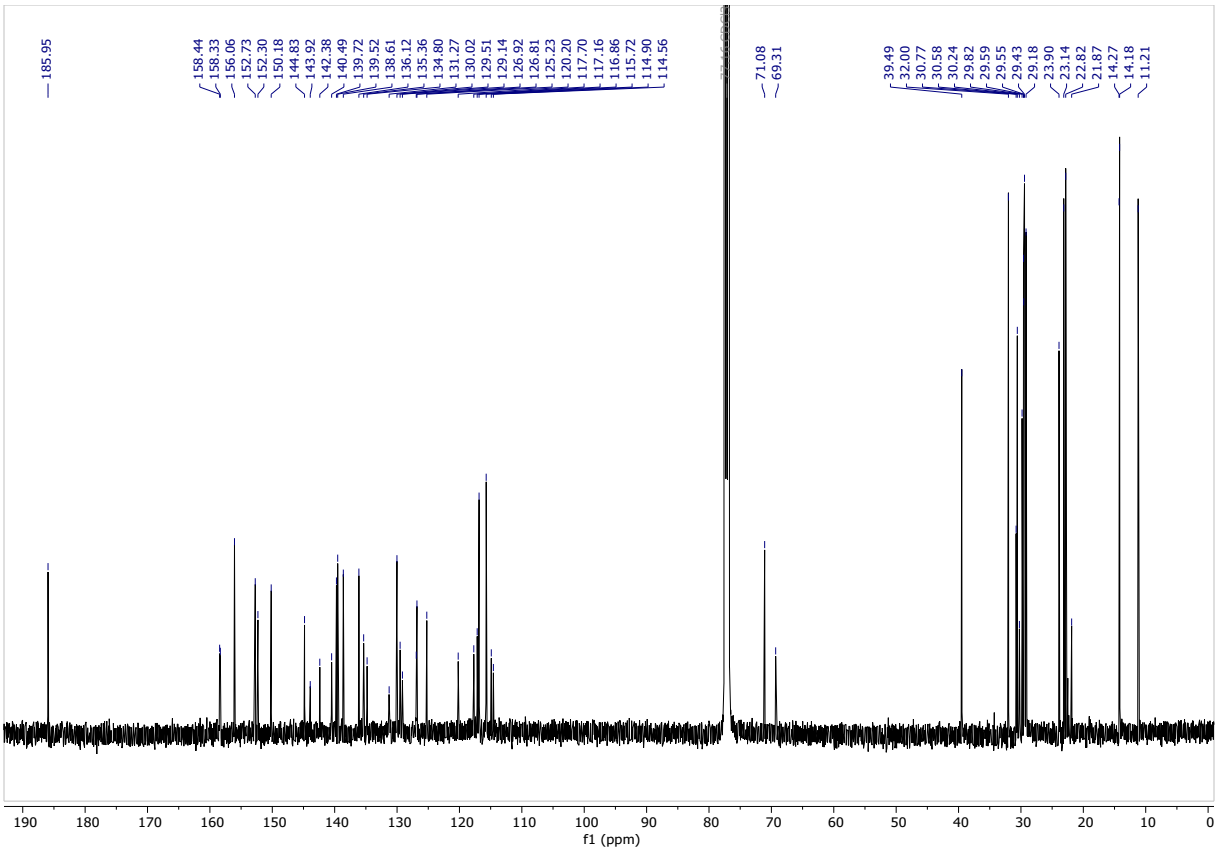

Figure S58. ^{13}C NMR of compound **BTT$_{R8}$-4Cl**

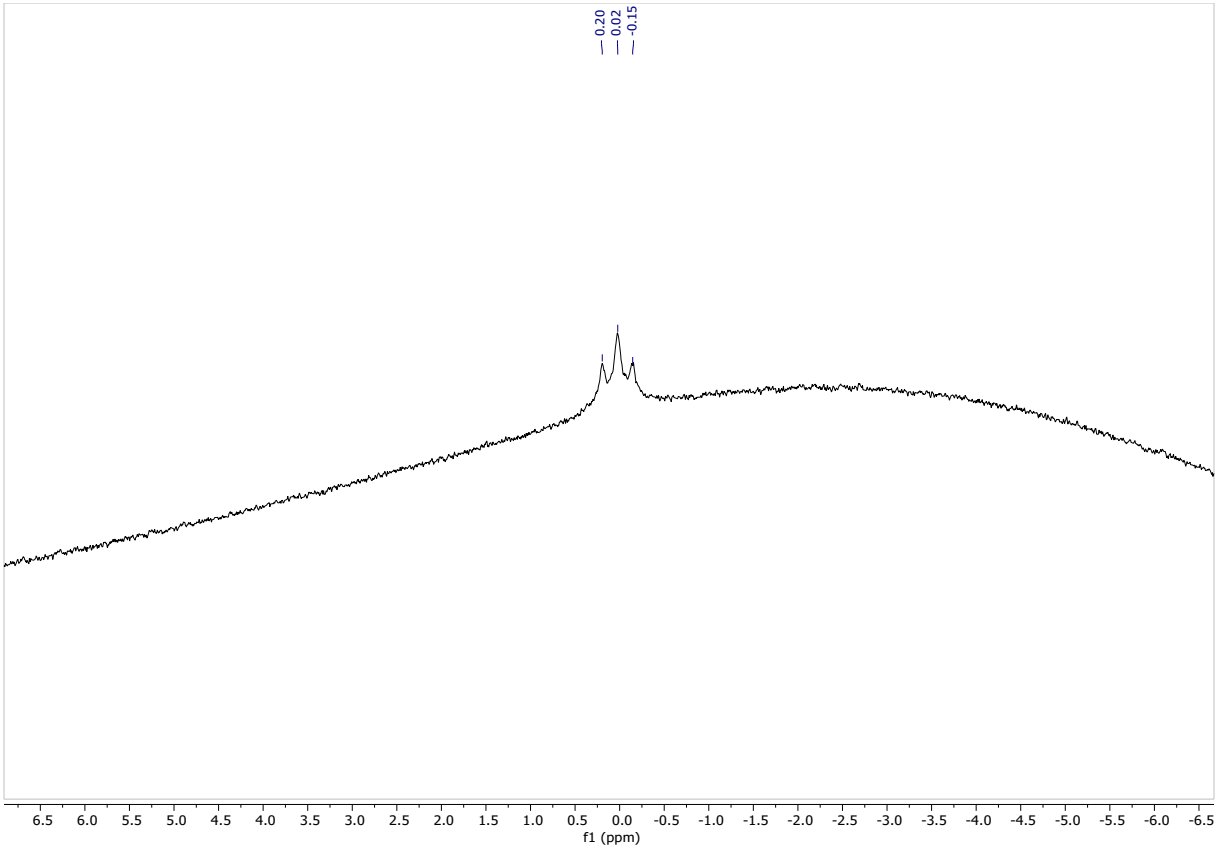

Figure S59. ^{11}B NMR of compound **BTT$_{R8}$-4Cl**

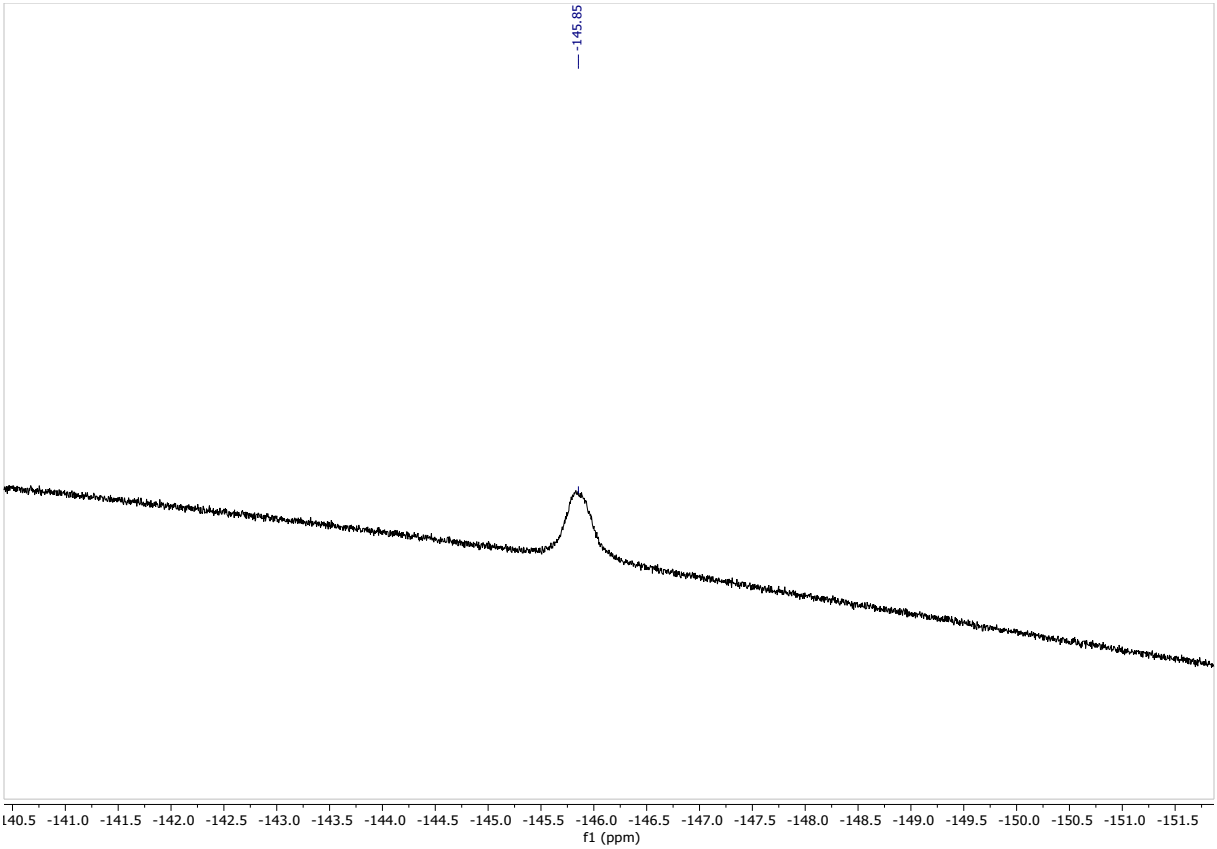

Figure S60. ^{19}F NMR of compound **BTT_{R8}-4Cl**

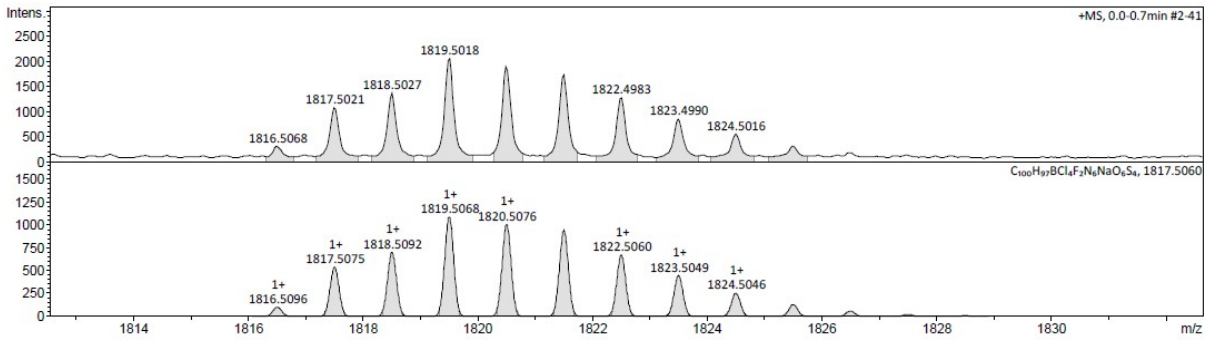

Figure S61. HRMS of compound **BTT_{R8}-4Cl**

TGA measurements

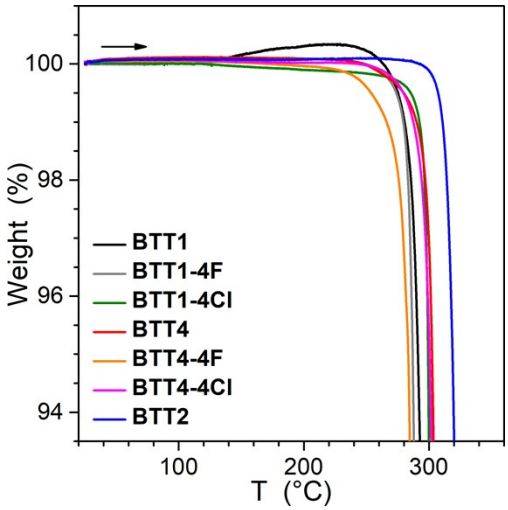

Figure S62. TGA curves of the sample series (Q50 from TA Instruments; conditions: 5°C/min, air).

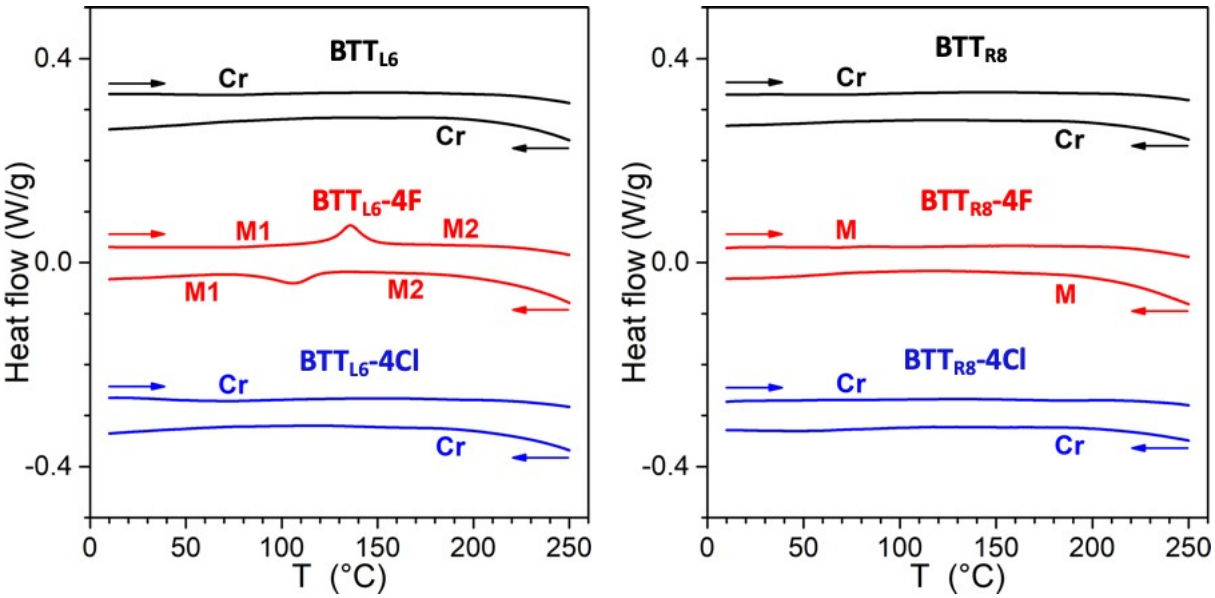

Figure S63. DSC curves on second heating and cooling (DSC Q1000 from TA Instruments; conditions: 5°C/min, endotherm up). Phase type from POM, DSC and SWAXS: Cr = crystal; M, M1, M2 = mesophases

SWAXS measurements

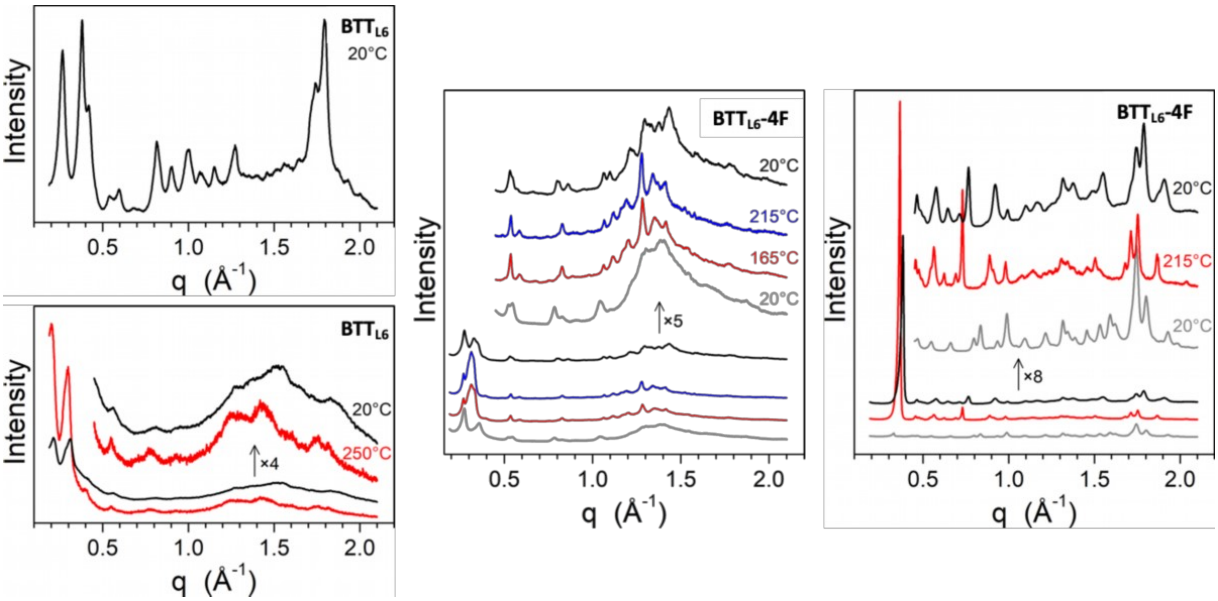

Figure S64. Small- and wide-angle scattering (SWAXS) patterns of **BTT$_{L6}$** and **BTT$_{L6}$** derivative series, in the room temperature pristine state (grey), on heating at high temperature (red) and on cooling to room temperature (black). For **BTT$_{L6}$**, note the broad scattering signals centered at 1.4 Å^{-1} and the overlapping sharp reflections.

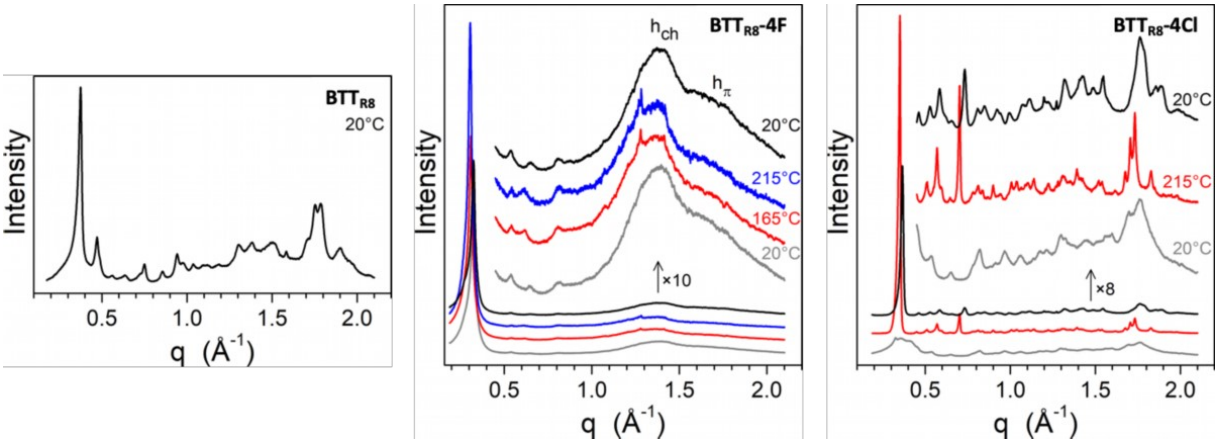

Figure S65. Small- and wide-angle scattering (SWAXS) patterns of **BTT$_{R8}$** and **BTT$_{R8}$** derivative series, in the room temperature pristine state (grey), on heating at high temperature (red) and on cooling to room temperature (black). For **BTT$_{R8}$**, note the wide q-range composed of broad scattering signals h_{ch} and h_{π} from the local-range arrangement within the domains of molten chain and conjugated units.

DFT and TD-DFT calculations

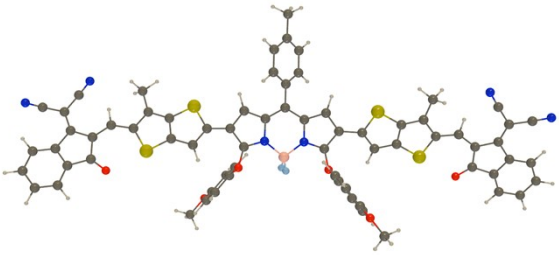

0.00 (A)

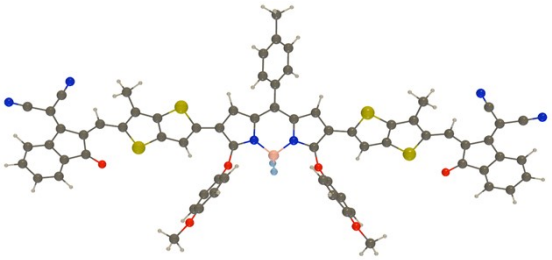

0.47 (B)

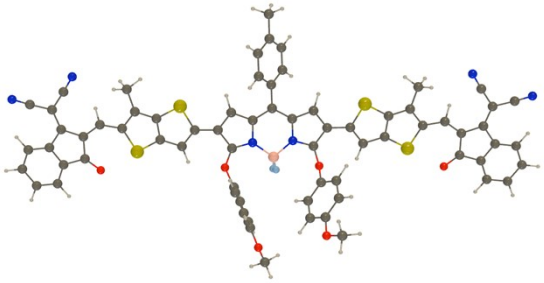

1.01

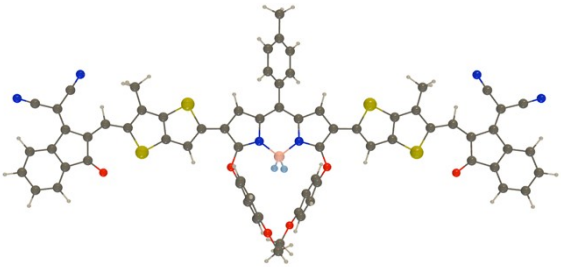

0.70 (C)

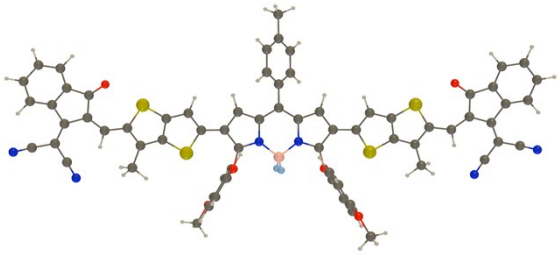

1.10

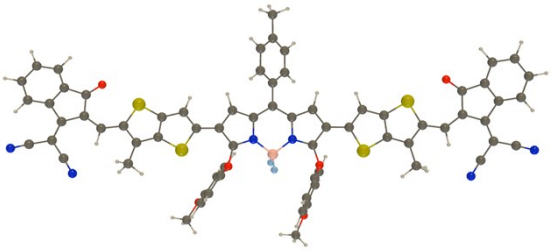

1.27

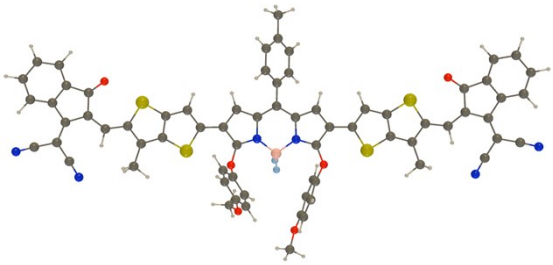

1.17

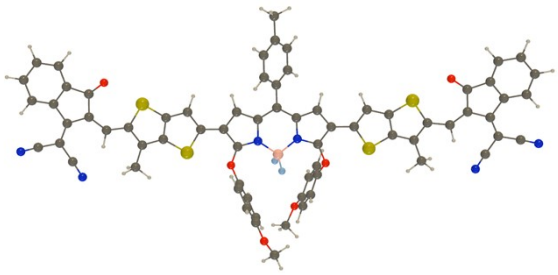

0.50 (D)

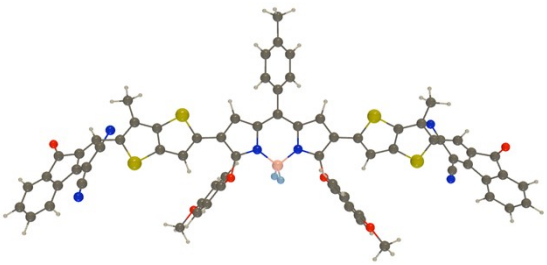

7.86

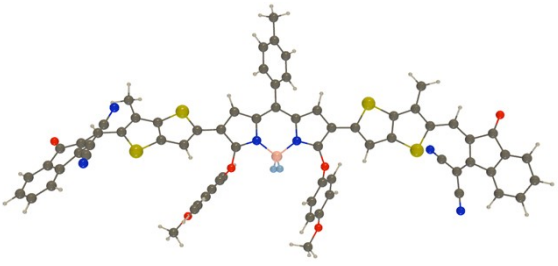

8.73

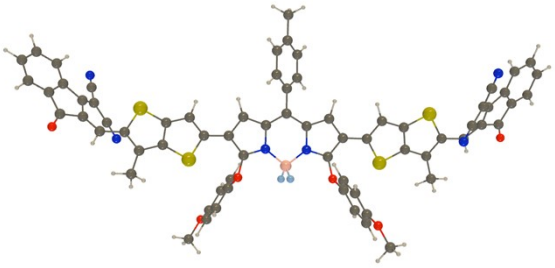

9.35

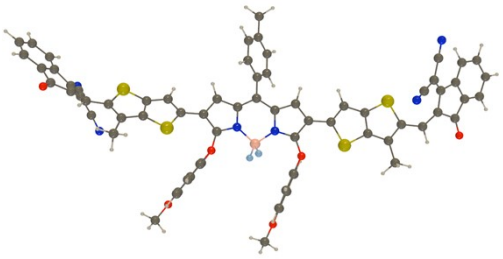

9.36

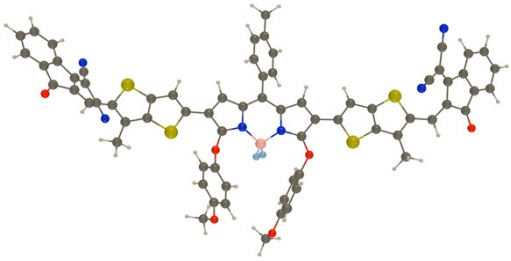

7.50

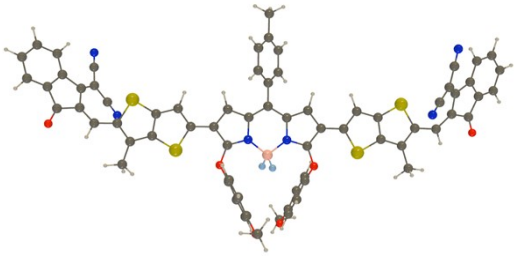

8.77

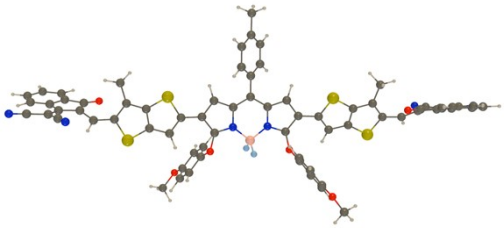

7.43

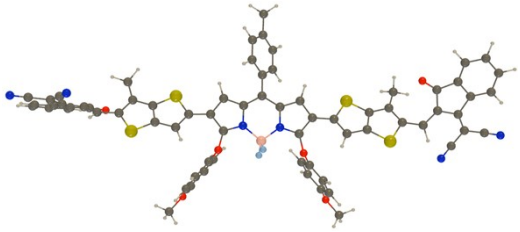

7.89

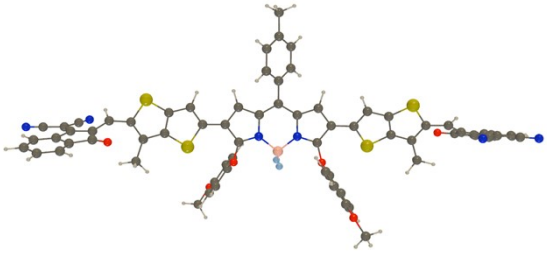

8.77

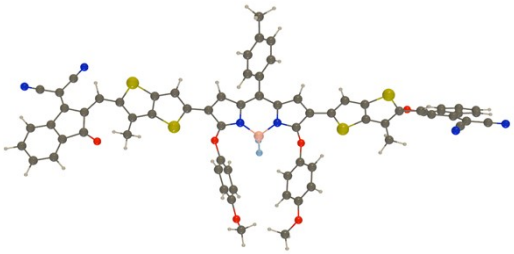

7.21

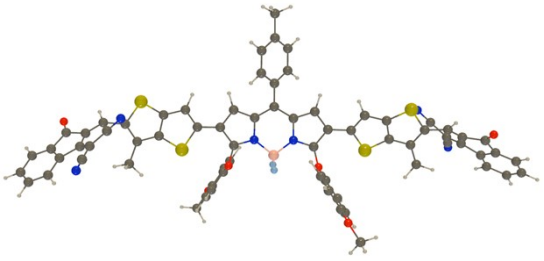

9.15

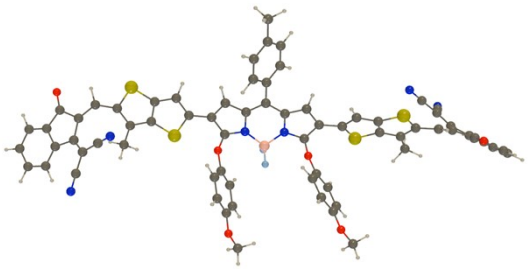

9.21

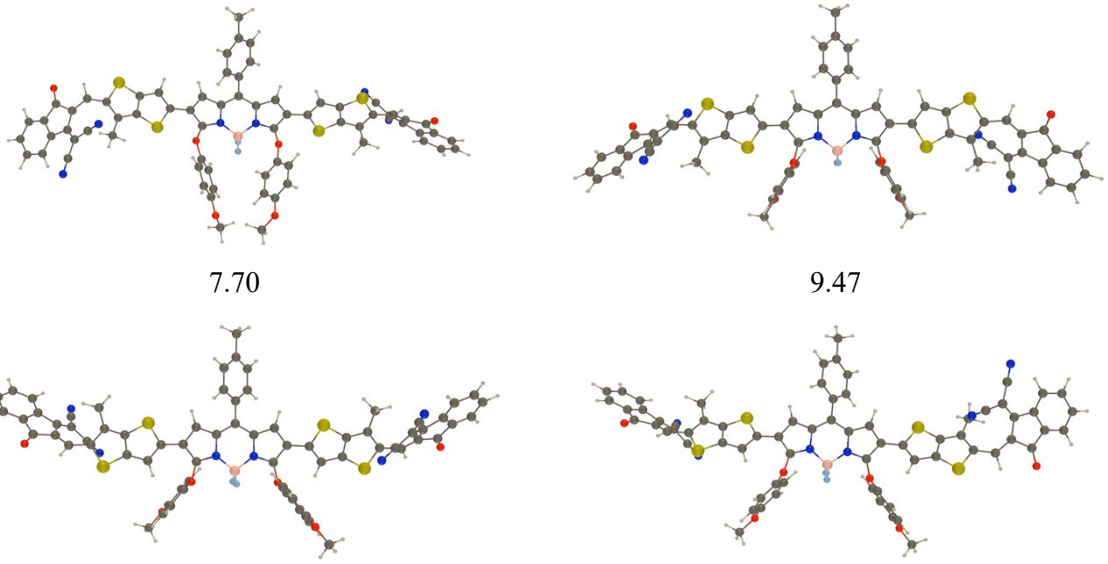

Figure S66. Representation of the various conformers found for (the model) of **BTT1**. The values indicated are the relative PCM($CHCl_3$)-MN15/6-31G(d) E+ZPVE in kcal.mol^{-1}. The four more stable are indicated by A, B, C, D letters.

Table S1. Relative *E*+ZPVE energies (kcal.mol^{-1}), frontier MO energies (in eV) and vertical transition wavelength (in nm) for the four more stable structures of Figure S66. All calculations at the PCM($CHCl_3$)-MN15/6-31+G(d,p)//PCM($CHCl_3$)-MN15/6-31G(d) level.

Compound	Conformer	*E*+ZPVE	HOMO (eV)	LUMO (eV)	λ (nm)
BTT	A	0.00	-6.393	-3.086	600
	B	0.47	-6.392	-3.097	602
	C	0.70	-6.214	-3.051	631
	D	0.50	-6.227	-3.044	631
BTT-4F	A	0.00	-6.448	-3.164	604
	B	0.38	-6.450	-3.170	605
	C	0.62	-6.267	-3.135	636
	D	0.49	-6.284	-3.125	636
BTT-4Cl	A	0.00	-6.456	-3.202	611
	B	0.42	-6.462	-3.207	611
	C	0.65	-6.279	-3.170	642
	D	0.55	-6.295	-3.159	641

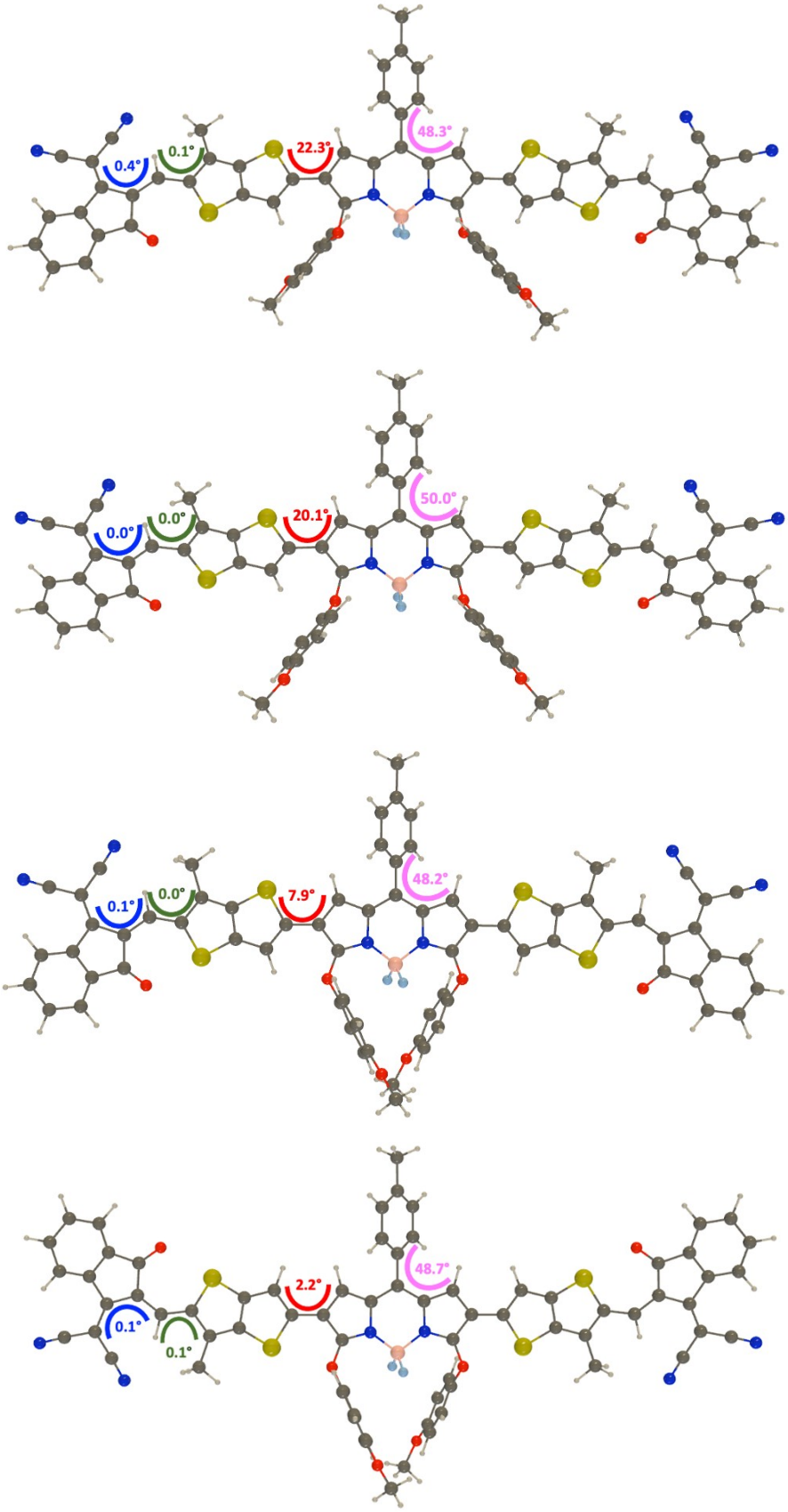

Figure S67. Key dihedral angles in **BTT** obtained at the PCM($CHCl_3$)-MN15/6-31G(d) level of theory on structures (from top to bottom) A, B, C, and D of Figure S66.

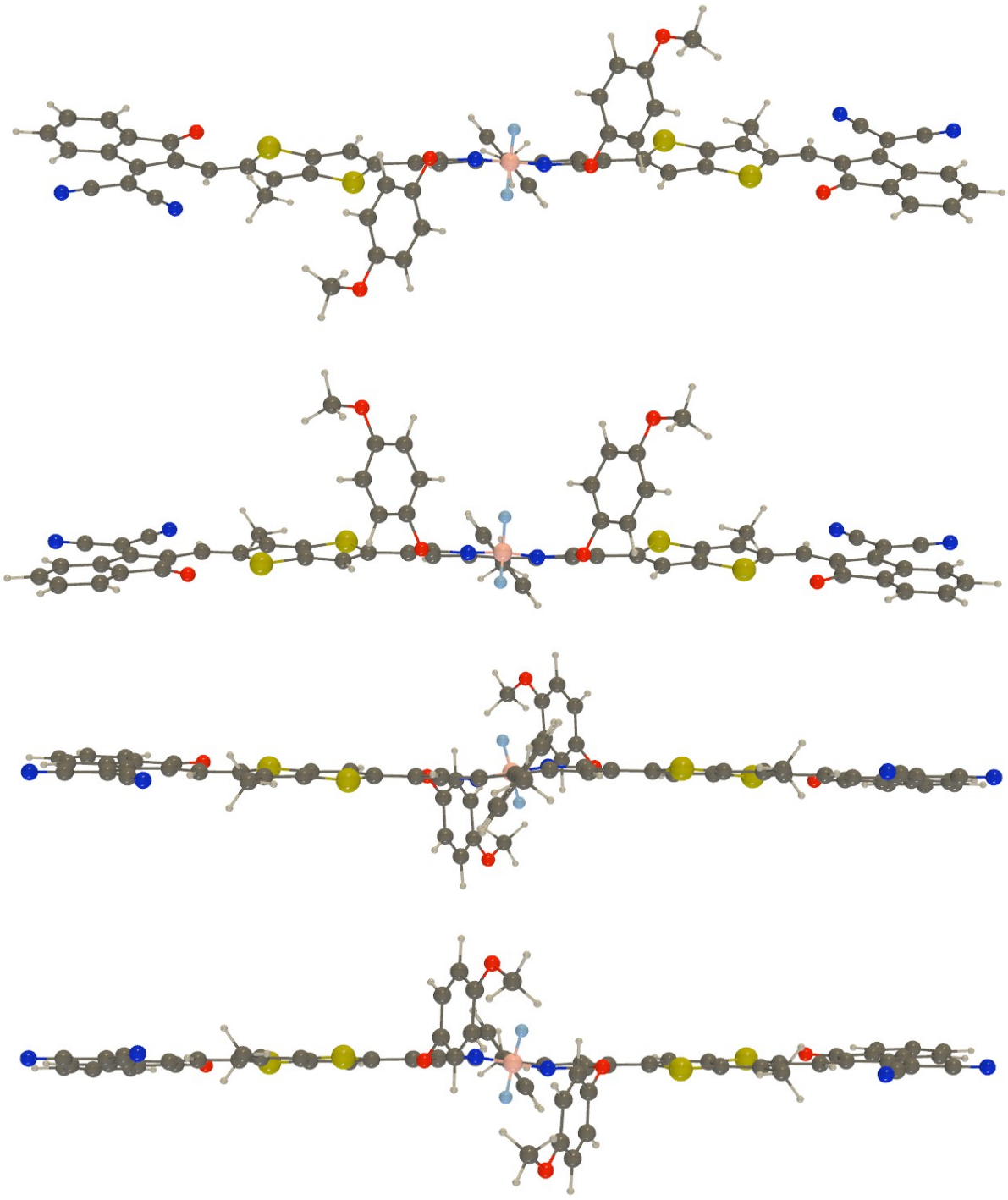

Figure S68. Side view of the **BTT** obtained at the PCM($CHCl_3$)-MN15/6-31G(d) level of theory on structures (from top to bottom) A, B, C, and D of Figure S67.

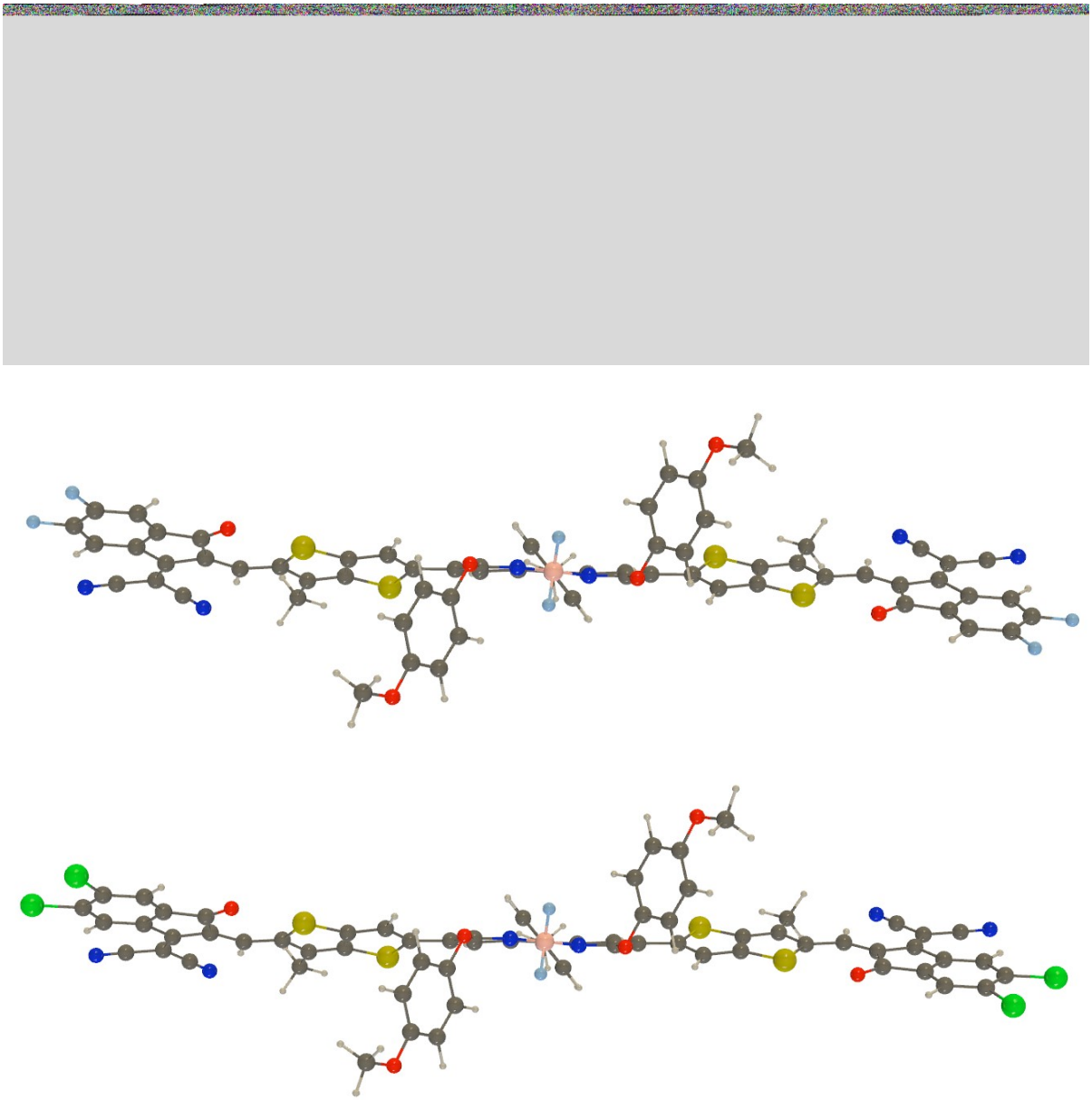

Figure S69. Side view of the **BTT**, **BTT-4F**, and **BTT-4Cl** (from top to bottom) obtained at the PCM($CHCl_3$)-MN15/6-31G(d) level of theory.

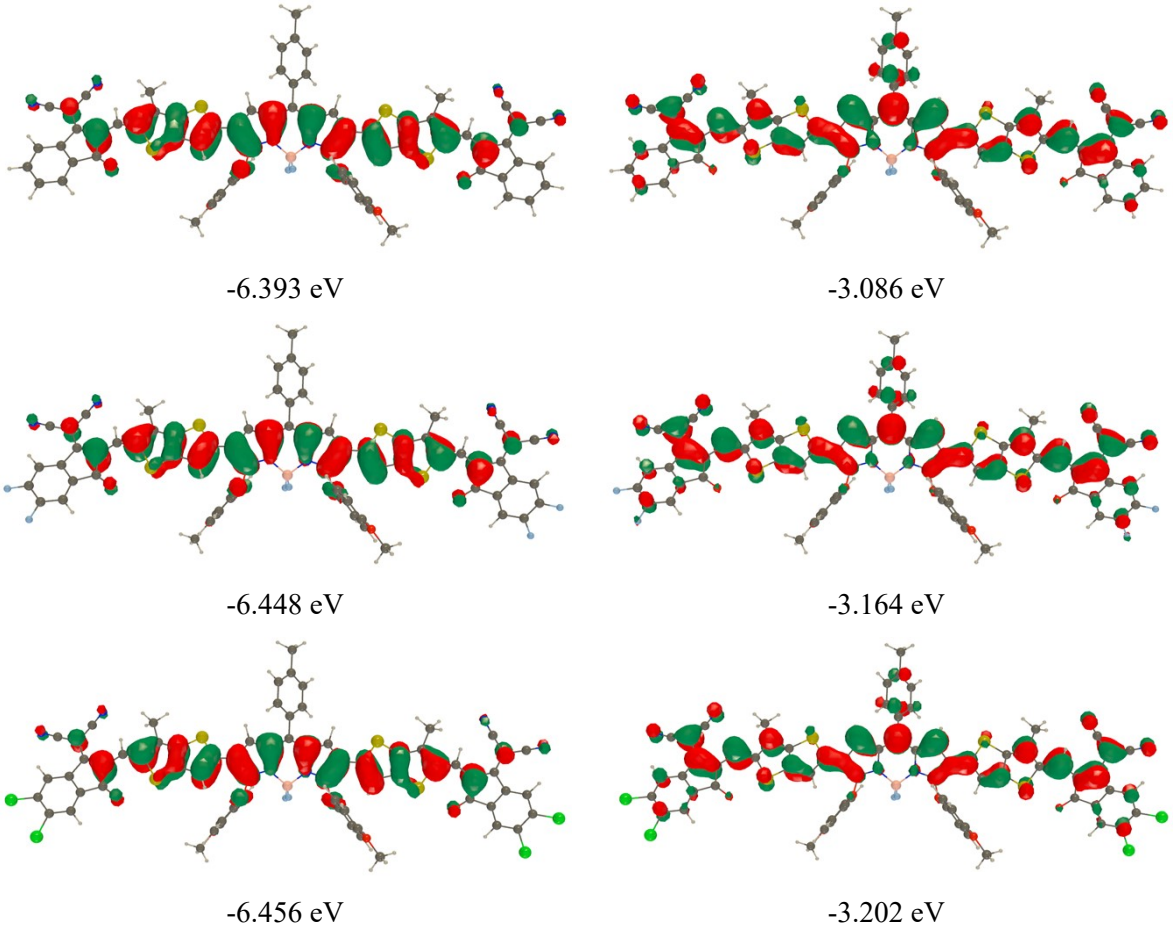

Figure S70. Frontier orbitals of **BTT**, **BTT-4F**, and **BTT-4Cl** (from top to bottom) obtained at the PCM($CHCl_3$)-MN15/6-31+G(d,p)//PCM($CHCl_3$)-MN15/6-31G(d) level of theory on structure A of Figure S66. The HOMO (left) and LUMO (right) are plotted with a contour threshold of 0.02 au and their energies are given eV.

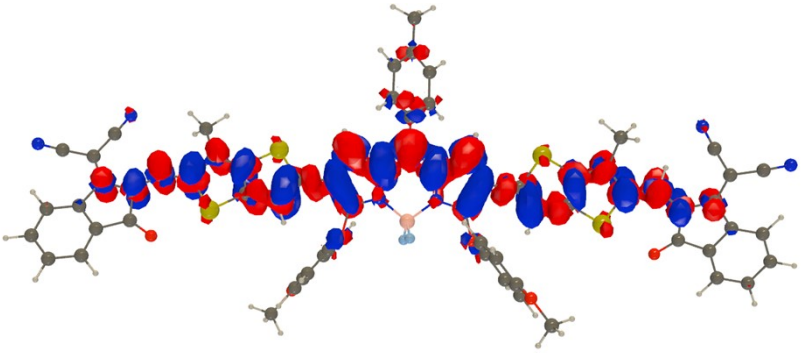

600 nm (*f*=3.48)

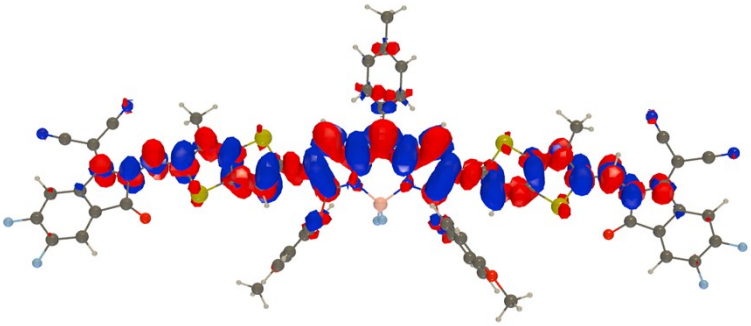

604 nm (*f*=3.56)

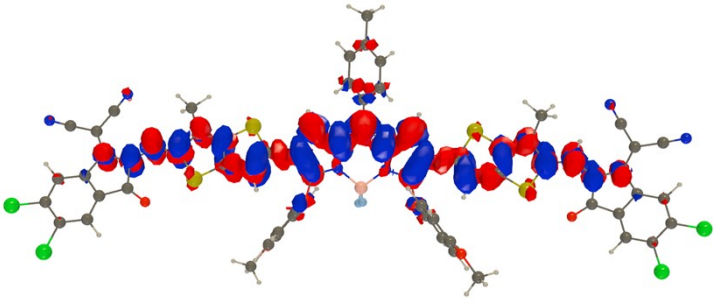

611 nm (*f*=3.70)

Figure S71. Density difference plot corresponding to the lowest excitation for **BTT**, **BTT-4F**, and **BTT -4Cl** (from top to bottom) obtained at the PCM($CHCl_3$)-MN15/6-31+G(d,p)//PCM($CHCl_3$)-MN15/6-31G(d) level of theory. The blue and red lobes indicate decrease and increase of density upon absorption respectively. A contour threshold of 0.0005 au is used, and the vertical excitation wavelengths (in nm) and corresponding oscillator strengths are given. The most stable structures are considered.

Optical properties

Table S2. Spectroscopy data for all BODIPY in solution at 25°C

Compound	λ_{abs} (nm)	ε ($M^{-1}.cm^{-1}$)	λ_{em} (nm)	Φ_f[(a)]	τ (ns)	k_r (10^8 Hz)	k_{nr} (10^8 Hz)	Δ_{SS} (cm^{-1})	Solvent
1	551	88900	567	0.51	-	-	-	512	DCM
2	549	100100	570	>1%	N.D.	-	-	671	DCM
3	547	124800	568	>1%	N.D.	-	-	644	DCM
5	640	66000	721	0.05	1.0	0.50	9.5	1755	DCM
6	639	55100	722	0.05	1.1	0.46	8.6	1799	DCM
7	631	74600	687	0.21	2.2	0.96	3.6	1292	DCM
8	629	79500	689	0.23	2.0	1.2	3.9	1384	DCM
BTT_{L6}	717	174100	764	0.08	0.8	1.0	12	857	DCM
	723	178700	770	0.09	1.1	0.82	8.3	844	$CHCl_3$
BTT_{L6}-4F	725	191300	770	0.11	1.0	1.1	8.9	806	DCM
	730	194000	776	0.11	1.0	1.1	8.9	812	$CHCl_3$
BTT_{L6}-4Cl	Partially soluble								DCM
	737	222800	783	0.15	1.1	1.4	7.7	797	$CHCl_3$
BTT_{R8}	716	170100	763	0.07	0.8	0.88	12	860	DCM
	724	193600	768	0.08	1.0	0.80	9.2	791	$CHCl_3$
BTT_{R8}-4F	723	192200	774	0.08	1.2	0.67	7.7	911	DCM
	731	210300	775	0.10	1.1	0.91	8.2	776	$CHCl_3$
BTT_{R8}-4Cl	731	215500	781	0.10	1.1	0.91	8.2	876	DCM
	738	202100	782	0.09	1.1	0.82	8.3	762	$CHCl_3$

(a) A reported BODIPY dye (φ_{ref} = 0.49 in DCM, λ_{ex} = 650 nm) was used as reference.

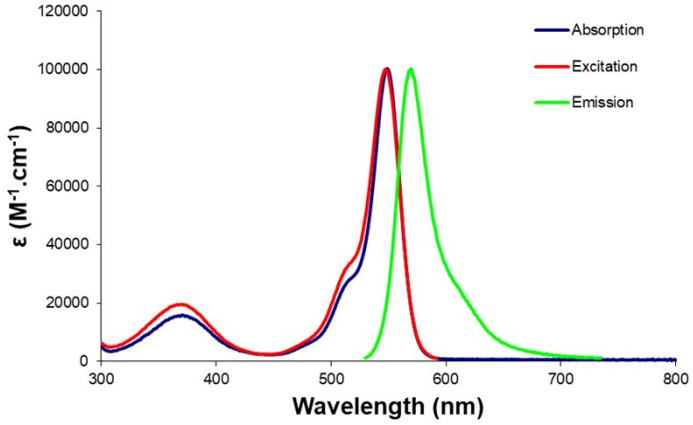

Figure S72. UV-Vis, emission and excitation spectra of compound **2** (DCM)

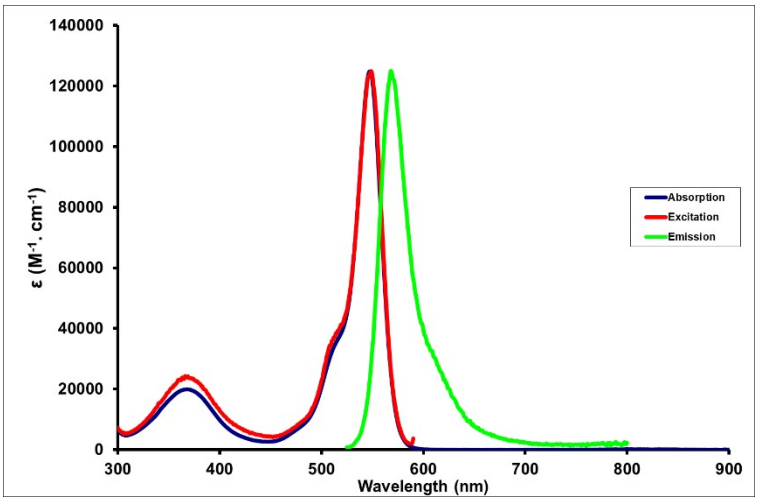

Figure S73. UV-Vis, emission and excitation spectra of compound **3** (DCM)

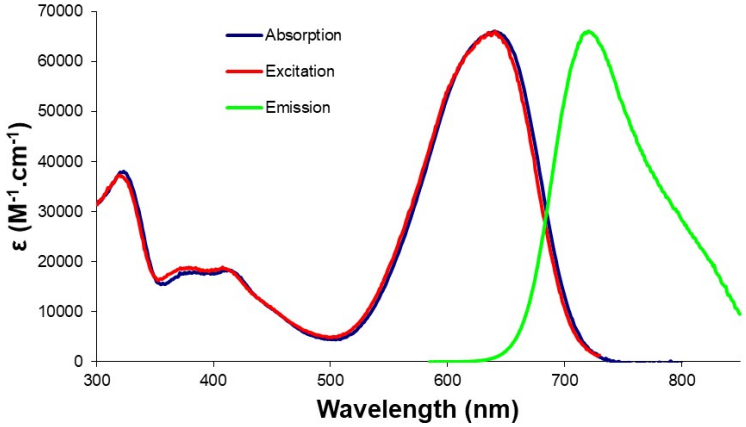

Figure S74. UV-Vis, emission and excitation spectra of compound **5** (DCM)

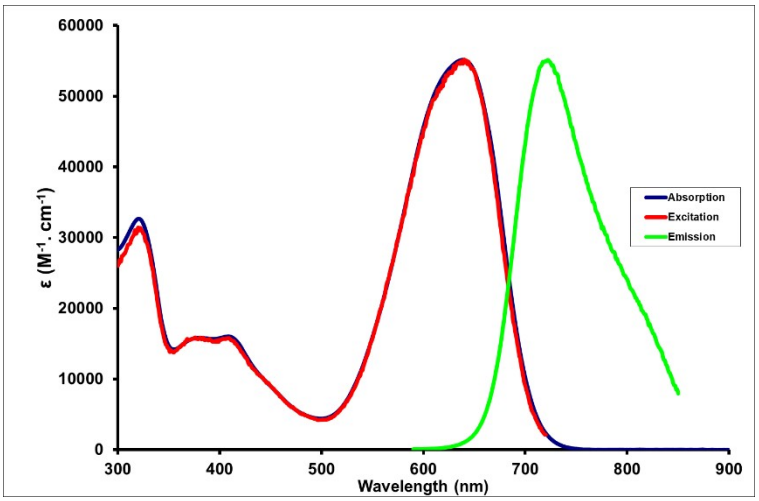

Figure S75. UV-Vis, emission and excitation spectra of compound **6** (DCM)

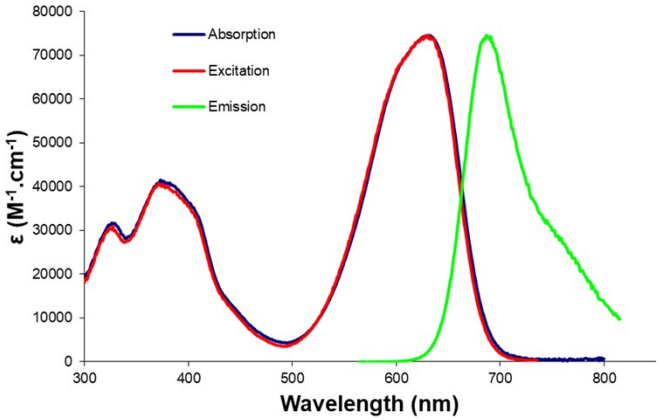

Figure S76. UV-Vis, emission and excitation spectra of compound **7** (DCM)

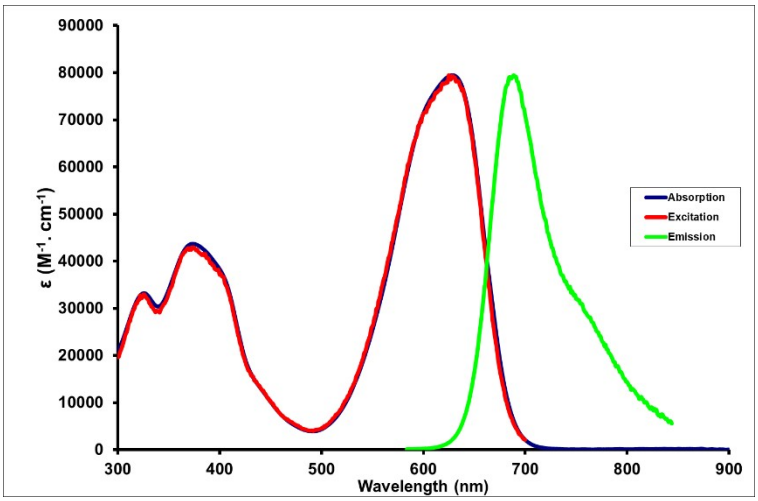

Figure S77. UV-Vis, emission and excitation spectra of compound **8** (DCM)

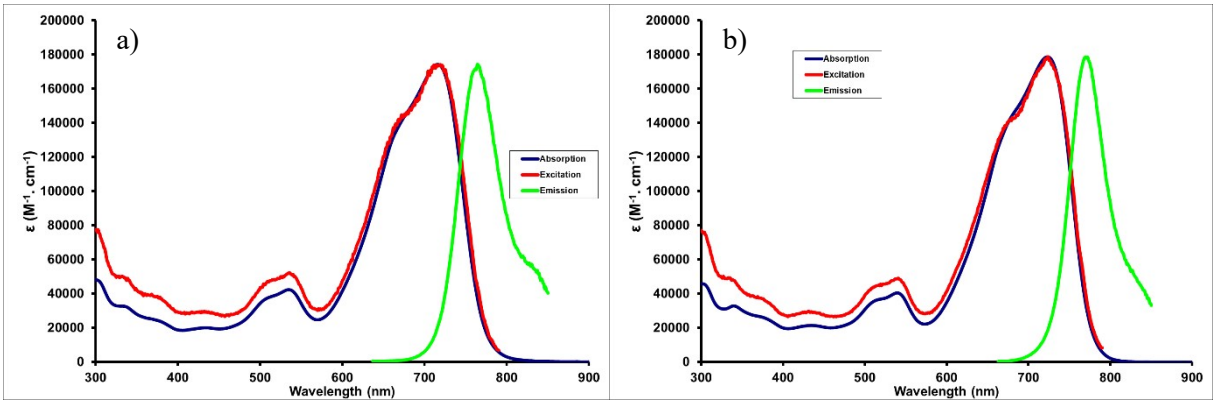

Figure S78. UV-Vis, emission and excitation spectra of compound $\mathbf{BTT_{L6}}$ a) DCM b) $CHCl_3$

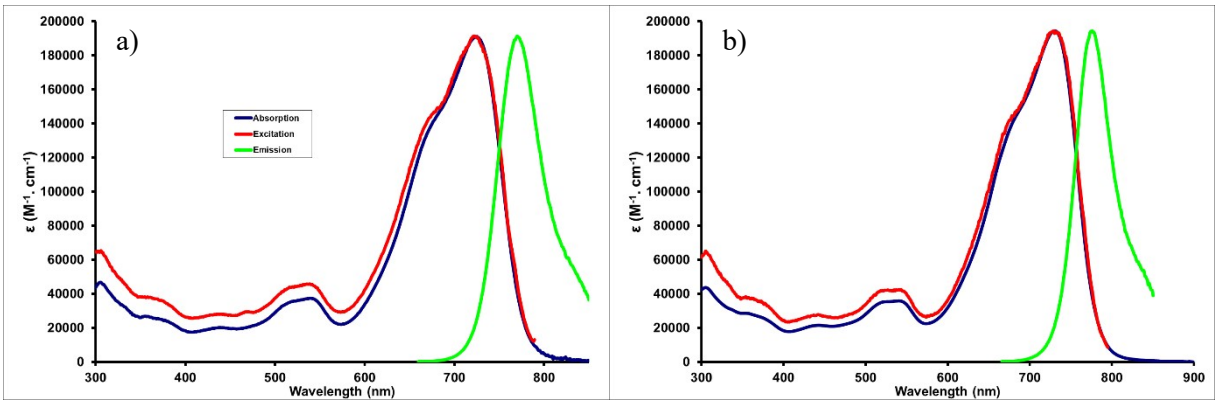

Figure S79. UV-Vis, emission and excitation spectra of compound **BTT_{L6}-4F** a) DCM b) $CHCl_3$

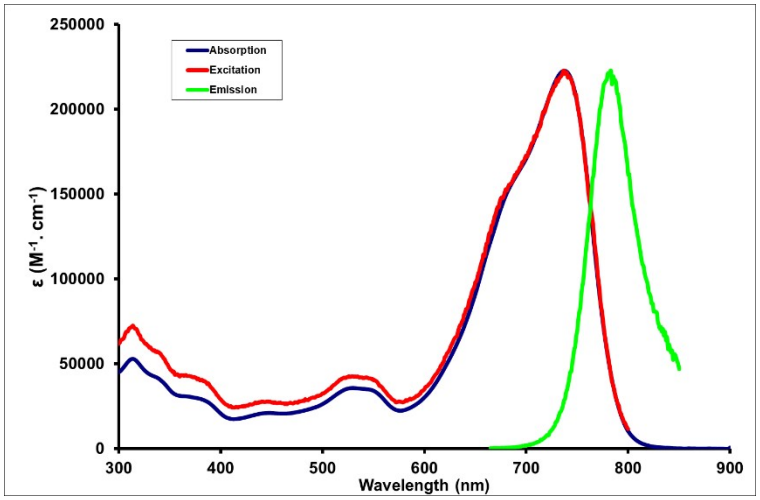

Figure S80 UV-Vis, emission and excitation spectra of compound **BTT_{L6}-4Cl** ($CHCl_3$)

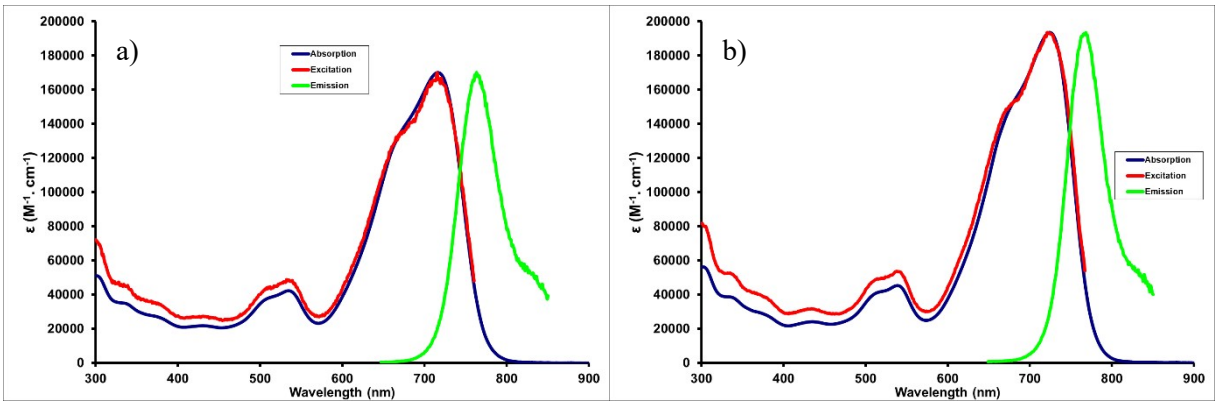

Figure S81. UV-Vis, emission and excitation spectra of compound **BTT_{R8}** a) DCM b) $CHCl_3$

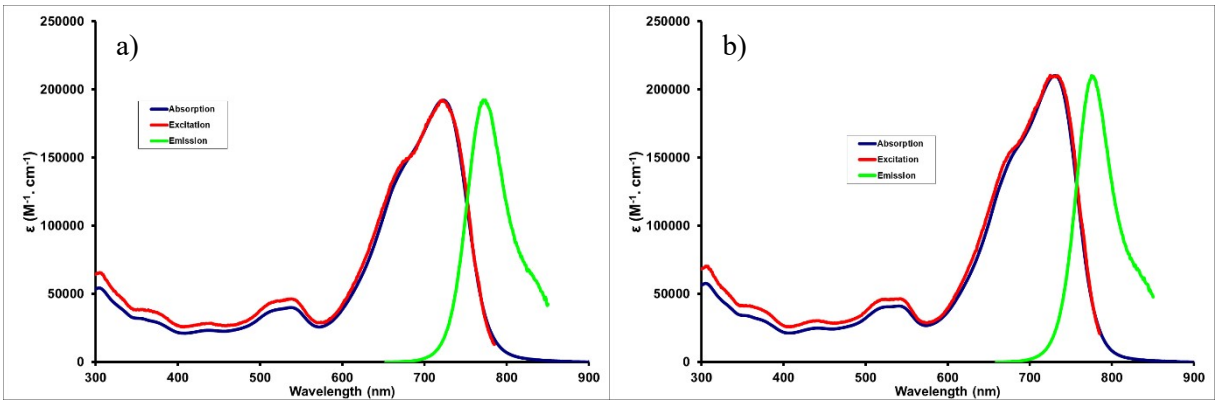

Figure S82. UV-Vis, emission and excitation spectra of compound **BTT_{R8}-4F** a) DCM b) $CHCl_3$

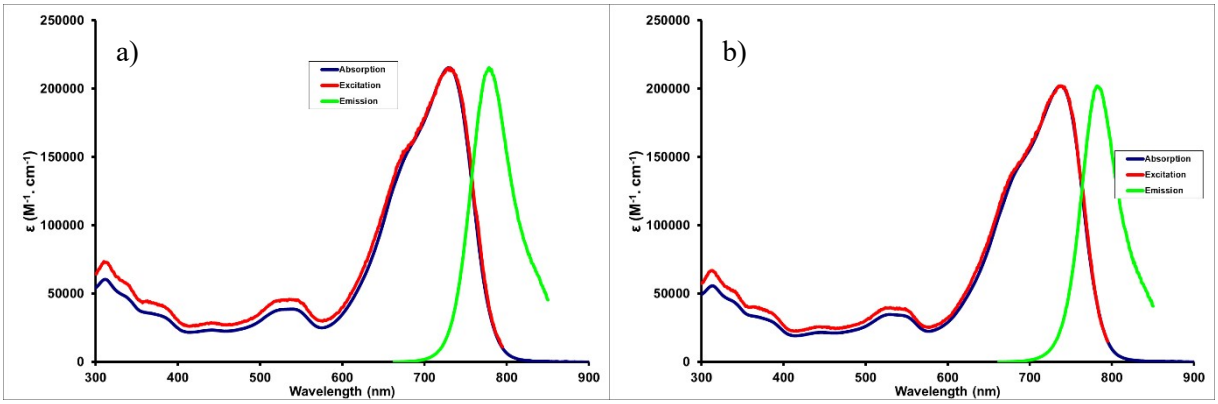

Figure S83. UV-Vis, emission and excitation spectra of compound **BTT_{R8}-4Cl** a) DCM b) $CHCl_3$

Cyclic Voltammetry

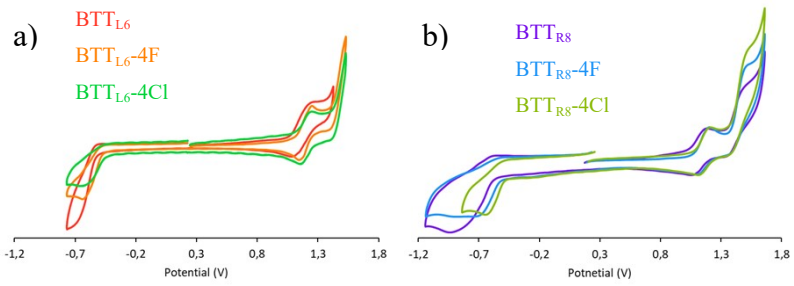

Figure S84. Cyclic voltammograms of a) BTT_{L6}, BTT_{L6}-4F and BTT_{L6}-4Cl b) BTT_{R8}, BTT_{R8}-4F and BTT_{R8}-4Cl (in DCM + 0.2 M NBu_4PF_6, sweeping rate: 100 $mV.S^{-1}$, 25°C)

Charge transport properties

Table S3. Charge carrier mobilities extracted in the saturation regime from OFETs transfer characteristics and from SCLC electron-mobility only devices. μ_h is the hole mobility and μ_e the electron one.

Compound	OFET ($cm^2/V.s$)						SCLC ($cm^2/V.s$)
	$\mu_e^{(a)}$	$\mu_h^{(a)}$	$\mu_e^{(b)}$	$\mu_h^{(b)}$	$\mu_e^{(c)}$	$\mu_h^{(c)}$	$\mu_e^{(a)}$
BTT_{L6}	$(4.9 \pm 1.1)\times10^{-3}$	-	$(5.7 \pm 0.9)\times10^{-3}$	$(1.9 \pm 0.4)\times10^{-4}$	$(3.7 \pm 0.7)\times10^{-3}$	$(3.3 \pm 0.6)\times10^{-4}$	$(3.2 \pm 0.4)\times10^{-3}$
BTT_{L6}-4F	$(2.5 \pm 0.7)\times10^{-3}$	-	$(3.6 \pm 1.0)\times10^{-3}$	-	$(1.9 \pm 0.2)\times10^{-3}$	-	-
BTT_{L6}-4Cl	$(5.2 \pm 2.0)\times10^{-3}$	-	$(6.6 \pm 1.9)\times10^{-3}$	-	$(1.0 \pm 0.3)\times10^{-3}$	-	-
BTT_{R8}	$(4.1 \pm 1.7)\times10^{-3}$	-	$(7.4 \pm 1.1)\times10^{-3}$	$(5.1 \pm 0.7)\times10^{-4}$	$(5.4 \pm 1.7)\times10^{-3}$	$(7.9 \pm 1.1)\times10^{-4}$	$(2.2 \pm 0.5)\times10^{-4}$
BTT_{R8}-4F	$(3.4 \pm 0.5)\times10^{-3}$	-	$(1.4 \pm 0.5)\times10^{-3}$	-	$(3.6 \pm 0.8)\times10^{-4}$	-	$(3.4 \pm 0.2)\times10^{-4}$
BTT_{R8}-4Cl	$(2.1 \pm 0.6)\times10^{-2}$	-	$(3.5 \pm 0.5)\times10^{-2}$	-	$(1.5 \pm 1.4)\times10^{-3}$	$(7.4 \pm 0.6)\times10^{-4}$	$(7.4 \pm 0.6)\times10^{-4}$

(a): as cast. (b) annealed 10 minutes at 100°C. (c) annealed 10 minutes at 150°C.

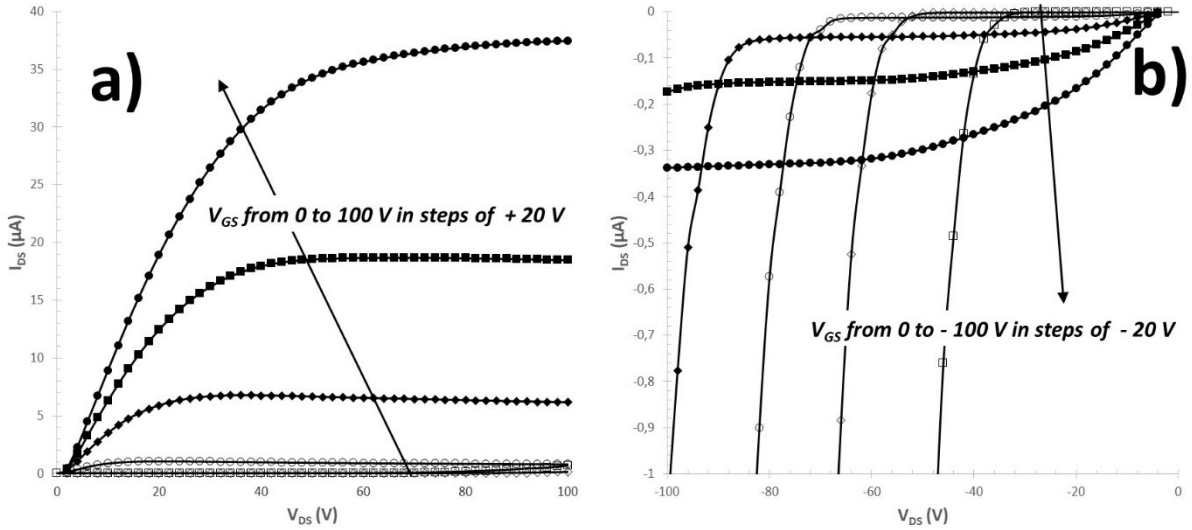

Figure S85. Output characteristics for an OFET annealed at 100°C for 10 minutes with a **BTT_{L6}** molecule channel. (a) electron output characteristic and (b) hole output characteristic.

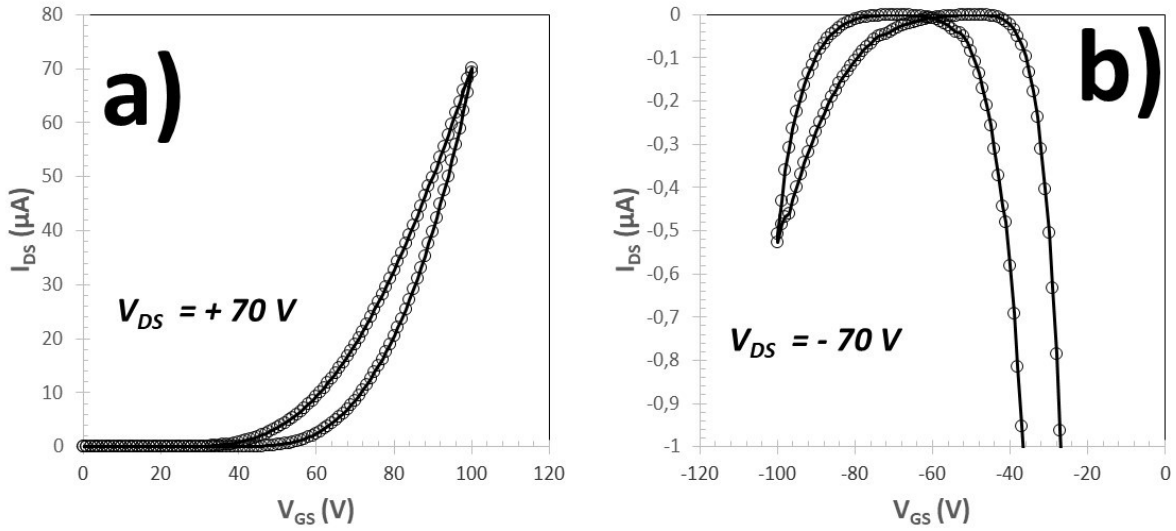

Figure S86. Transfer characteristics in the saturation mode for an OFET annealed at 100°C for 10 minutes with a $\mathbf{BTT_{L6}}$ molecule channel. (a) electron transfer characteristic and (b) hole transfer characteristic.

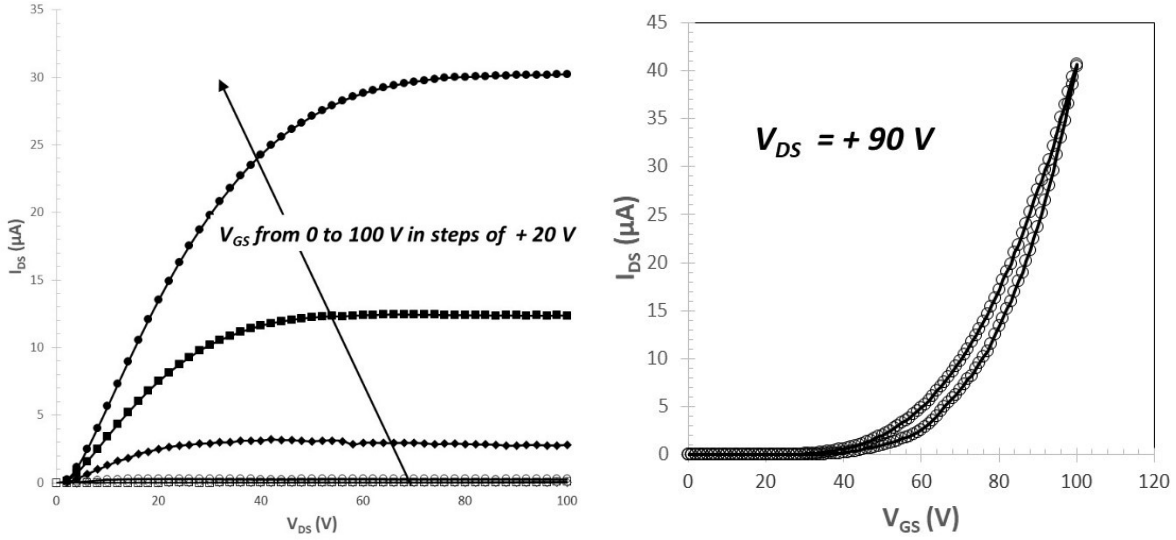

Figure S87. Electron output characteristics (left) and transfer characteristic in the saturation mode (right) for an OFET annealed at 100°C for 10 minutes with a $\mathbf{BTT_{L6}}$**-4F** molecule channel.

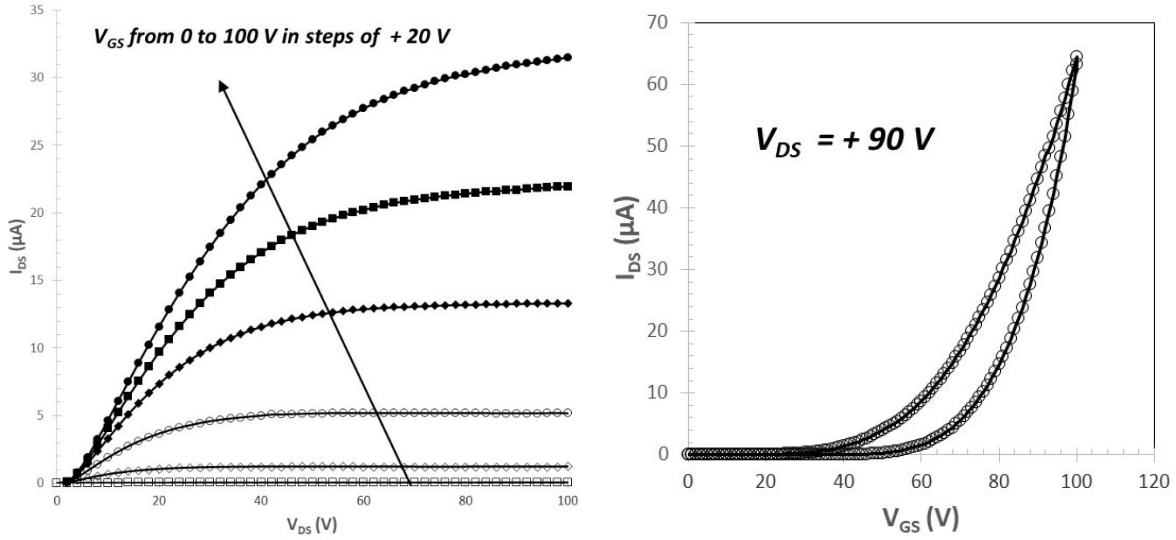

Figure S88. Electron output characteristics (left) and transfer characteristic in the saturation mode (right) for an OFET annealed at 100°C for 10 minutes with a **BTT_{L6}-4Cl** molecule channel.

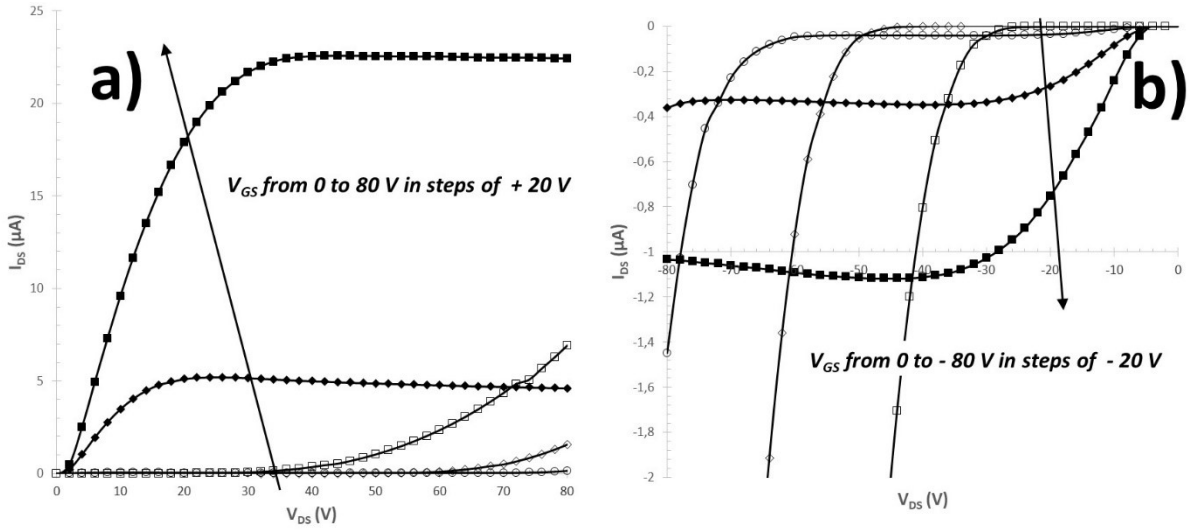

Figure S89. Output characteristics for an OFET annealed at 100°C for 10 minutes with a **BTT_{R8}** molecule channel. (a) electron output characteristic and (b) hole output characteristic.

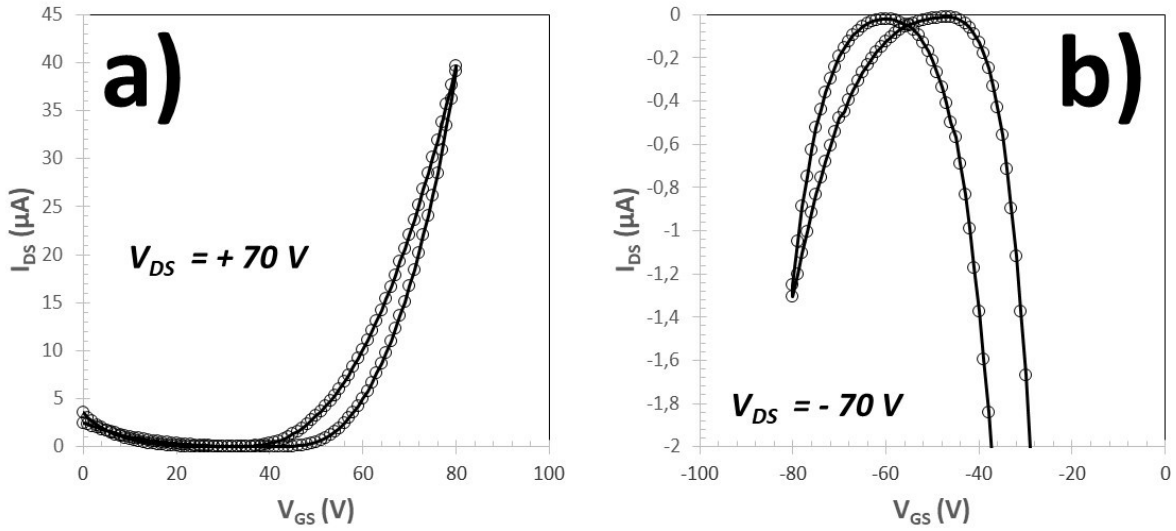

Figure S90. Transfer characteristics in the saturation mode for an OFET annealed at 100°C for 10 minutes with a $\mathbf{BTT_{R8}}$ molecule channel. (a) electron transfer characteristic and (b) hole transfer characteristic.

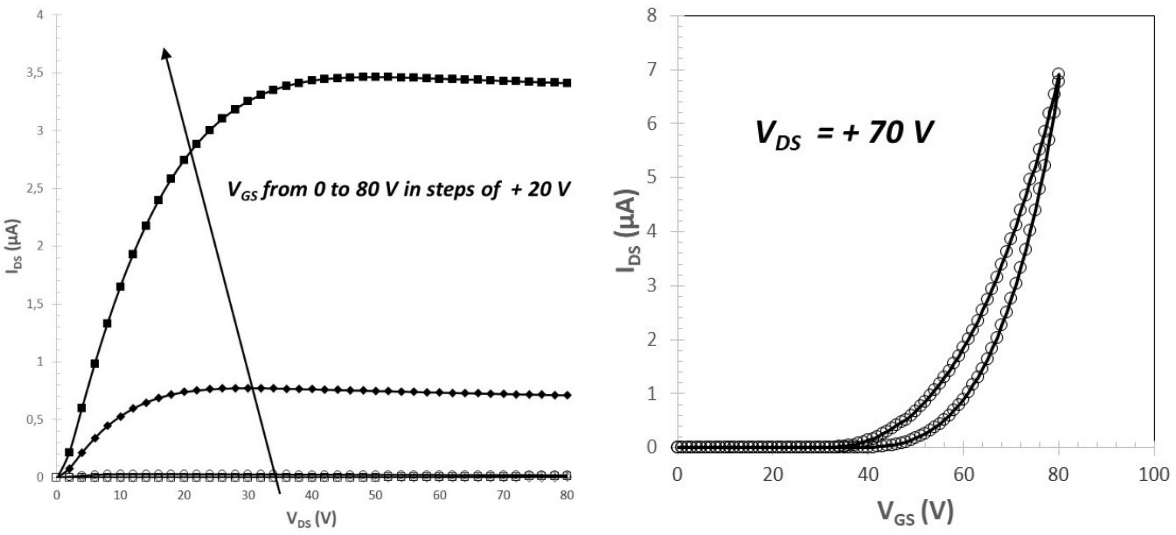

Figure S91. Electron output characteristics (left) and transfer characteristic in the saturation mode (right) for an OFET annealed at 100°C for 10 minutes with a $\mathbf{BTT_{R8}}$**-4F** molecule channel.

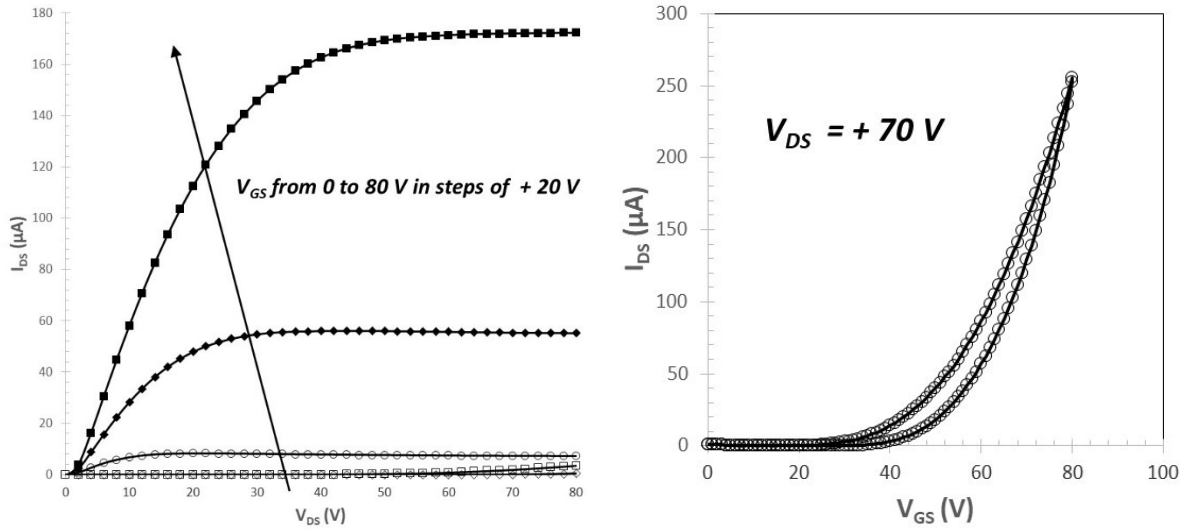

Figure S92. Electron output characteristics (left) and transfer characteristic in the saturation mode (right) for an OFET annealed at 100°C for 10 minutes with a **BTT_{R8}-4Cl** molecule channel.

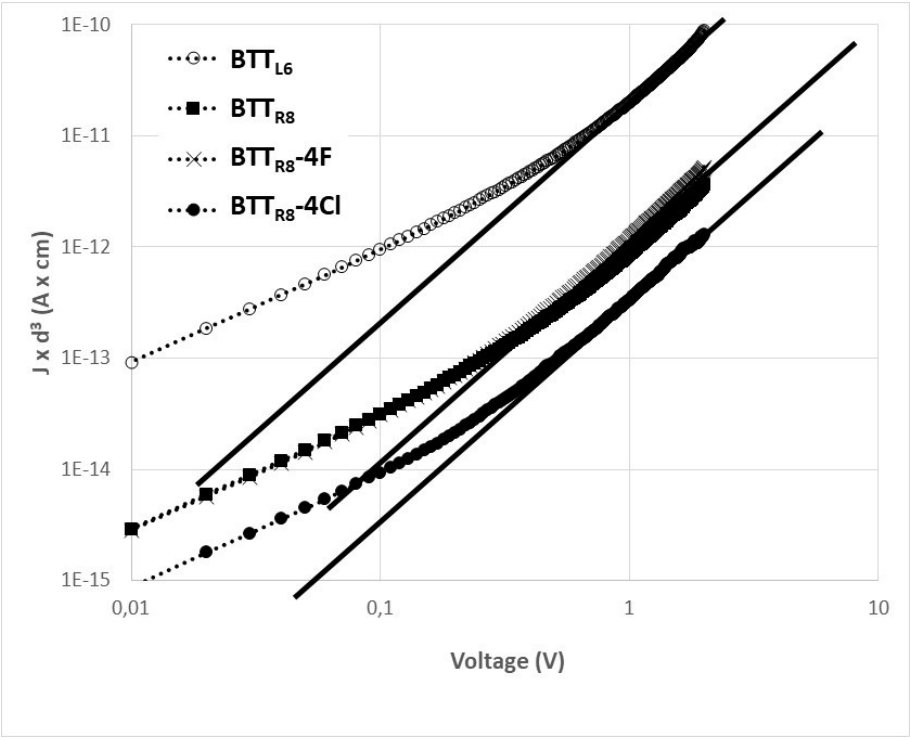

Figure S93. Current density (*J*) times d^3 (where *d* is the organic film thickness) versus the voltage (*V*) for SCLC electron-only diodes. The full line is an eye-guide for the SCLC regime.

GIWAXS

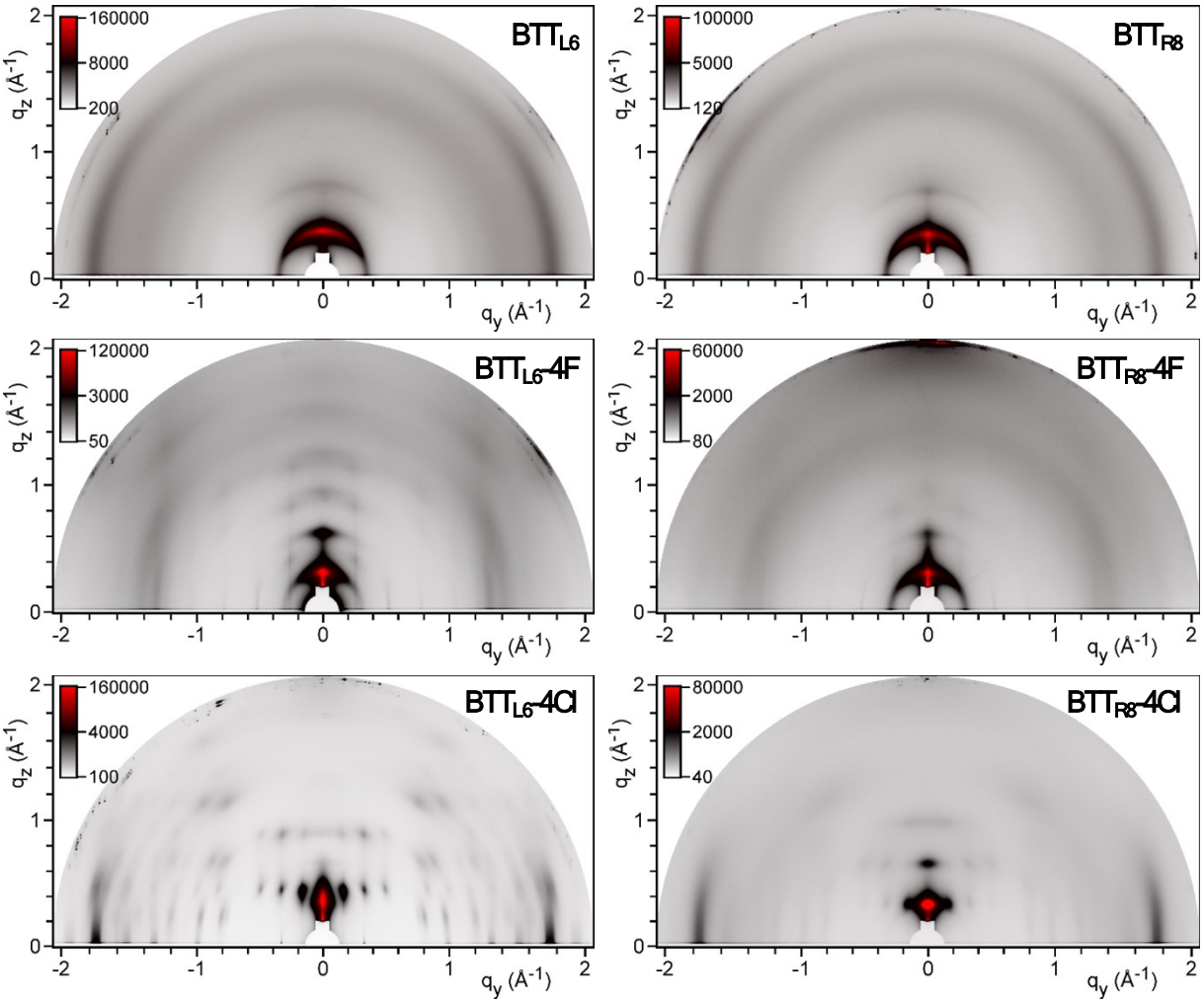

Figure S94. GIWAXS patterns of thin films of the BTT series, (beamline 9A, PLS-II synchrotron, South Korea), which were spin-coated on bare silicon from 10 mg/ml $CHCl_3$ solution.

Organic Solar Cells

For some of the most efficient devices (**BTT$_{L6}$-4F** as electron-acceptor), the photovoltaic parameters were measured as a function of the light-power using neutral filters. While the short-circuit current density (J_{sc}) exhibit, as expected for reasonably efficient devices, a linear dependence on light power, the open-circuit voltage (V_{oc}) dependence on light-power gives some informations on the main recombination mechanism in the OSCs.

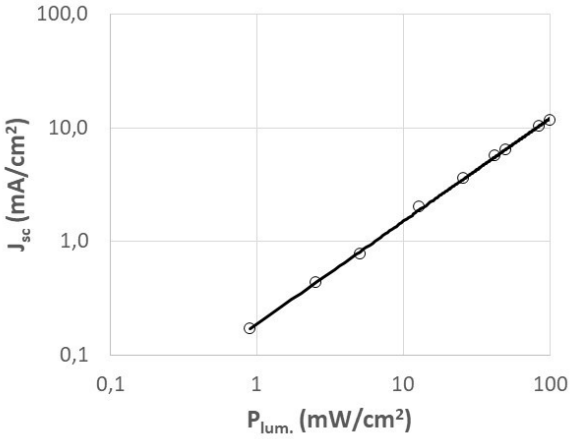

Figure S95. Short-circuit current density (J_{sc}) as a function of the incident light power.

J_{sc} shows an almost linear dependence on light power from 0.1 to 100 mW/cm² following:

$$J_{sc} = KP_{lum.}^{0.9} \quad (4)$$

This variation indicates a limited charge-carrier recombination rate in short-circuit conditions. On the contrary, the open-circuit voltage follows:

$$V_{oc} = A + B\frac{k_B T}{q} Ln(P_{lum.}) \quad (5)$$

where A is not depending on the light power, k_B is the Boltzmann's constant, T the temperature and q the elementary charge. B indicates a purely bimolecular recombination process when equal to one and efficient trap-assisted recombinations when substantial deviations from 1 are observed.[5] In our case, B is equal to 1.5 in the high illumination power range (from 10 to 100 mW/cm²). We can therefore conclude that trap-assisted recombinations are a major recombination process in [PM6:**BTT$_{L6}$-4F**] OSCs.

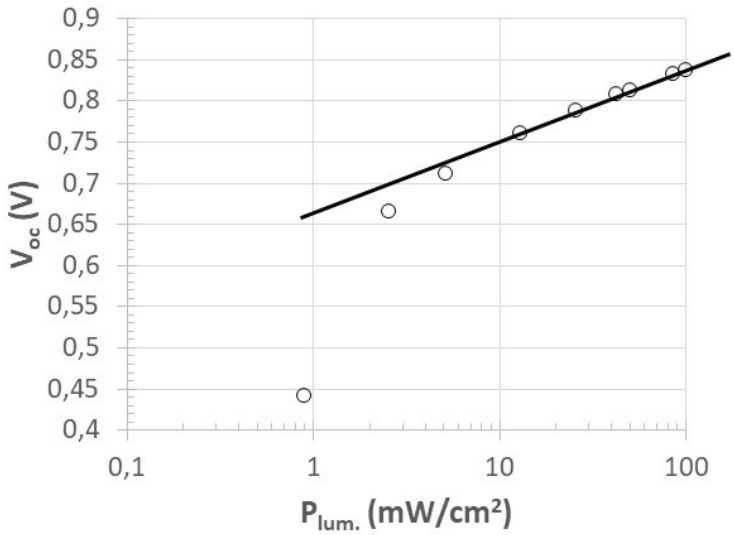

Figure S96. Open-circuit voltage (V_{oc}) as a function of the incident light power.

References

[1] M. J. Frisch, *et al.* Gaussian 16 Rev. A.03, Wallingord, CT, USA, **2016**.

[2] J. Tomasi, B. Mennucci and R. Cammi, *Chem. Rev.*, 2005, **105**, 2999.

[3] H. S. Yu, X. He, S. L. Li, and D. G. Truhlar, *Chem. Sci.,* 2016, **7**, 5032.

[4] B. Le Guennic and D. Jacquemin, *Acc. Chem. Res.,* 2015, **48**, 530.

[5] A. Chelouche, G. Magnifouet, A. Al Ahmad, N. Leclerc, T. Heiser and P. Lévêque, *J. Appl. Physics*, 2016, **120**, 225501.